Christian-Albrechts Universität zu Kiel
Institut für Theoretische und Astrophysik

Master thesis

Strongly Degenerate Nonideal Fermi Systems: Configuration Path Integral Monte Carlo Simulation

Simon Groth

Kiel, July 2014

1st examiner: Prof. Dr. Michael Bonitz

2nd examiner: Prof. Dr. Eckhard Pehlke

Abstract

Based on first principles, the configuration path integral Monte Carlo (CPIMC) approach allows for the exact computation of thermodynamic properties of strongly degenerate fermionic many-body systems with arbitrary pair-interaction. Due to the fermion sign problem, this regime is not accessible with (standard) direct path integral Monte Carlo methods. In this work, a Worm algorithm within the CPIMC formalism is presented which, in addition to standard thermodynamic observables, is capable of providing exact results for imaginary time correlation functions, i.e., in particular for the Matsubara Green function. The method is tested for a two-dimensional system of spin polarized, Coulomb interacting fermions in a harmonic trap. The obtained results are compared to an exact diagonalization method and to the Hartree-Fock approximation.

Zusammenfassung

Die sogenannte configuration path integral Monte Carlo Methode (CPIMC) ermöglicht die exakte Berechnung thermodynamischer Eigenschaften von stark entarteten fermionischen Vielteilchensystemen mit beliebiger Paarwechsel-wirkung. Auf Grund des fermionischen Vorzeichenproblems ist dieser Bereich mit herkömmlichen Pfadintegral-Methoden nicht zugänglich. In dieser Arbeit wird der Worm algorithmus innerhalb des CPIMC Formalismus vorgestellt. Zusätzlich zu den thermodynamischen Observablen können damit exakte Erwartungswerte für imaginärzeitabhängige Korrelationsfunktionen gewonnen werden, d.h. insbesondere für die Matsubara-Green-Funktion. Als Testsystem für die entwickelte Methode dienen spin-polarisierte, Coulomb-wechselwirkende Fermionen in einer zweidimensionalen harmonischen Falle. Die erhaltenen Ergebnisse werden mit einer exakten Diagonalisierungsmethode und der Hartree-Fock Näherung verglichen.

Contents

Contents

1. Introduction

The ab initio simulation of interacting fermionic many-body systems without approximations represents a challenging and highly interesting research field of theoretical physics and chemistry. Even for systems in equilibrium, a general approach allowing for simulations at arbitrary temperatures and densities still remains to be found. In particular for strongly degenerate systems, exact calculations can be carried out only for small particle numbers. The regime of high degeneracy, where quantum effects play an important role, is found at high densities, i.e., weakly to moderately coupled systems at low temperatures. Physical examples of such systems are fermions in optical lattices, electrons in quantum dots, dense and quark-gluon plasmas, conduction electrons in metals as well as warm dense matter inside large astrophysical objects.

Finite temperature quantum Monte Carlo (QMC) methods belong to the most promising approaches concerning the exact[1] computation of equilibrium properties of interacting many-body systems. With (standard) direct path integral Monte Carlo (DPIMC) [1, 2], which is based on Feynman's path integral formulation of quantum mechanics [3] (in imaginary time), accurate calculations for large bosonic systems can be performed, even at high degeneracy. But, for fermions, this method suffers from the so called *fermion sign problem* [4, 5], which causes an exponential increase of the statistical error with the system size and inverse temperature. In addition, for DPIMC, the fermion sign problem becomes worse the higher the degeneracy of the simulated system. Several optimizations of the standard DPIMC still allow for the simulation of moderately degenerate systems (depending on the coupling, at sufficiently high temperatures) [6, 7]. Another exact approach that reduces the sign problem is the multi-level blocking algorithm [8]. However, the regime of strong degeneracy is practically inaccessible with DPIMC methods. Of course, there exist many approximations. Regarding QMC methods, the most successful is the so called restricted path integral Monte Carlo (RPIMC) [4], which avoids the fermion sign problem by introducing an (uncontrollable) systematic error.

The recently developed configuration path integral Monte Carlo (CPIMC)

---

[1] In fact, the obtained results are exact up to a small statistical error, which reduces with the computation time converging to the exact value. Further, in practice, QMC methods usually introduce a systematic error due to a finite number of basis functions (CPIMC) or time slices (DPIMC). By ensuring the convergence of the observables with respect to these quantities, the remaining systematic error is much smaller than the statistical error.

method [9] allows for the first principle simulation of such strongly degenerate systems without approximations. This method has a sign problem complementary to that of DPIMC concerning the degeneracy of the system, i.e., there is no sign problem for the ideal quantum limit, whereas strongly interacting systems are not accessible [10, 11]. The main idea of CPIMC consists in employing the reformulation of quantum mechanics in terms of second quantization, which results in paths in imaginary time in the space of Slater-determinants in occupation number representation, unlike in DPIMC, where the paths are in coordinate space. Further, CPIMC is based on the continuous time QMC [12], which has been applied to lattice models. Within the CPIMC formalism, fermionic systems with (arbitrary) pair-interaction, i.e., in particular long range interaction, can be simulated requiring much more elaborate Monte Carlo updates than for lattice models (with short range pair-interaction). In fact, QMC in occupation number representation goes back to the less sophisticated Stochastic Series Expansion (SSE) [13] that has been applied to lattice models, too.

In addition to standard thermodynamic observables, we are also interested in the computation of imaginary time correlation functions. In particular, the one- and two-particle Matsubara Green functions (MGF) give access to dynamical properties, namely the single-particle spectral function and the dynamical structure factor[14]. However, to extract this information from the correlation function, a Laplace-like transformation has to be inverted. Several methods exist to perform the inversion but these require very accurate data for the MGF since the inversion is an ill-posed problem [15, 16]. Therefore, exact data for the MGF taking into account all correlation effects is necessary to obtain correct spectral properties.

For non- to moderately degenerate systems, the so called Worm algorithm (WA) within the DPIMC formalism yields exact results for the one-particle MGF [17]. For the continuous time QMC of lattice models, there also exists a WA [18].

In this work, a WA for the CPIMC method is presented, which, based on the ideas in [18], has been developed mainly within the PhD thesis of T. Schoof and to some extent within this master thesis. The main part of this work constitutes the development of the concrete sampling procedure of the one-particle MGF. In addition, due to the formulation of CPIMC in second quantization, the underlying one-particle basis in which the simulation is performed is in general arbitrary. Already in standard CPIMC [9], it turned out that the canonical finite temperature Hartree-Focck (FTHF) basis reduces the sign problem of the method. However, this is not always the case, and moreover, the exact mechanism that reduces the sign problem remained to be understood. For that reason, the ground state and finite temperature HF approach are investigated in more detail to determine the best basis for CPIMC calculations.

Finally, the method is applied to a two-dimensional test system of spin polarized, Coulomb interacting fermions in a harmonic trap. The MGF is directly linked to the one-particle density matrix, which can be used to compute the particle density. These densities (from the MGF) are compared to the results obtained from Configuration Interaction (CI) [19, 20] and FTHF [21] calculations. Since CI represents an exact diagonalization method, this verifies the correctness of the presented algorithm. Eventually, the imaginary time MGF is compared to the MGF in HF approximation to demonstrate the necessity of taking into account the interaction beyond the mean-field approximation.

1.1. Outline

This work is organized as follows:

In chapter 2, a brief but self-consistent review on Metropolis Monte Carlo and second quantization of quantum mechanics is given, which represent the basis of the CPIMC approach.

In chapter 3, first, the expansion of the of the partition function that is used for the standard CPIMC approach is derived. Then, the expansion is modified suitable for a WA and a similar expansion of the MGF is found. Together, these define the total configuration space of the WA. In the next part of this chapter, the developed Monte Carlo steps of the CPIMC WA are explained and discussed in detail.

In chapter 4, the estimators of the thermodynamic observables of interest are derived. It follows the presentation of different developed estimators for the MGF. Finally, a sufficiently fast converging estimator for the MGF is found.

Chapter 5 gives a brief introduction into the HF approximation. In particular the utilized ground state and finite temperature HF algorithm is explained.

In chapter 6, the test system is specified. Then, the ground state and finite temperature HF method is applied to the test system and investigated concerning the convergence behavior and the obtained solutions. Next, the fermion sign problem for CPIMC calculations in different HF basis sets is explored to find the optimal HF basis. Afterwards, the particle density obtained from the developed estimator of the MGF is compared to the density of CI and HF calculations. It follows a comparison of the (imaginary) time-dependent MGF from CPIMC calculations with the MGF in HF approximation. Finally, the fermion sign problem of canonical and grand canonical CPIMC calculations

is discussed for the test system.

Chapter 7 summarizes the main results and gives an outlook on possible future work.

1.2. Frequently used abbreviations

- **ONV**:Occupation number vector (see Sec. 2.2.2)

- **MGF**: Matsubara Green function. In this work, MGF refers to the one-particle MGF if not explicitly pointed out else.

- **CPIMC:** Configuration path integral Monte Carlo

- **standard CPIMC:** Refers to the former CPIMC method without the Worm algorithm. It has been developed by T. Schoof within his diploma thesis and is explained in [9, 10, 11].

- **WA**: Worm algorithm

- **CPIMC WA**: Refers to the Worm algorithm within the CPIMC approach which is presented in this work.

- **(standard) DPIMC**: Refers to the Direct path integral Monte Carlo approach without WA [1, 22].

- **DPIMC WA**: Refers to the WA within the DPIMC approach [17].

- **HF**: Hartree-Fock

- **FTHF**: Finite temperature Hartree-Fock

- **CI**: Configuration interaction

2. Theory

In this chapter, based on [10], an introduction to the basic theory required for the CPIMC formalism is given. First, the *Metropolis-algorithm* [23] is explained, which is capable of sampling random variables according to an arbitrary distribution without knowing its normalization. Second, a short but self-consistent review on second quantization of quantum mechanics is presented. Especially the derivation of the *Slater-Condon-rules*, which are utterly important for the CPIMC formalism, is briefly outlined. Readers that are familiar with the second quantization might just skip through the corresponding part to get to know the utilized notation.

2.1. Metropolis Monte Carlo

In statistical physics, the expectation value of an observable $\hat{O}$ can be written in the general form

$$\langle \hat{O} \rangle = \sum_{C} \!\!\!\!\!\diagup\, O(C) \frac{W(C)}{Z} \qquad \text{with} \qquad Z = \sum_{C} \!\!\!\!\!\diagup\, W(C) \,. \tag{2.1}$$

Here, C denotes a high dimensional multi-variable that consists of continuous and/or discrete one dimensional variables. For that reason, the symbol $\sum\!\!\!\!\!\diagup$ is used. In terms of Metropolis Monte Carlo, C is commonly interpreted as a *(system) configuration*[1]. Each configuration contributes to the partition function Z with its weight $W(C)$. If the weight function $W(C)$ is strictly positive, then $P(C) = \frac{W(C)}{Z}$ is the probability for the configuration C to be realized. The value of the observable in the system configuration C is given by $O(C)$. It is called the *estimator* of the observable. Hence, the expectation value is nothing but the summation over all these contributions weighted with the corresponding probability.

Sure, if we could directly compute the partition function Z, then we could apply standard relations of statistical physics to calculate any observable since a system in thermodynamic equilibrium is completely described by this function. Due to the high dimensionality of the summation, this is not possible in most

---

[1]This should not be confused with a true physical micro-state. Rather, the multi-variable C represents an abstract or mathematical system configuration.

cases. However, Monte Carlo methods are a very powerful tool when it comes to the computation of such high dimensional integrals. Suppose we have a set of system configurations $\{C_i\}$, $i = 1 \ldots N_{\mathrm{MC}}$ that are distributed with $P(C)$. Then, a good estimate of the expectation value (2.1) is given by

$$\langle \hat{O} \rangle \approx \frac{1}{N_{\mathrm{MC}}} \sum_{i=1}^{N_{\mathrm{MC}}} O(C_i) \ . \tag{2.2}$$

Of course, such a set of configurations can not be computed directly since this would require the knowledge of the normalization Z. Fortunately, utilizing the *Metropolis algorithm* [23], we can compute a sequence of states $C_0, C_1, \ldots$ that are eventually distributed with $P(C)$ without knowing the underlying normalization. For that purpose, we define a *transition probability* $T(C_i \rightarrow \widetilde{C}_{i+1})$ that defines the probability for the system to transition into the configuration $\widetilde{C}_{i+1}$ from the configuration C_i. This transition probability has to fulfil the so called *detailed balance* equation[2]

$$P(C_i)T(C_i \rightarrow \widetilde{C}_{i+1}) = P(\widetilde{C}_{i+1})T(\widetilde{C}_{i+1} \rightarrow C_i) \ .$$

Choosing the possible solution for the transition probability

$$T(C_i \rightarrow \widetilde{C}_{i+1}) = \min \left[1, \frac{P(\widetilde{C}_{i+1})}{P(C_i)} \right] = \min \left[1, \frac{W(\widetilde{C}_{i+1})}{W(C_i)} \right] , \tag{2.3}$$

we directly see that the normalization cancels.

Supposing the system is in the configuration C_i, the Metropolis algorithm works as follows: First, propose a transition to a different configuration $\widetilde{C}_{i+1}$ and evaluate Eq. (2.3). Then draw a random number[3] from $[0, 1)$ and accept the transition if it is smaller than the transition probability, i.e., $C_{i+1} = \widetilde{C}_{i+1}$. If it is larger than the transition probability, the system stays in the configuration C_i and it is $C_{i+1} = C_i$. Starting from a random initial configuration C_1, the sequence of configurations will eventually be distributed with $P(C)$ if the proposed transitions address a sufficient degree of freedom of the multi-variable C. More strictly speaking, the different proposals, also called *Monte Carlo steps*, have to be *ergodic* which means that all possible system configurations C must be accessible within a finite number of Monte Carlo steps. Therefore, given some expectation value in the form of Eq. (2.1), we will usually need a couple of different Monte Carlo steps addressing different degrees of freedom of C.

The explained algorithm is only valid if we propose each transition with equal probability. In most cases, it is more efficient to choose some system

---

[2]There exist weaker conditions but in practice, the detailed balance equation is used.

[3]The quality of the used random number generator is crucial for the reliability of the results.

changes more frequently than others. This can formally be incorporated in the detailed balance by splitting the transition probability into a *sampling probability* $S(C_i \rightarrow \widetilde{C}_{i+1})$ and an *acceptance probability* $A(C_i \rightarrow \widetilde{C}_{i+1})$ which have to fulfil the generalized detailed balance equation

$$P(C_i)A(C_i \rightarrow \widetilde{C}_{i+1})S(C_i \rightarrow \widetilde{C}_{i+1}) = P(\widetilde{C}_{i+1})A(\widetilde{C}_{i+1} \rightarrow C_i)S(\widetilde{C}_{i+1} \rightarrow C_i)$$
(2.4)

with the possible solution for the acceptance probability

$$A(C_i \rightarrow \widetilde{C}_{i+1}) = \min \left[1, \frac{S(\widetilde{C}_{i+1} \rightarrow C_i)W(\widetilde{C}_{i+1})}{S(C_i \rightarrow \widetilde{C}_{i+1})W(C_i)} \right] . \qquad (2.5)$$

The generalized algorithm is also called the *Metropolis Hastings algorithm* [22]. Further, the number of Monte Carlo steps that have to be performed until the correlations to the initial configuration C_1 have vanished is referred to as the *equilibration time*. Moreover, since the acceptance probability for the transition to the next configuration only depends on the current configuration, the computed sequence of configurations $C_1, C_2, \ldots, C_{N_{\mathrm{MC}}}$ represents a *Markov chain* of length N_{MC}.

However, finding a good set of different Monte Carlo steps that ensure ergodicity[4] can be very hard. Besides the ergodicity, the average acceptance probability of each step should be sufficiently large while changing the configuration C as much as possible. The concrete form of the multi-variable C depends on the chosen representation of the partition function. For a quantum system, the partition function is given by the trace over the N-particle density operator[5] $\hat{\rho}$

$$Z = \mathrm{Tr}\, \hat{\rho} \, ,$$

where the actual form of the density operator is determined by the chosen ensemble. Obviously, there exists an infinite number of possibilities to evaluate this expression for there exists an infinite number of N-particle basis sets in which the trace can be performed. Further, we could switch to the Heisenberg or the Interaction picture, or add an arbitrary number of unit operators and/or apply a reasonable approximation for the density operator. All those representations (or expansions in the form of Eq. (2.1)) of the partition function describe the same physical system, but most of them define a different multi-variable C and hence require different Monte Carlo steps. Of course, only a few representations are suitable for the application of the Metropolis algorithm. Besides, note

---

[4]In the majority of cases it is not possible to actually proof the ergodicity of the steps.

[5]Commonly, in terms of Monte Carlo, the density operator is usually not normalized, e.g., in the canonical ensemble it is $\hat{\rho} = e^{-\beta \hat{H}}$.

that we can not directly compute the partition function with the Metropolis algorithm but only expectation values according to Eq. (2.2).

So far we have assumed that the weight function $W(C)$ is strictly positive. Unfortunately, the partition function describing a fermionic system in general has negative and positive weights. If we still want to apply the Metropolis algorithm, then we have to rewrite (2.1) as follows:

$$\langle \hat{O} \rangle = \frac{\sum_C O(C) W(C)}{\sum_C W(C)} = \frac{\frac{1}{Z'} \sum_C O(C) S(C) |W(C)|}{\frac{1}{Z'} \sum_C S(C) |W(C)|} = \frac{\langle \hat{O} S \rangle'}{\langle S \rangle'} \, , \quad (2.6)$$

where we have introduced the primed partition function

$$Z' := \sum_C |W(C)| \, .$$

$S(C) = \operatorname{sgn}[W(C)]$ denotes the sign of the weight of the configuration C. We directly see that the expectation value $\langle O \rangle$ in the physical system, described by the true partition function Z, can be expressed by the expectation value of two different observables $\hat{O}S$ and S in the primed system described by Z' (denoted by $\langle \rangle'$). Since $P'(C) = \frac{|W(C)|}{Z'}$ is a true probability distribution, we can apply the Metropolis algorithm to that system by simply inserting the modulus of the weights $|W(C)|$ in Eq. (2.5). Having computed a Markov chain for the primed system, we can utilize Eq. (2.2) to estimate the desired expectation value of the observable in the true physical system:

$$\langle \hat{O} \rangle \approx \frac{\sum_{i=1}^{N_{MC}} O(C_i) S(C_i)}{\sum_{i=1}^{N_{MC}} S(C_i)} =: \frac{\overline{OS}'}{\overline{S}'} = \overline{O}. \quad (2.7)$$

In practice, not the whole configurations of the Markov chain are stored but only the value of the observables of each configuration, i.e. $O_i = O(C_i)$ and $S_i = (C_i)$, $i = 1, \ldots, N_{\mathrm{MC}}$. The estimated expectation value (2.7) fluctuates around the true expectation value $\langle \hat{O} \rangle$. To properly estimate the statistical error, it is not sufficient to calculate the standard deviation of $\overline{O}$. First, we have to take into account that the configurations of the Markov chain are not independent but auto-correlated for we compute every configuration from its previous. Second, the estimated value $\overline{O}$ is calculated from the fraction of two quantities $\overline{OS}'$ and $\overline{S}'$ that are both estimated and thus have a statistical error. Moreover, the generated "measurements" (samples) $\{O_i S_i\}$ and $\{S_i\}$ are not only auto-correlated but also cross-correlated, i.e. $O_i S_i$ is cross-correlated with S_i. A good estimator of the relative error, which takes into account these aspects, is given by [24]

$$\frac{\Delta \overline{O}_{\mathrm{auto,cross}}}{\overline{O}} = \sqrt{\left(\frac{\Delta \overline{OS}'}{\overline{OS}'} \right)^2 + \left(\frac{\Delta \overline{S}'}{\overline{S}'} \right)^2 - \frac{2}{N_{MC}} \frac{\overline{OSS}' - \overline{OS}'\,\overline{S}'}{\overline{OS}'\,\overline{S}'} 2\tau_{int,OS,S}} \, ,$$

$$(2.8)$$

with the statistical errors of $\overline{OS}'$ and $\overline{S}'$

$$\Delta\overline{OS}' = \sqrt{\frac{\overline{(OS)^2}' - \overline{(OS)}'^2}{N_{MC}} 2\tau_{\text{int},OS}} \; ,$$

$$\Delta\overline{S}' = \sqrt{\frac{\overline{S^2}' - \overline{S}'^2}{N_{MC}} 2\tau_{\text{int},S}} \; , \tag{2.9}$$

which are both enhanced by their *integrated auto-correlation time*

$$\tau_{\text{int},OS} = \frac{1}{2} + \sum_{k=1}^{N_{MC}} \frac{\overline{(OS)_i(OS)_{i+K}} - \overline{OS}^2}{\overline{(OS)_i^2} - \overline{OS}^2} \tag{2.10}$$

with

$$\overline{(OS)_i(OS)_{i+k}} = \frac{1}{N_{MC} - k} \sum_{i=1}^{N_{MC}-k} (OS)_i(OS)_{i+k}$$

and

$$\tau_{\text{int},S} = \frac{1}{2} + \sum_{k=1}^{N_{MC}} \frac{\overline{S_iS_{i+k}} - \overline{S}^2}{\overline{S_i^2} - \overline{S}^2} \quad \text{with} \quad \overline{S_iS_{i+k}} = \frac{1}{N_{MC} - k} \sum_{i=1}^{N_{MC}-k} S_iS_{i+k} \; . \tag{2.11}$$

The statistical errors (2.9) can be reduced by the square root of the number of samples N_{MC}. The enhancement by the integrated auto-correlation time τ can be interpreted in such a way that we have effectively computed $\frac{N_{\text{MC}}}{2\tau}$ uncorrelated samples. The third term under the square root in Eq. (2.8) accounts for the cross-correlation of OS and S, which is measured by the *integrated cross-correlation time*

$$\tau_{\text{int},OS,S} = \frac{1}{2} + \sum_{k=1}^{N_{MC}} \frac{\overline{O_iS_iS_{i+k}}' - \overline{OS}'\,\overline{S}'}{\overline{OSS}' - \overline{OS}'\,\overline{S}'} \tag{2.12}$$

with

$$\overline{O_iS_iS_{i+k}}' = \frac{1}{N_{MC} - k} \sum_{i=1}^{N_{MC}-k} O_iS_iS_{i+k} \; .$$

Note that the evaluation of the Eqs. (2.10),(2.11) and (2.12) requires the storage of all samples and does not allow for on the fly averaging. Moreover, binning analysis, which is used to reduce the required amount of stored samples, is not trivially possible due to the cross-correlation time (2.12). Finally, if the average acceptance probability of the steps is small, then the auto-correlation time is long, and we would waste storage by saving all samples. Instead, it is more sophisticated to propose N_{cycle} steps before saving the next sample, whereby the auto-correlation of the (stored) samples is reduced. We refer to N_{cycle} as the *cycle length*.

2.1.1. Fermion sign problem

From Eq. (2.6) it seems that Metropolis Monte Carlo of fermionic systems is no problem at all. But, if the average sign $\langle S \rangle'$ becomes much smaller than one, then we obviously have to determine $\langle OS \rangle'$ very precisely to obtain a reliable result for $\overline{O}$. Indeed, the average sign is by definition (cf. (2.6)) smaller or equal one, i.e.

$$\langle S \rangle' = \frac{Z}{Z'} \leq 1 \;.$$

In the canonical ensemble, where we have $Z = e^{-\beta N f}$ with β the inverse temperature of the system and f the free energy per particle, we can further write

$$\langle S \rangle' = e^{-\beta N (f - f')} \;. \tag{2.13}$$

Hence, the average sign goes to zero with increasing product of the inverse temperature and particle number. Upon a closer examination of the relative statistical error (2.8), we find that

$$\frac{\Delta \overline{O}_{\text{auto,sign}}}{\overline{O}} \propto \frac{1}{\overline{S}' \sqrt{N_{MC}}} \;.$$

and, assuming that $\langle S \rangle' \approx \overline{S}'$, it follows

$$\frac{\Delta \overline{O}_{\text{auto,sign}}}{\overline{O}} \propto \frac{1}{\sqrt{N_{MC}}} e^{\beta N (f - f')} \;.$$

The relative statistical error is inversely proportional to the average sign[6], which decreases exponentially with the system size and the inverse temperature. Unfortunately, the error can only be reduced by the square root of the number of samples. Given a certain error after a certain computation time, we have to compute a hundred times longer to reduce the error by one order of magnitude. This is the well known *fermion sign problem*. It occurs whenever we do Metropolis Monte Carlo with a partition functions that has sign changing weights[7]. Moreover, the chosen representation of the partition function strongly influences the sign problem. Even though there exist a few fermionic systems that do not suffer from the sign problem [25, 26], a general solution is unlikely since it has been shown to be NP-complete [5] for a chosen representation. For bosons and boltzmannons, Metropolis Monte Carlo can be done without sign problem, and, in contrast to fermions, very large systems can be simulated.

---

[6]In fact, this is only true for small average signs.

[7]Many other methods also suffer from a similar sign problem for fermions like e.g., diffusion Monte Carlo for ground state simulations.

2.2. Second quantization

In first quantization of quantum mechanics, the observables are represented by Hermitian operators acting on state vectors in Hilbert space. In a chosen basis representation, the state vectors become wave functions. This formulation of quantum mechanics is not very handy when it comes to the description of many-body systems of identical particles since the wave function has to be (anti-)symmetrized, especially, if the particle number is not fixed. With second quantization, there exist another, in many cases advantageous, formalism to describe such systems. In the context of that formalism, the so called creation and annihilation operators are introduced. Both, operators of observables and wave functions can be expressed in terms of these operators. In this section, only a very brief review of second quantization shall be given to introduce the required relations and notations for the CPIMC formalism. For more details see e.g. [27] and [28].

2.2.1. Slater determinants

We start with the ideal system of N identical particles with mass m. In first quantization, the Hamiltonian[8] takes the form

$$\hat{H}_0 = \sum_{\alpha=1}^{N} \hat{h}_\alpha \quad \text{with} \quad \hat{h}_\alpha = \frac{\hat{p}_\alpha^2}{2m} + \hat{v}_\alpha \,, \tag{2.14}$$

where $\hat{h}_\alpha$ denotes the one-particle Hamiltonian of the particle α consisting of the kinetic energy operator $\frac{\hat{p}_\alpha^2}{2m}$ and an external potential $\hat{v}_\alpha$. The eigenstates of the one-particle Hamiltonian $\{|i\rangle_\alpha\}$ with corresponding eigenvalues ϵ_i form an orthonormal basis in the one-particle Hilbert space $\mathcal{H}_1$. The quantum number i is a multi-index including the spin projection of the particle α, i.e., the spin orbitals are given by $\langle \vec{r}, \sigma | i \rangle = \Phi(\vec{r}, \sigma)$. Due to the separation of the ideal N-particle Hamiltonian (2.14) into a sum of one-particle Hamiltonians, we can construct the solution of the N-particle eigenvalue problem $\hat{H}_0 |\Psi\rangle = E |\Psi\rangle$ from product-states of one particle states $|i\rangle$

$$|i_1 i_2 \ldots i_N\rangle := \prod_{\beta=1}^{N} |i_\beta\rangle_\beta = |i_1\rangle_1 |i_2\rangle_2 \ldots |i_N\rangle_N \,. \tag{2.15}$$

It is straightforward to show that these product-states are eigenstates of the ideal Hamiltonian $\hat{H}_0$

$$\sum_{\alpha=1}^{N} \hat{h}_\alpha \prod_{\beta=1}^{N} |i_\beta\rangle_\beta = \sum_{\alpha=1}^{N} \left(\prod_{\substack{\beta=1 \\ \beta \neq \alpha}}^{N} |i_\beta\rangle_\beta \right) \hat{h}_\alpha |i_\alpha\rangle_\alpha = \sum_{\alpha=1}^{N} \epsilon_{i_\alpha} \prod_{\beta=1}^{N} |i_\beta\rangle_\beta \,.$$

---

[8]In this thesis, natural units are used, i.e., it is $\hbar = k_B = 1$.

These product-states form a basis of the N-particle Hilbert space $\mathcal{H} = \bigotimes_{\alpha=1}^{N} \mathcal{H}_1$. However, the indistinguishability of the particles has not been taken into account since in the product state (2.15) we know that particle α is in the state $|i_\alpha\rangle$. In order to do this, we define the two-particle exchange operator $\hat{P}_{\alpha,\beta}$

$$\hat{P}_{\alpha,\beta} |\ldots i_\alpha \ldots i_\beta \ldots\rangle = |\ldots i_\beta \ldots i_\alpha \ldots\rangle \quad \forall \alpha, \beta .$$

This operator can only have the eigenvalues ± 1 as

$$\hat{P}_{\alpha,\beta} |\ldots i_\alpha \ldots i_\beta \ldots\rangle = \lambda |\ldots i_\alpha \ldots i_\beta \ldots\rangle$$
$$\Leftrightarrow \quad |\ldots i_\alpha \ldots i_\beta \ldots\rangle = \hat{P}_{\alpha,\beta}\hat{P}_{\alpha,\beta} |\ldots i_\alpha \ldots i_\beta \ldots\rangle = \lambda^2 |\ldots i_\alpha \ldots i_\beta \ldots\rangle$$
$$\Leftrightarrow \quad \lambda^2 = 1 .$$

Since the Hamiltonian is invariant under particle exchange, i.e., $\left[\hat{\mathcal{H}}_0, \hat{P}_{\alpha,\beta}\right] = 0$, both operators $\hat{\mathcal{H}}_0$ and $\hat{P}_{\alpha,\beta}$ must have the same eigenstates. It turns out that only those N-particle states are realized that either always have the eigenvalue -1, under arbitrary two-particle exchange, or $+1$. Moreover, states with $\lambda = +1$ are referred to as being (totally) symmetric, and particles that are described by symmetric states are called bosons. The (totally) anti-symmetric states (with $\lambda = -1$) describe fermions. In this work, we are interested in the latter. A totally anti-symmetric, normalized N-particle state that is still an eigenstate of $\hat{H}_0$ can be written as a superposition of all $N!$ permuted product states (2.15) as follows

$$|i_1 i_2 \ldots i_N\rangle_- = \frac{1}{\sqrt{N!}} \sum_{\pi \in S_N} (-1)^P |i_1\rangle_{\pi(1)} |i_2\rangle_{\pi(2)} \ldots |i_N\rangle_{\pi(N)} , \qquad (2.16)$$

where π is an element in the N-body permutation group S_N, and P is the number of two-particle exchanges in which the permutation π can be decomposed. In spin-coordinate representation (with the abbreviation $x = \{\vec{r}, \sigma\}$) and with the definition of determinants, we obtain

$$\langle x_1 x_2 \ldots x_N | i_1 i_2 \ldots i_N\rangle_- = \Psi_-(x_1, \ldots, x_N)$$
$$= \frac{1}{\sqrt{N!}} \begin{vmatrix} \phi_{i_1}(x_1) & \phi_{i_2}(x_1) & \cdots & \phi_{i_N}(x_1) \\ \phi_{i_1}(x_2) & \phi_{i_2}(x_2) & \cdots & \phi_{i_N}(x_2) \\ \vdots & \vdots & & \vdots \\ \phi_{i_1}(x_N) & \phi_{i_2}(x_N) & \cdots & \phi_{i_N}(x_N) \end{vmatrix} . \quad (2.17)$$

These so called *Slater determinants* are obviously anti-symmetric under two-particle exchanges since this corresponds to the interchange of two rows which changes the sign of the determinant. Further, the determinant vanishes if two or more columns are linear dependent, for instance, if two or more of the

quantum numbers i_α are equal. In other words, no two fermions can occupy the same spin orbital. This is the well known *Pauli Principle*.

The anti-symmetric product-states (2.16) form a basis in the anti-symmetric Hilbert space $\mathcal{H}_-^N \subset \mathcal{H}^N$. Hence, we can expand any fermionic N-particle state into a linear combination of anti-symmetric product-states (2.16) constructed from an arbitrary one particle basis $\{|i\rangle\}$.

2.2.2. Occupation number representation

The anti-symmetric N-particle states (2.16), or equivalent the Slater determinants (2.17), are uniquely defined by the N quantum numbers $i_1, i_2 \ldots i_N$ of the N occupied one-particle orbitals. Therefore, we can write

$$|i_1 \ldots i_N\rangle_\pm \equiv |n_0 n_1 n_2 \ldots\rangle =: |\{n\}\rangle \ ,$$

where $n_i \in \{0, 1\}$ denotes the occupation number of the i-th one-particle orbital, i.e., those with $n_i = 1$ form the corresponding Slater determinant. Actually, we could choose any arbitrary mapping of occupation numbers to one-particle orbitals, but once defined, the mapping has to remain unchanged. Then, an occupation number vector (ONV) $|\{n\}\rangle$ uniquely defines a Slater determinant, and it is common to refer to the ONV itself as a Slater determinant. As we consider a quantum system of N fermions, it is $N = \sum_{i=0}^{\infty} n_i$. It follows that the ONVs form a basis in the anti-symmetric Hilbert space $\mathcal{H}_-^N$, i.e., it is

$$\sum_{\{n\}} |\{n\}\rangle \langle\{n\}| \, \delta_{\sum_i n_i, N} = \hat{1}_N \ , \tag{2.18}$$

where the short form

$$\sum_{\{n\}} := \sum_{n_0=0}^{1} \sum_{n_1=0}^{1} \cdots$$

for the summation over all occupation numbers is used. Further, the OVNs fulfil the orthogonality relation

$$\langle\{n\}|\{\bar{n}\}\rangle = \prod_{i=0}^{\infty} \delta_{n_i, \bar{n}_i} =: \delta_{\{n\},\{\bar{n}\}} \ . \tag{2.19}$$

In this occupation number representation of Slater determinants, we only have to drop the restriction $N = \sum_{i=0}^{\infty}$ to obtain states of varying particle number, whereas in terms of Slater determinants, we have to deal with determinants of different dimension. The ONVs of varying particle number form a basis in the anti-symmetric Fock space $\mathcal{F}_-$ that is defined as being the direct sum of the anti-symmetric Hilbert spaces with $0, 1, 2, \ldots$ particles, i.e., it is

$$\mathcal{F}_- := \mathcal{H}^0 \oplus \mathcal{H}^1 \oplus \mathcal{H}_-^2 \ldots \ .$$

In $\mathcal{H}^0$, there is exactly one state with zero particles $|n\rangle = |000\ldots\rangle$ containing only zeros. This state is also referred to as the vacuum state. The orthogonality relation (2.19) is valid for the ONVs in Fock space, too, and the completeness relation (2.18) changes slightly to

$$\sum_{\{n\}} |\{n\}\rangle \langle\{n\}| = \hat{1} \; .$$

Hence, we can expand the state vector $|\Psi\rangle$ of a fermionic system with varying particle number, e.g., in the grand canonical ensemble, into a linear combination of OVNs

$$|\Psi\rangle = \sum_{\{n\}} c_{\{n\}} |\{n\}\rangle \; ,$$

where the OVNs are defined with respect to an arbitrary one-particle basis $\{|i\rangle\}$.

2.2.3. Creation and annihilation operators

The creation and annihilation operators represent the most important tool of second quantization. For fermions, the creation operator $\hat{a}_i^\dagger$ is defined by

$$\hat{a}_i^\dagger |\{n\}\rangle = (1 - n_i)(-1)^{\alpha_{\{n\},i}} |\ldots, n_i + 1, \ldots\rangle \; . \tag{2.20}$$

Hence, it maps an ONV of particle number N onto an ONV of particle number $N + 1$ by adding a particle in the orbital i. The prefactor $(1 - n_i)$ results in the vanishing of the ONV if there is already a particle in the orbital i (Pauli principle). The phase factor $(-1)^{\alpha_{\{n\},i}}$ with

$$\alpha_{\{n\},i} := \sum_{l=0}^{i-1} n_l \tag{2.21}$$

is in agreement with the representation of the ONVs as anti-symmetric product-states (2.16) since it corresponds to the number of two-particle exchanges to correctly sort the new orbital $|i\rangle$ into the product. This, of course, corresponds to the number or column interchanges in (2.17) required to place ϕ_i in the correct column. In accordance with (2.20), the fermionic annihilation operator is defined by

$$\hat{a}_i |\{n\}\rangle = n_i(-1)^{\alpha_{\{n\},i}} |\ldots, n_i - 1, \ldots\rangle \; . \tag{2.22}$$

It vanishes if there is no particle in the orbital i to be annihilated. The Hermitian adjoint of the creation operator is the annihilation operator and vice

versa, which is indicated by the notation. Further, they fulfil the important relations

$$\{\hat{a}_i^\dagger, \hat{a}_j^\dagger\} = \{\hat{a}_i, \hat{a}_j\} = 0 \; ,$$
$$\{\hat{a}_i, \hat{a}_j^\dagger\} = \delta_{i,j} \tag{2.23}$$

with the anti-commutator of two operators $\{\hat{A}, \hat{B}\} := \hat{A}\hat{B} + \hat{B}\hat{A}$. Utilizing the creation operator, any Fock state can be constructed from the vacuum state:

$$|\{n\}\rangle = \left(\prod_{i=0}^{\infty}(\hat{a}_i^\dagger)^{n_i}\right)|\{0\}\rangle \; .$$

Due to the relations (2.23), the ordering of the creation operators on the r.h.s. must be the same as the ordering of the orbitals in the ONV on the l.h.s..With the orthogonality relation (2.19) and the definitions (2.20), (2.22), we immediately write down the matrix elements of the creation and annihilation operators

$$\langle\{n\}|\hat{a}_k^\dagger|\{\bar{n}\}\rangle = (-1)^{\alpha_{\{n\},k}}\delta_{\{n\},\{\bar{n}\}}^{k}\delta_{n_k,1}\delta_{n_k,\bar{n}_k+1} \; ,$$
$$\langle\{n\}|\hat{a}_k|\{\bar{n}\}\rangle = (-1)^{\alpha_{\{n\},k}}\delta_{\{n\},\{\bar{n}\}}^{k}\delta_{n_k,0}\delta_{n_k,\bar{n}_k-1} \; ,$$
$$\text{with} \quad \delta_{\{n\},\{\bar{n}\}}^{k} := \prod_{\substack{i=0 \\ i\neq k}}^{\infty} \delta_{n_i,\bar{n}_i} \; . \tag{2.24}$$

Similarly, matrix elements of products of two or more creation and annihilation operators can be computed. In particular, there is the hermitian occupation number operator $\hat{n}_i := \hat{a}_i^\dagger \hat{a}_i$, which is diagonal in occupation number representation with the eigenvalues being the occupation number n_i of the $i-$th one-particle orbital, i.e., it is

$$\hat{n}_i |\{n\}\rangle = n_i |\{n\}\rangle \; .$$

The total number of particles $N = \sum_{i=0}^{\infty} n_i$ of an ONV is an eigenvalue of the total particle number operator $\hat{N}$ defined as

$$\hat{N} := \sum_{i=0}^{\infty} \hat{n}_i \; .$$

Finally, the creation and annihilation operators can be transformed into another one-particle basis according to

$$\hat{a}_\nu^\dagger = \sum_{i=0}^{\infty} \langle i|\nu\rangle \, \hat{a}_i^\dagger \; ,$$
$$\hat{a}_\nu = \sum_{i=0}^{\infty} \langle \nu|i\rangle \, \hat{a}_i \; . \tag{2.25}$$

In the continuous basis of spin-coordinate states $\{|x\rangle\}$, $x = (\mathbf{r}, \sigma)$, the creation and annihilation operators are called *field operators*. Using Eq. (2.25), these can be expressed in terms of creation and annihilation operators of an arbitrary discrete one-particle basis $\{|i\rangle\}$:

$$\hat{\Psi}^\dagger(x) := \hat{a}_x^\dagger = \sum_{i=0}^\infty \langle i|x\rangle\, \hat{a}_i^\dagger = \sum_{i=0}^\infty \phi_i^*(x)\hat{a}_i^\dagger \,,$$

$$\hat{\Psi}(x) := \hat{a}_x = \sum_{i=0}^\infty \langle x|i\rangle\, \hat{a}_i = \sum_{i=0}^\infty \phi_i(x)\hat{a}_i \,, \tag{2.26}$$

where $\hat{\Psi}^\dagger(x)$ creates and $\hat{\Psi}(x)$ annihilates a particle at space point $\mathbf{r}$ with spin projection σ.

2.2.4. One-particle operators in second quantization

The operator of the kinetic energy or an external potential of a N-particle system is of the form

$$\hat{B} = \sum_{\alpha=1}^N \hat{b}_\alpha \,, \tag{2.27}$$

where $\hat{b}_\alpha$ is a one-particle operator acting on particle α. Though misleadingly, $\hat{B}$ is referred to as a one-particle operator while actually, $\hat{B}$ is a N-particle operator acting on N-particle states $|\Psi\rangle \in \mathcal{H}_N$. The representation of the one-particle operators $\hat{b}$ in an arbitrary one-particle basis $\{|i\rangle\}$ is given by

$$\hat{b} = \sum_{i,j=0}^\infty b_{ij} \,|i\rangle_\alpha \langle j|\,\alpha$$

with one-particle integrals[9]

$$b_{ij} = \langle i|\hat{b}|j\rangle = \int \mathrm{d}x\, \phi_i^*(x) b(x) \phi_j(x) \,. \tag{2.28}$$

Inserting this into (2.27), we obtain the matrix representation of the N-particle operator

$$\hat{B} = \sum_{i,j=0}^\infty b_{ij} \sum_{\alpha=1}^N |i\rangle_\alpha \langle j|_\alpha \tag{2.29}$$

Provided that the N-particle state $|\Psi\rangle$ is an anti-symmetrized product state (2.16) constructed from the same one-particle basis $\{|i\rangle\}$, it is straightforward

---

[9]Integration over $x = (\mathbf{r}, \sigma)$ includes summation over the spin projections.

to show that the action of the operator (2.29) on the anti-symmetric product state corresponds to the following action of creation and annihilation operators on the ONV $|\{n\}\rangle$ that is uniquely defined by $|\Psi\rangle$:

$$\sum_{i,j=0}^{\infty} b_{ij} \hat{a}_i^\dagger \hat{a}_j \, |\{n\}\rangle = \sum_{i,j=0}^{\infty} b_{ij} \sum_{\alpha=1}^{N} |i\rangle_\alpha \, \langle j|_\alpha \, |\Psi\rangle \; . \tag{2.30}$$

Thus, the l.h.s. of (2.30) is the second quantized form of the N-particle operator (2.27), i.e.,

$$\hat{B} = \sum_{i,j=0}^{\infty} b_{ij} \hat{a}_i^\dagger \hat{a}_j \; . \tag{2.31}$$

Note that this operator, unlike the first quantized form (2.29), does not depend on the particle number, and its action on Fock states $|\{n\}\rangle$ of different particle number is well defined. To compute the matrix elements of (2.31) in Fock space, we have to compute the matrix elements of a product of an arbitrary creation and annihilation operator. Using the matrix elements of the creation and annihilation operator (2.24) and the completeness relation in Fock space (2.19), we find for $k \neq l$

$$
\begin{aligned}
\langle\{n\}|\hat{a}_l^\dagger \hat{a}_k|\{\bar{n}\}\rangle &= \sum_{\{n'\}} \langle\{n\}|\hat{a}_l^\dagger|\{n'\}\rangle \, \langle\{n'\}|\hat{a}_k|\{\bar{n}\}\rangle \\
&= \sum_{\{n'\}} (-1)^{\alpha_{\{n'\},l}+\alpha_{\{\bar{n}\},k}} \delta_{\{n\},\{n'\}}^l \delta_{\{n'\},\{\bar{n}\}}^k \delta_{n_l',0} \delta_{n_l,1} \delta_{\bar{n}_k,1} \delta_{n_k',0} \\
&= (-1)^{\alpha_{\{n\},l}+\alpha_{\{\bar{n}\},k}} \delta_{\{n\},\{\bar{n}\}}^{kl} \delta_{n_l,1} \delta_{\bar{n}_k,1} \delta_{\bar{n}_l,0} \delta_{n_k,0}
\end{aligned}
$$

and for $k = l$

$$\langle\{n\}|\hat{a}_k^\dagger \hat{a}_k|\{\bar{n}\}\rangle = \langle\{n\}|\hat{n}_k|\{\bar{n}\}\rangle = n_k \delta_{\{n\},\{\bar{n}\}} \; .$$

Splitting $\hat{B}$ into these two cases, it follows

$$
\begin{aligned}
\langle\{n\}|\hat{B}_1|\{\bar{n}\}\rangle &= \sum_{k=0}^{\infty} b_{kk} \, \langle\{n\}|\hat{a}_k^\dagger \hat{a}_k|\{\bar{n}\}\rangle + \sum_{\substack{k,l=0 \\ k \neq l}}^{\infty} b_{lk} \, \langle\{n\}|\hat{a}_l^\dagger \hat{a}_k|\{\bar{n}\}\rangle \\
&= \delta_{\{n\},\{\bar{n}\}} \sum_{k=0}^{\infty} b_{kk} n_k \\
&\quad + \sum_{k=0}^{\infty} \sum_{\substack{l=0 \\ l \neq k}}^{\infty} b_{lk} (-1)^{\alpha_{\{n\},l}+\alpha_{\{\bar{n}\},k}} \delta_{\{n\},\{\bar{n}\}}^{kl} \delta_{n_l,1} \delta_{\bar{n}_k,1} \delta_{\bar{n}_l,0} \delta_{n_k,0} \; .
\end{aligned}
$$

$$\tag{2.32}$$

Obviously, these matrix elements do not vanish in only two cases: The ONVs $|\{n\}\rangle$ and $|\{\bar{n}\}\rangle$ either have to be equal or differ in exactly two orbitals. The phase factor can be further simplified. Assuming that $k < l$ we have (cf. Def. (2.21))

$$
\begin{aligned}
(-1)^{\alpha_{\{n\},l}+\alpha_{\{\bar{n}\},k}} &= (-1)^{\sum_{i=0}^{l-1} n_i + \sum_{i=0}^{k-1} \bar{n}_i} = (-1)^{\sum_{i=0}^{k-1} n_i + \sum_{i=k}^{l-1} n_i + \sum_{i=0}^{k-1} \bar{n}_i} \\
&= (-1)^{2\left(\sum_{i=0}^{k-1} n_i\right)} (-1)^{\sum_{i=k}^{l-1} n_i} \\
&= (-1)^{\sum_{i=k+1}^{l-1} n_i} ,
\end{aligned}
\tag{2.33}
$$

where in the second line we have used the fact that $|\{n\}\rangle$ and $|\{\bar{n}\}\rangle$ only differ in the orbitals k and l. The last line is correct since n_k has to be zero for a non-vanishing matrix element in (2.32). Likewise, we can simplify the phase factor for $k > l$. Both cases can be written in the compact form

$$
(-1)^{\alpha_{\{n\},l}+\alpha_{\{\bar{n}\},k}} = (-1)^{\sum_{\min(k,l)+1}^{max(k,l)-1}} .
\tag{2.34}
$$

If we define $|\{n\}_q^p\rangle$ to be the ONV that results from $|\{n\}\rangle$ by removing a particle from orbital $|p\rangle$ and adding one to orbital $|q\rangle$, i.e., assuming $q < p$, it is

$$
|\{n\}_q^p\rangle = |\ldots, n_q - 1, \ldots, n_p + 1, \ldots\rangle ,
\tag{2.35}
$$

then we can finally combine (2.32) and (2.34) to obtain a very compact form of the matrix elements:

$$
\langle\{n\}|\hat{B}|\{\bar{n}\}\rangle = \begin{cases} \sum_{k=0}^{\infty} b_{kk} n_k, & \{n\} = \{\bar{n}\} \\ b_{pq}(-1)^{\sum_{l=\min(p,q)+1}^{\max(p,q)-1} n_l}, & \{n\} = \{\bar{n}\}_q^p \\ 0, & \text{else} \end{cases} .
\tag{2.36}
$$

Summarizing the above, we get a contribution of b_{kk} to the diagonal matrix elements for all occupied orbitals in the ONV. Only in case the two ONVs differ in exactly two orbitals $|p\rangle$ and $|q\rangle$, the off-diagonal elements do not vanish and its phase factor is determined by the number of occupied orbitals between $|q\rangle$ and $|p\rangle$ (or $|p\rangle$ and $|q\rangle$). It should be mentioned that the one-particle integrals b_{pq} can be negative, i.e., in addition to the phase factor, giving rise to another sign change of the matrix element.

2.2.5. Two-particle operators in second quantization

The interaction operator of an N-particle system is typically of the form

$$
\hat{W} = \frac{1}{2} \sum_{\alpha \neq \beta = 1}^{N} \hat{w}_{\alpha,\beta} ,
\tag{2.37}
$$

where $\hat{w}_{\alpha,\beta}$ is the two-particle interaction operator acting on the particles α and β, e.g., for Coulomb interaction it is

$$\hat{w}_{\alpha,\beta} = \frac{e^2}{|\hat{\underline{r}}_\alpha - \hat{\underline{r}}_\beta|} \; . \tag{2.38}$$

In second quantization, this operator can also be written in terms of creation and annihilation operators[10]:

$$\hat{W} = \frac{1}{2} \sum_{i,j,k,l=0}^{\infty} w_{ijkl} \hat{a}_i^\dagger \hat{a}_j^\dagger \hat{a}_l \hat{a}_k \; ,$$

with the two-particle integrals[11]

$$w_{ijkl} = \langle ij|\hat{w}|kl\rangle = \int \mathrm{d}x \int \mathrm{d}y \, \phi_i^*(x)\phi_j^*(y)w(x,y)\phi_k(x)\phi_l(y) \; . \tag{2.39}$$

Note the interchange of k and l in the ordering of the indices in the two-particle integral and the product of annihilators. For fermions, this order directly follows from the anti-commutation relations (2.23) and is essential. The invariance of the interaction operator with respect to particle interchange, i.e., $w(x,y) = w(y,x)$, and the fact that the interaction $w(x,y)$ is real, i.e., $w^*(x,y) = w(x,y)$, result in the following two symmetry properties of the two-particle integrals (2.39)

$$\begin{aligned} w_{ijkl} &= w_{jilk} \; , \\ w_{ijkl}^* &= w_{klij} \; . \end{aligned} \tag{2.40}$$

For the description of interacting fermions in second quantization, we have to compute the matrix elements $\langle \{n\}|\hat{W}|\{\bar{n}\}\rangle$. For that purpose, we can use the above symmetries of the two-particle integrals to recast the interaction operator into a more advantageous form

$$\hat{W} = \sum_{i=0}^{\infty} \sum_{j=i+1}^{\infty} \sum_{k=0}^{\infty} \sum_{l=k+1}^{\infty} w_{ijkl}^- \; \hat{a}_i^\dagger \hat{a}_j^\dagger \hat{a}_l \hat{a}_k \; ,$$

with the anti-symmetrized two-particle integrals $w_{ijkl}^- = w_{ijkl} - w_{ijlk}$. Since $i < j$ and $k < l$, there are six possibilities for different products of creation and

---

[10] The second quantized form of $\hat{W}$ is also derived from the action of (2.37) on an anti-symmetric product-state (2.16).

[11] Assuming that the two-particle operator $\hat{w}$, like (2.38), is diagonal in spin-coordinate representation.

annihilation operators in which we can split $\hat{W}$:

$$
\begin{aligned}
\hat{W} = \ & \sum_{i=0}^{\infty}\sum_{j=i+1}^{\infty} w_{ijij}^{-}\,\hat{a}_j^\dagger\hat{a}_i^\dagger\hat{a}_i\hat{a}_j + \sum_{i=0}^{\infty}\sum_{j=i+1}^{\infty}\sum_{\substack{l=i+1\\l\neq j}}^{\infty} w_{ijil}^{-}\,\hat{a}_j^\dagger\hat{a}_i^\dagger\hat{a}_i\hat{a}_l \\
& + \sum_{i=0}^{\infty}\sum_{j=i+1}^{\infty}\sum_{\substack{k=0\\k\neq i}}^{j-1} w_{ijkj}^{-}\,\hat{a}_j^\dagger\hat{a}_i^\dagger\hat{a}_k\hat{a}_j + \sum_{i=0}^{\infty}\sum_{j=i+1}^{\infty}\sum_{k=0}^{i-1} w_{ijki}^{-}\,\hat{a}_j^\dagger\hat{a}_i^\dagger\hat{a}_k\hat{a}_i \\
& + \sum_{i=0}^{\infty}\sum_{j=i+1}^{\infty}\sum_{l=j+1}^{\infty} w_{ijjl}^{-}\,\hat{a}_j^\dagger\hat{a}_i^\dagger\hat{a}_j\hat{a}_l + \sum_{i=0}^{\infty}\sum_{j=i+1}^{\infty}\sum_{\substack{k=0\\k\neq i,j}}^{\infty}\sum_{\substack{l=k+1\\l\neq i,j}}^{\infty} w_{ijkl}^{-}\,\hat{a}_j^\dagger\hat{a}_i^\dagger\hat{a}_k\hat{a}_l \ .
\end{aligned}
$$

It takes some time, but it is straightforward to compute the matrix elements $\langle\{n\}|\hat{a}_j^\dagger\hat{a}_i^\dagger\hat{a}_k\hat{a}_l|\{\bar{n}\}\rangle$ for these six cases. After rearranging the terms, we eventually end up with

$$
\begin{aligned}
\langle\{n\}|\hat{W}|\{\bar{n}\}\rangle = \ & \delta_{\{n\},\{\bar{n}\}}\sum_{i=0}^{\infty}\sum_{j=i+1}^{\infty} w_{ijij}^{-}n_i n_j \\
& + \sum_{p=0}^{\infty}\sum_{q=0}^{\infty}\delta_{\{n\},\{\bar{n}\}}^{pq}\delta_{n_p,1}\delta_{\bar{n}_p,0}\delta_{n_q,0}\delta_{\bar{n}_q,1} \\
& \qquad\quad \cdot\sum_{i=0}^{\infty} w_{ipiq}^{-}(-1)^{\alpha_{\{n\},i}+\alpha_{\{\bar{n}\},i}+\alpha_{\{n\},p}+\alpha_{\{\bar{n}\},q}}\Theta(i,p,q)n_i \\
& + \sum_{p=0}^{\infty}\sum_{q=p+1}^{\infty}\sum_{r=0}^{\infty}\sum_{s=r+1}^{\infty}\delta_{\{n\},\{\bar{n}\}}^{pqrs}\delta_{n_p,1}\delta_{\bar{n}_p,0}\delta_{n_q,1}\delta_{\bar{n}_q,0}\delta_{n_r,0}\delta_{\bar{n}_r,1}\delta_{n_s,0}\delta_{\bar{n}_s,1} \\
& \qquad\quad \cdot\, w_{pqrs}^{-}(-1)^{\alpha_{\{n\},p}+\alpha_{\{n\},q}+\alpha_{\{\bar{n}\},r}+\alpha_{\{\bar{n}\},s}} \ ,
\end{aligned}
$$

where we have defined the function

$$
\Theta(i,p,q) := \begin{cases} -1 & \text{if} \quad p < i < q, \ \text{ or } \ q < i < p \\ \ \ 0 & \text{if} \quad i = p \ \text{ or } \ i = q \\ \ \ 1 & \text{else} \end{cases} \ ,
$$

that ensures the correct phase factor. Similar to (2.33), we can further simplify the phase factors yielding

$$
\hat{W}_{\{n\},\{\bar{n}\}} := \langle\{n\}|\hat{W}|\{\bar{n}\}\rangle = \hat{W}^{\mathrm{I}}_{\{n\},\{\bar{n}\}} + \hat{W}^{\mathrm{II}}_{\{n\},\{\bar{n}\}} + \hat{W}^{\mathrm{III}}_{\{n\},\{\bar{n}\}}\ ,
$$

$$
\hat{W}^{\mathrm{I}}_{\{n\},\{\bar{n}\}} = \delta_{\{n\},\{\bar{n}\}} \sum_{i=0}^{\infty} \sum_{j=i+1}^{\infty} w^{-}_{ijij} n_i n_j\ ,
$$

$$
\hat{W}^{\mathrm{II}}_{\{n\},\{\bar{n}\}} = \sum_{p,q=1}^{\infty} \delta^{pq}_{\{n\},\{\bar{n}\}} \delta_{n_p,1}\delta_{\bar{n}_p,0}\delta_{n_q,0}\delta_{\bar{n}_q,1} \sum_{\substack{i=0 \\ i\neq p,q}}^{\infty} w^{-}_{ipiq}(-1)^{\sum_{l=\min(p,q)+1}^{\max(p,q)-1} n_l} n_i\ ,
$$

$$
\hat{W}^{\mathrm{III}}_{\{n\},\{\bar{n}\}} = \sum_{p=1}^{\infty} \sum_{q=p+1}^{\infty} \sum_{r=1}^{\infty} \sum_{s=r+1}^{\infty} \delta^{pqrs}_{\{n\},\{\bar{n}\}} \delta_{n_p,1}\delta_{\bar{n}_p,0}\delta_{n_q,1}\delta_{\bar{n}_q,0}\delta_{n_r,0}\delta_{\bar{n}_r,1}\delta_{n_s,0}\delta_{\bar{n}_s,1}
$$
$$
\cdot\, w^{-}_{pqrs}(-1)^{\sum_{l=p}^{q-1} n_l + \sum_{l=r}^{s-1} \bar{n}_l}\ .
$$

The Kronecker deltas in the three summands define the three cases for the left and right ONV that result in a non-vanishing matrix element $\langle\{n\}|\hat{W}|\{\bar{n}\}\rangle$: First, both ONVs are equal, i.e., $|\{n\}\rangle = |\{\bar{n}\}\rangle$. Second, the ONVs differ in exactly two orbitals $|p\rangle$ and $|q\rangle$ with $|\{n\}\rangle = |\{\bar{n}\}^p_q\rangle$ (cf. Def. (2.35)). The third summand does not vanish if the two ONVs differ in exactly four orbitals $|p\rangle, |q\rangle, |r\rangle$ and $|s\rangle$ with $p < q$ and $r < s$. Defining $|\{n\}^{p<q}_{r<s}\rangle$ as the ONV that is obtained from $|\{n\}\rangle$ by adding a particle to the orbitals $|p\rangle$ and $|q\rangle$ and removing one from $|r\rangle$ and $|s\rangle$ allows for the compact writing of the matrix elements of the interaction operator [9]:

$$
\langle\{n\}|\hat{W}|\{\bar{n}\}\rangle = \begin{cases} \displaystyle\sum_{i=0}^{\infty}\sum_{j=i+1}^{\infty} w^{-}_{ijij} n_i n_j, & \{n\} = \{\bar{n}\} \\[2em] \displaystyle\sum_{\substack{i=0 \\ i\neq p,q}}^{\infty} w^{-}_{ipiq}(-1)^{\sum\limits_{l=\min(p,q)+1}^{\max(p,q)-1} n_l} n_i, & \{n\} = \{\bar{n}\}^p_q \\[2em] w^{-}_{pqrs}(-1)^{\sum\limits_{l=p}^{q-1} n_l + \sum\limits_{l=r}^{s-1}\bar{n}_l}, & \{n\} = \{\bar{n}\}^{p<q}_{r<s} \\[1.5em] 0, & \text{else} \end{cases}
\qquad. \quad (2.41)
$$

These are the well-known *Slater-Condon-rules* [27], which are of prime importance for the CPIMC method.

3. Configuration path integral Monte Carlo

In this chapter, first, the expansion of the partition function (see Sec. 2.1) that is used for the standard CPIMC approach is derived following [10]. Afterwards, the expansion is modified such that it is suitable for a Worm algorithm (WA). Then, a similar expansion for the Matsubara Green function (MGF) is found, which, together with the partition function, defines the total configuration space of the developed WA. Finally, the developed Monte Carlo steps of the WA are presented and discussed in detail.

3.1. Paths in the ONV picture

We consider a general system described by the Hamiltonian $\hat{H}$ in the canonical ensemble, i.e., with fixed particle number N in a volume V at temperature T. The partition function is given by the trace over the (not normalized) density operator $\hat{\rho} = e^{-\beta\hat{H}}$, where $\beta = \frac{1}{T}$ is the inverse temperature

$$Z(N, \beta, V) = \operatorname{Tr} e^{-\beta\hat{H}} . \tag{3.1}$$

The trace can be performed in an arbitrary N-particle basis $\{|\Psi_i\rangle\}$. In such an arbitrary basis, we can formally split the Hamiltonian into a diagonal part $\hat{D}$ and a off-diagonal part $\hat{Y}$, i.e., it is $\hat{H} = \hat{D} + \hat{Y}$ with[1]

$$\langle\Psi_i|\hat{H}|\Psi_j\rangle = \begin{cases} \langle\Psi_i|\hat{D}|\Psi_i\rangle = D_i & \text{if} \quad i = j \\ \langle\Psi_i|\hat{Y}|\Psi_j\rangle = Y_{i,j} & \text{if} \quad i \neq j \end{cases} . \tag{3.2}$$

Now we can switch to the interaction picture[2] in imaginary time with respect to the diagonal operator $\hat{D}$

$$\hat{Y}(\tau) = e^{\tau\hat{D}}\hat{Y}e^{-\tau\hat{D}} \quad \text{with} \quad \tau \in [0, \beta] . \tag{3.3}$$

---

[1]Here, i and j are multi-variables of all quantum numbers defining the N-particle states.

[2]In this work, the notation of the operators in the interaction picture does only differ to that of Schrödinger operators by the presence of a time argument.

3. Configuration path integral Monte Carlo

In this picture, we define the time ordering operator $\hat{T}_\tau$ by

$$\hat{T}_\tau[\hat{A}(\tau_1)\hat{B}(\tau_2)] := \begin{cases} \hat{A}(\tau_1)\hat{B}(\tau_2) \,, & \text{if} \quad \tau_1 > \tau_2 \\ \hat{A}(\tau_2)\hat{B}(\tau_1) \,, & \text{if} \quad \tau_2 > \tau_1 \end{cases}$$

and expand the density operator as follows

$$e^{-\beta\hat{H}} = e^{-\beta\hat{D}}\, e^{-\int_0^\beta \hat{Y}(\tau)\mathrm{d}\tau}$$

$$= e^{-\beta\hat{D}} \sum_{K=0}^\infty \int_0^\beta \mathrm{d}\tau_1 \dots \int_0^\beta \mathrm{d}\tau_K \frac{(-1)^K}{K!} \hat{T}_\tau[\hat{Y}(\tau_1)\hat{Y}(\tau_2)\cdot\dots\cdot\hat{Y}(\tau_K)] \,.$$

Due to the time-ordering operator, for each K, there are $K!$ equal terms of time ordered off-diagonal products. Therefore, we can modify the integral boundaries such that the operators are already time ordered, thereby obtaining

$$e^{-\beta\hat{H}} = e^{-\beta\hat{D}} \sum_{K=0}^\infty \int_0^\beta \mathrm{d}\tau_1 \int_{\tau_1}^\beta \mathrm{d}\tau_2 \dots \int_{\tau_{K-1}}^\beta \mathrm{d}\tau_K (-1)^K \hat{Y}(\tau_K)\hat{Y}(\tau_{K-1})\cdot\dots\cdot\hat{Y}(\tau_1) \,.$$

(3.4)

This expansion is inserted into Eq. (3.1). Performing the trace in the N-particle basis of ONVs[3] $\{|\{n\}\rangle\}$ with fixed particle number[4] $N = \sum_{i=0}^\infty n_i$, yields[5]

$$Z = \sum_{K=0}^\infty \sum_{\{n\}} \int_0^\beta \mathrm{d}\tau_1 \int_{\tau_1}^\beta \mathrm{d}\tau_2 \dots \int_{\tau_{K-1}}^\beta \mathrm{d}\tau_K$$

$$(-1)^K e^{-\beta D_{\{n\}}} \langle\{n\}|\hat{Y}(\tau_K)\hat{Y}(\tau_{K-1})\cdot\dots\cdot\hat{Y}(\tau_1)|\{n\}\rangle \,.$$

Next, we insert $K-1$ unity operators $\hat{1} = \sum_{\{n^{(i)}\}} |\{n^{(i)}\}\rangle \langle\{n^{(i)}\}|$ of the anti-symmetrized N-particle Hilbert space $\mathcal{H}_-^N$

$$Z = \sum_{K=0}^\infty \sum_{\{n\}} \sum_{\{n^{(1)}\}} \cdots \sum_{\{n^{(K-1)}\}} \int_0^\beta \mathrm{d}\tau_1 \int_{\tau_1}^\beta \mathrm{d}\tau_2 \dots \int_{\tau_{K-1}}^\beta \mathrm{d}\tau_K (-1)^K e^{-\beta D_{\{n\}}}$$

$$\langle\{n\}|\,|\hat{Y}(\tau_K)\,|\{n^{(K-1)}\}\rangle \langle\{n^{(K-1)}\}|\,\hat{Y}(\tau_{K-1})\,|\{n^{(K-2)}\}\rangle \cdot\dots$$

$$\dots\cdot \langle\{n^{(1)}\}|\,\hat{Y}(\tau_1)\,|\{n\}\rangle \,.$$

The matrix elements of the off-diagonal operators in the interaction picture are readily computed:

$$\langle\{n^{(i)}\}|\hat{Y}(\tau_K)|\{n^{(j)}\}\rangle = \langle\{n^{(i)}\}|e^{\tau_K\hat{D}}\hat{Y}e^{-\tau_K\hat{D}}|\{n^{(j)}\}\rangle$$

$$= e^{\tau_K D_{\{n^{(i)}\}}} Y_{\{n^{(i)}\},\{n^{(j)}\}} e^{-\tau_K D_{\{n^{(j)}\}}} \,.$$

---

[3]Since we consider fermions, it is $n_i \in \{0,1\}$.

[4]Here, summation over all occupation numbers implies conservation of the total particle number N.

[5]Note that by definition it is $\hat{D}\,|\{n\}\rangle = D_{\{n\}}\,|\{n\}\rangle$ (cf. Eq. (3.2) with $|\Psi_i\rangle = |\{n\}\rangle$).

Thus, it follows

$$Z = \sum_{K=0}^{\infty} \sum_{\{n\}} \sum_{\{n^{(1)}\}} \cdots \sum_{\{n^{(K-1)}\}} \int_0^{\beta} d\tau_1 \int_{\tau_1}^{\beta} d\tau_2 \cdots \int_{\tau_{K-1}}^{\beta} d\tau_K$$

$$(-1)^K \exp\left\{-\sum_{i=0}^{K} D_{\{n^{(i)}\}}(\tau_{i+1} - \tau_i)\right\} \prod_{i=1}^{K} Y_{\{n^{(i)}\},\{n^{(i-1)}\}} \, .$$

Further, we take into account that, by definition, the diagonal elements of the off-diagonal operators are zero, i.e., $Y_{\{n^{(i)}\},\{n^{(i)}\}} = 0$. After excluding these terms in the summation over the ONVs and rearranging the factors, we finally end up with

$$Z(N,V,\beta) = \sum_{\substack{K=0, \\ K\neq 1}}^{\infty} \sum_{\substack{\{n\}, \\ =\{n^{(0)}\}=\{n^{(K)}\}}} \sum_{\substack{\{n^{(1)}\}, \\ \neq\{n^{(0)}\}}} \cdots \sum_{\substack{\{n^{(K-1)}\}, \\ \neq\{n^{(K-2)}\}\neq\{n^{(K)}\}}} \int_0^{\beta} d\tau_1 \int_{\tau_1}^{\beta} d\tau_2 \cdots \int_{\tau_{K-1}}^{\beta} d\tau_K$$

$$(-1)^K \exp\left\{-\sum_{i=0}^{K} D_{\{n^{(i)}\}}(\tau_{i+1} - \tau_i)\right\} \prod_{i=0}^{K-1} Y_{\{n^{(i+1)}\},\{n^{(i)}\}} =: \sum_{C} W(C) \, ,$$

$$(3.5)$$

where we have $\{n\} = \{n^{(0)}\} = \{n^{(K)}\}$, $\tau_0 = 0$ and $\tau_{k+1} = \beta$. Each contribution W to the partition function is uniquely defined by the K ONVs $|\{n^{(i)}\}\rangle$, $i = 0, \ldots, K-1$ and times τ_i, $i = 1, \ldots, K$. Therefore, in this expansion of the partition function, the multi-variable C, defining a system configuration (cf. Eq. (2.1)), is given by[6]

$$C = \Big((K), \{n^{(0)}\}, \{n^{(1)}\}, \ldots, \{n^{(K-1)}\}, \tau_1, \tau_2, \ldots, \tau_K\Big)$$

with the weight function

$$W\Big(C = \Big(K, \tau_1, \tau_2, \ldots, \tau_K, \{n^{(0)}\}, \{n^{(1)}\}, \ldots, \{n^{(K-1)}\}\Big)\Big) = \qquad (3.6)$$

$$(-1)^K \exp\left\{-\sum_{i=0}^{K} D_{\{n^{(i)}\}}(\tau_{i+1} - \tau_i)\right\} \prod_{i=0}^{K-1} Y_{\{n^{(i+1)}\},\{n^{(i)}\}}.$$

In analogy to the path integral picture in coordinate space, these system configurations can be visualized as $\beta-$periodic paths in Fock space, i.e., in the space of ONVs, where the ONV $|\{n^i\}\rangle$ is realized on the interval (τ_i, τ_{i+1}) giving a contribution of $D_{\{n^i\}}(\tau_{i+1} - \tau_i)$ to the exponential term of the weight function $W(C)$. Further, at each time point τ_i, there is a change of the ONV

---

[6]Of course, K is already defined by the number of ONVs. Therefore, it is written in brackets.

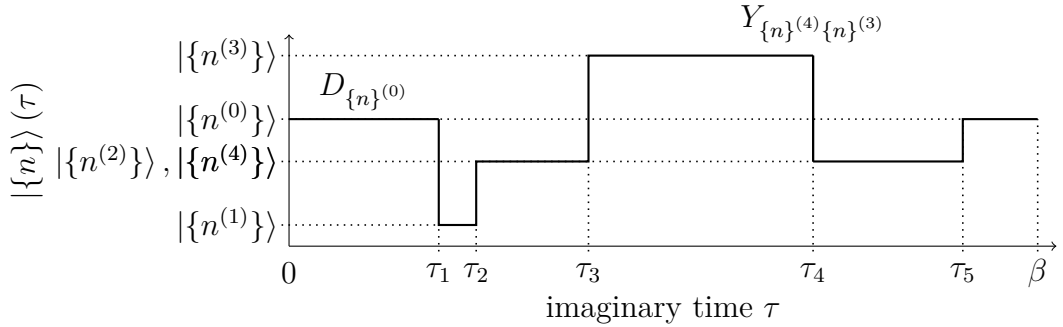*3. Configuration path integral Monte Carlo*

Figure 3.1.: Possible path in imaginary time. Horizontal lines correspond to diagonal matrix elements $D_{\{n^{(i)}\}}$, whereas vertical lines correspond to off-diagonal elements $Y_{\{n^{(i+1)}\},\{n^{(i)}\}}$. The ordering of the ONVs is arbitrary.

$|\{n\}\rangle\,(\tau)$ corresponding to an off-diagonal factor $Y_{\{n^{(i+1)}\},\{n^{(i)}\}}$ in $W(C)$. Fig. 3.1 shows a possible path for $K = 5$. In this picture, times at which the ONV $|\{n\}\rangle\,(\tau)$ changes appear as kinks in the paths. Therefore, we refer to K as the number of *kinks*.

It shall be mentioned that the derivation of Eq. (3.5) can be done without switching to the interaction picture. Instead the *Trotter Formula* [29] can be used, which leads to discrete paths. Unlike to the DPIMC method, where paths are discrete with respect to the imaginary time, the limit of continuous paths can eventually be carried out analytically yielding Eq. (3.5). (For details, see [9], where the notation "configuration path integral Monte Carlo" has been introduced.)

So far, the expansion of the partition function (3.5) is in principle valid for any fermionic systems[7] in the canonical or grand canonical[8] ensemble since we can split any Hamiltonian $\hat{H}$ into a diagonal and off-diagonal part. In this thesis, we are interested in the general case of interacting fermions in some external potential, i.e., the N-particle Hamiltonian is of the form

$$\hat{H} = \hat{H}_0 + \hat{W}$$

with $\hat{H}_0$ the Hamiltonian of the ideal system (as defined in Eq. (2.14)) and $\hat{W}$ the interaction operator (cf. Eq. (2.37)). In second quantization, $\hat{H}$ is represented by (cf. Sec. 2.2.4 and 2.2.5)

$$\hat{H} = \sum_{i,j} h_{ij} \hat{a}_i^\dagger \hat{a}_j + \sum_{i<j,k<l} w_{ijkl}^- \hat{a}_i^\dagger \hat{a}_j^\dagger \hat{a}_l \hat{a}_k \ . \tag{3.7}$$

---

[7]For bosons, we only have to change the summation over the occupation numbers from $n_i \in \{0,1\}$ to $n_i \in \mathbb{N}$.

[8]For the grand canonical ensemble, we only have to modify the interaction picture in Eq. (3.3) by replacing $\hat{D}$ with $\hat{D} - \mu\hat{N}$, where μ is the chemical potential.

With the matrix elements of general one-particle operators (Eq. (2.36)) and the Slater-Condon rules for the interaction operator (Eq. (2.41)), we can compute the matrix elements of the diagonal and off-diagonal operator in the partition function (3.5) according to

$$D_{\{n^{(k)}\}} = \sum_{i=1}^{\infty} h_{ii} n_i^{(k)} + \sum_{i=0}^{\infty} \sum_{j=i+1}^{\infty} w_{ijij}^- n_i^{(k)} n_j^{(k)} , \qquad (3.8)$$

and

$$Y_{\{n^{(k)}\}\{n^{(l)}\}} = \begin{cases} \left(h_{pq} + \sum_{\substack{i=0 \\ i \neq p,q}}^{\infty} w_{ipiq}^- n_i^{(k)} \right) (-1)^{\sum\limits_{m=\min(p,q)+1}^{\max(p,q)-1} n_m^{(k)}}, & \{n^{(k)}\} = \{n^{(l)}\}_q^p \\[2em] w_{pqrs}^- (-1)^{\sum\limits_{m=p}^{q-1} n_m^{(k)} + \sum\limits_{m=r}^{s-1} n_m^{(l)}}, & \{n^{(k)}\} = \{n^{(l)}\}_{r<s}^{p<q} \\[1em] 0, & \text{else.} \end{cases}$$

$$(3.9)$$

Consequently, paths can only have kinks $Y_{\{n^{(i+1)}\},\{n^{(i)}\}}$ where the consecutive ONVs $|\{n^{(i)}\}\rangle$ and $|\{n^{(i+1)}\}\rangle$ differ in exactly two or four orbitals, i.e., they are equal except for either a one- or two-particle excitation. In all other cases, the weight function is zero due to a vanishing off-diagonal element, and hence, such paths do not exist. Note that by performing the trace in occupation number representation and evaluating the matrix elements of the field operators in the Hamiltonian (3.7) according to the fermionic anti-commutation relations (2.23), we automatically included the correct spin statistics.

Furthermore, there are three sources of sign changes in the weight function (3.6): First, we have the number of kinks $(-1)^K$. Second, the one-particle integrals h_{pq} (cf. Eq. (2.28)) and the anti-symmetrized two-particle integrals w_{pqrs}^- (cf. Eq. (2.39)), which are calculated in an arbitrary one-particle basis $\{|i\rangle\}$, in general have both positive and negative values. Third, each kink includes a fermionic phase factor $(-1)^\alpha$ determined by the occupied orbitals in between the differing orbitals. Depending on the simulated system, these are the potential sources for a serious sign problem.

Finally, we note that Eq. (3.5) represents a perturbation expansion concerning the off-diagonal matrix elements. Therefore, if we use the ideal basis, which diagonalizes the ideal Hamiltonian $\hat{H}_0$, we have a perturbation expansion of the partition function in terms of the interaction.

3.2. Paths in the kink picture

The partition function (3.5) is well-suited for Monte Carlo simulations via the Metropolis algorithm (standard CPIMC). Some important estimators and

an ergodic set of Monte Carlo steps are described in detail in [10]. Apart from the sign problem, the presented standard CPIMC algorithm has three major drawbacks. First, depending on the system size, the average acceptance probabilities of the steps are of the order $\mathcal{O}(10^{-4})$. Even though small acceptance probabilities of Monte Carlo steps do not necessarily imply an inefficient algorithm, e.g., if the steps result in large changes of the system configurations, average acceptance probabilities smaller than 10^{-3} are unlikely to be efficient. Second, while the expectation values of standard thermodynamic observables like the total energy or heat capacity can be calculated up to a relative statistical error of about 10^{-4}, it turned out that the statistical error of the one- and two-particle density matrix is very large. Third, and most importantly, the standard CPIMC method does not allow for the sampling of the one- and two-particle MGF, which give access to the single-particle spectral function and the dynamical structure factor, respectively (see [15, 16, 14] and references therein).

The Worm algorithm (WA) of the DPMC method [17, 30] has been shown to be much more efficient in sampling the exchange of particles than the standard DPIMC methods[1], and at the same time, the WA gives direct access to the MGF. However, due to the fermion sign problem within the DPIMC approach, strongly degenerate fermionic systems cannot be simulated, whereas this is possible with the CIPIMC method. Therefore, a WA for CPIMC had to be developed to provide exact data for the MGF of strongly degenerate systems. In addition, we hoped that the mentioned problems of small acceptance probabilities and poor results for the one-particle density matrix could be solved or improved due to a reformulation of the standard CPIMC approach in terms of a WA. The basic idea of the WA for Metropolis Monte Carlo in determinant space has been developed by Prokof'ev *et al.*[18], where only bosonic lattice models are considered. In fact, for lattice models, things are much simpler since the corresponding Hamiltonians in second quantization do not contain a true two-particle interaction operator consisting of two creation and annihilation operators with different indices.

For the WA, we rewrite the partition function (3.5) by taking into account that consecutive ONVs in the path can only differ by two or four orbitals, i.e., many summands in (3.5) are redundant[9]. Actually, a path, as shown in Fig. 3.1, is specified by the first ONV $|n^{(0)}\rangle$ and the consecutive one- and two-particle excitations with corresponding times. Hence, instead of summing over K different ONVs, we only have to sum over a single ONV and all consecutive one- and two-particle excitations. The formal derivation of this apparently simple conclusion is fairly elaborate for continuous models and, as far as I know, has

---

[9]For the standard CPIMC method described in [10], summing over configurations with vanishing weights is not relevant since in the Monte Carlo algorithm proposing not allowed excitations is simply rejected.

not been performed or published anywhere else. We start from the actual form of the off-diagonal operator. According to the second quantized form of the Hamiltonian (3.7) and the definition of the off-diagonal operator (3.2), it is

$$
\hat{Y} = \sum_{\substack{i,k=0 \\ i\neq k}}^{\infty} h_{ik}\hat{a}_i^\dagger \hat{a}_k + \sum_{\substack{i,j,k,l=0 \\ i<j,k<l, \\ i\neq k \text{ if } j=l,\ j\neq l \text{ if } i=k}}^{\infty} w_{ijkl}^{-}\hat{a}_i^\dagger \hat{a}_j^\dagger \hat{a}_l \hat{a}_k
$$

$$
= \sum_{\substack{i,k=0 \\ i\neq k}}^{\infty} h_{ik}\hat{a}_i^\dagger \hat{a}_k + \sum_{\substack{i,k=0 \\ i\neq k}}^{\infty}\sum_{\substack{j=0 \\ j>i \\ j>k}}^{\infty} w_{ijkj}^{-}\hat{a}_i^\dagger \hat{a}_j^\dagger \hat{a}_j \hat{a}_k \qquad (3.10)
$$

$$
+ \sum_{\substack{j,l=0 \\ j\neq l}}^{\infty}\sum_{\substack{i=0 \\ i<j \\ i<l}}^{\infty} w_{ijil}^{-}\hat{a}_i^\dagger \hat{a}_j^\dagger \hat{a}_l \hat{a}_i + \sum_{\substack{i,j,k,l=0 \\ i<j,k<l, \\ i\neq k,i\neq l,j\neq k,j\neq l}}^{\infty} w_{ijkl}^{-}\hat{a}_i^\dagger \hat{a}_j^\dagger \hat{a}_l \hat{a}_k \ .
$$

Using the anti-commutator relations (2.23) and the symmetries of the anti-symmetric two-electron integrals (2.40), we can further rewrite the third term

$$
\sum_{\substack{j,l=0 \\ j\neq l}}^{\infty}\sum_{\substack{i=0 \\ i<j \\ i<l}}^{\infty} w_{ijil}^{-}\hat{a}_i^\dagger \hat{a}_j^\dagger \hat{a}_l \hat{a}_i = \sum_{\substack{j,l=0 \\ j\neq l}}^{\infty}\sum_{\substack{i=0 \\ i<j \\ i<l}}^{\infty} w_{jili}^{-}\hat{a}_j^\dagger \hat{a}_i^\dagger \hat{a}_i \hat{a}_l \underset{\substack{j\leftrightarrow i \\ l\to k}}{=} \sum_{\substack{i,k=0 \\ i\neq k}}^{\infty}\sum_{\substack{j=0 \\ j<i \\ j<k}}^{\infty} w_{ijkj}^{-}\hat{a}_i^\dagger \hat{a}_j^\dagger \hat{a}_j \hat{a}_k \ .
$$

Thereby, we can combine the second and the third term in Eq. (3.10), which yields

$$
\hat{Y} = \sum_{\substack{i,k=0 \\ i\neq k}}^{\infty}\left(h_{ik}\hat{a}_i^\dagger \hat{a}_k + \sum_{\substack{j=0 \\ j\neq i,k}}^{\infty} w_{ijkj}^{-}\hat{a}_i^\dagger \hat{a}_j^\dagger \hat{a}_j \hat{a}_k \right) + \sum_{\substack{i,j,k,l=0 \\ i<j,k<l, \\ i\neq k,i\neq l,j\neq k,j\neq l}}^{\infty} w_{ijkl}^{-}\hat{a}_i^\dagger \hat{a}_j^\dagger \hat{a}_l \hat{a}_k
$$

$$
= \sum_{\substack{i,k=0 \\ i\neq k}}^{\infty}\left(h_{ik} + \sum_{\substack{j=0 \\ j\neq i,k}}^{\infty} w_{ijkj}^{-}\hat{n}_j \right)\hat{a}_i^\dagger \hat{a}_k + \sum_{\substack{i,j,k,l=0 \\ i<j,k<l, \\ i\neq k,i\neq l,j\neq k,j\neq l}}^{\infty} w_{ijkl}^{-}\hat{a}_i^\dagger \hat{a}_j^\dagger \hat{a}_l \hat{a}_k \ , \qquad (3.11)
$$

where we could interchange the field operators to factor out $\hat{a}_i^\dagger \hat{a}_k$ since all indices in the summation are pairwise distinct, i.e., for each interchange of two field operators, we only have a sign change. In this form, the matrix elements of the off-diagonal operator (3.9) are obvious. Next, we define the so called *kink operator* $\hat{q}(s)$ by

$$
\hat{q}(s) := \begin{cases} \left(h_{ik} + \displaystyle\sum_{\substack{j=0 \\ j\neq i,k}}^{\infty} w_{ijkj}^{-}\hat{n}_j \right)\hat{a}_i^\dagger \hat{a}_k & \text{if} \quad s = (i,k) \in A \\[2em] w_{ijkl}^{-}\hat{a}_i^\dagger \hat{a}_j^\dagger \hat{a}_l \hat{a}_k & \text{if} \quad s = (i,j,k,l) \in B \end{cases} , \quad (3.12)
$$

where A and B are the sets of all possible one- and two-particle excitations, respectively

$$A := \{(i,k) \in \mathbb{N}^2 \mid i \neq j\} ,$$

$$B := \{(i,j,k,l) \in \mathbb{N}^4 \mid i < j,\ k < l,\ i \neq k,\ i \neq l,\ j \neq k,\ j \neq l\} . \quad (3.13)$$

The action of the generalized kink operator on an arbitrary ONV is given by

$$\hat{q}(s) \,|\{n\}\rangle = q_{\{\bar{n}\},\{n\}}(s) \,|\{\bar{n}\}(\{n\},s)\rangle . \quad (3.14)$$

The the resulting ONV $|\{\bar{n}\}\rangle$ is defined by the occupation numbers $\{n\}$ and the one- or two-particle excitation s. Hence, the matrix elements $q_{\{\bar{n}\},\{n\}}(s)$ are completely determined by s and $\{n\}$. The off-diagonal operator (3.11) and its matrix elements can now be expressed in terms of these kink operators

$$\hat{Y} = \sum_{s \in A \cup B} \hat{q}(s) , \qquad Y_{\{\bar{n}\},\{n\}} = \sum_{s \in A \cup B} q_{\{\bar{n}\},\{n\}}(s) . \quad (3.15)$$

Of course, except for that s' which is determined by $\{n\}$ an $\{\bar{n}\}$, all $q_{\{\bar{n}\},\{n\}}(s)$ vanish, and for s' it is $q_{\{\bar{n}\},\{n\}}(s') = Y_{\{\bar{n}\},\{n\}}$, which is calculated according to Eq. (3.9). Using this expansion of the off-diagonal operator into kink operators, we can rewrite the product of the off-diagonal elements in the partition function (3.5) as follows[10]

$$\prod_{i=0}^{K-1} Y_{\{n^{(i+1)}\},\{n^{(i)}\}} = \prod_{i=1}^{K} Y_{\{n^{(i)}\}\{n^{(i-1)}\}} = \sum_{s_1}\sum_{s_2}\cdots\sum_{s_K}\prod_{i=1}^{K} q_{\{n^{(i)}\}\{n^{(i-1)}\}}(s_i) ,$$

whereby we obtain

$$Z(N,V,\beta) = \sum_{\substack{K=0,\\ K\neq 1}}^{\infty} \sum_{\substack{\{n\},\\ =\{n^{(0)}\}=\{n^{(K)}\}}} \sum_{\substack{\{n^{(1)}\},\\ \neq\{n^{(0)}\}}} \cdots \sum_{\substack{\{n^{(K-1)}\},\\ \neq\{n^{(K-2)}\}\neq\{n^{(K)}\}}} \sum_{s_1}\sum_{s_2}\cdots\sum_{s_K}$$

$$\int' \mathrm{d}^K\tau (-1)^K \exp\left\{-\sum_{i=0}^{K} D_{\{n^{(i)}\}}(\tau_{i+1}-\tau_i)\right\} \prod_{i=1}^{K} q_{\{n^{(i)}\}\{n^{(i-1)}\}}(s_i) .$$

$$(3.16)$$

Additionally, we have used a compact notation for the integrals over the kink positions in imaginary time

$$\int' \mathrm{d}^K\tau := \int_0^{\beta} d\tau_1 \int_{\tau_1}^{\beta} d\tau_2 \ldots \int_{\tau_{K-1}}^{\beta} d\tau_K . \quad (3.17)$$

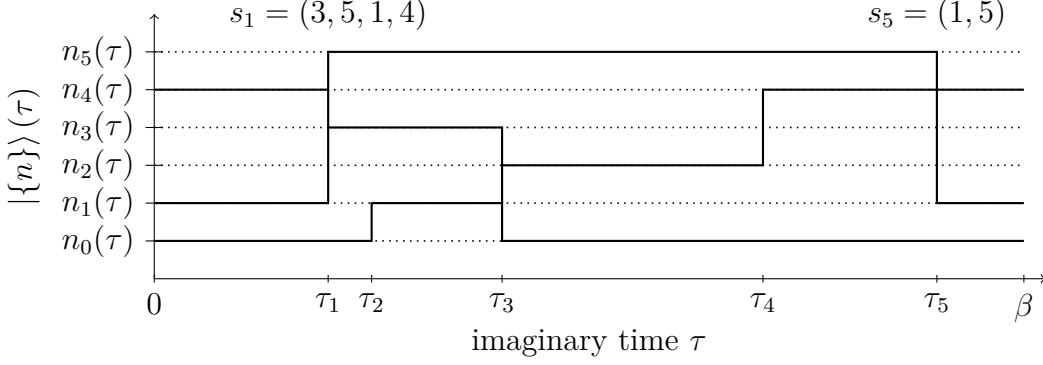[10]Summation over s implies summation over all $s \in A \cup B$ defined in the Eqs. (3.13).

Figure 3.2.: Possible path $\{n_0(\tau), n_1(\tau), \dots, n_5(\tau)\}$ in imaginary time of three particles in six orbitals in the kink picture. Each kink s represents either a one- or a two-particle excitation.

As already mentioned, the matrix elements of the kink operators are completely defined by one of the ONVs $|\{n^{(i-1)}\}\rangle$ or $|\{n^{(i)}\}\rangle$ and the excitation $s \in A \cup B$ (cf. Eq. (3.14)). Hence, in Eq. (3.16), the summations over the occupation numbers are redundant except for one, e.g., the one over $\{n\}$. Further, due to the restriction that the paths must be β-periodic, i.e., $\{n^{(0)}\} = \{n^{(K)}\}$, we can also drop the summation over s_K. It follows the final expansion of the partition function

$$
Z_{\mathrm{CP}} = \sum_{\substack{K=0, \\ K\neq 1}}^{\infty} \sum_{\{n\}} \sum_{s_1} \sum_{s_2} \cdots \sum_{s_{K-1}} \int' \mathrm{d}^K \tau
$$

$$
(-1)^K \exp\left\{-\sum_{i=0}^{K} D_{\{n^{(i)}\}}(\tau_{i+1} - \tau_i)\right\} \prod_{i=1}^{K} q_{\{n^{(i)}\}\{n^{(i-1)}\}}(s_i) =: \sum_{C_{\mathrm{CP}}} W_{\mathrm{CP}}(C_{\mathrm{CP}}) \,.
$$

(3.18)

A contribution to the partition function in this representation is uniquely defined by the first ONV $|\{n\}\rangle$ and the $K-1$ excitations (kinks) of type s_i that are consecutively applied to the ONV at times τ_i, where, due to the restriction of the integrals (cf. Eq. (3.17)), it is $\tau_0 < \tau_1 < \dots < \tau_K$. Thus, a system configuration, in terms of the WA referred to as a *closed path*, is given by

$$
C_{\mathrm{CP}} = ((K), \{n\}, s_1, s_2, \dots, s_{K-1}, \tau_1, \tau_2, \dots, \tau_K)
$$

(3.19)

with its corresponding weight function

$$
W(C_{\mathrm{CP}}) = (-1)^K \exp\left\{-\sum_{i=0}^{K} D_{\{n^{(i)}\}}(\tau_{i+1} - \tau_i)\right\} \prod_{i=1}^{K} q_{\{n^{(i)}\}\{n^{(i-1)}\}}(s_i) \,.
$$

These configurations can be visualized as paths in imaginary time, too. As an example, a possible path for three particles in six orbitals is shown in Fig.

3.2. In contrast to the paths $|\{n\}\rangle(\tau)$ in the ONV picture (cf. Fig. 3.1), where a path is represented by arbitrary ordered ONVs $|\{n^i\}\rangle$, $i = 0 \dots K - 1$, in this representation of the partition function, a path is given by the occupation number of each orbital $n_i(\tau)$ which can change at the kink times τ_i. Each kink s_i either defines a one- or a two-particle excitation (i.e., $s_i \in A$ or $s_i \in B$, see Def. (3.13)). If $s_i \in A$ ($s_i \in B$), then we refer to the kink s_i as being of *type 2 (4)*. In addition, these paths automatically include particle exchange, since in case of a type 4 kink, we cannot tell which particle is excited to which orbital.

We could now perform Metropolis Monte Carlo with this representation of the partition function if we transform the Monte Carlo steps of the ONV picture (standard CPIMC [10]) into this kink picture, but our goal is to develop a suitable WA in this picture.

3.3. Open paths in the kink picture

In this section, it is shown that the summation over all MGFs has a similar expansion to that of the partition function (3.18). The MGF is defined in the grand canonical ensemble, i.e., for a given temperature T, volume V and chemical potential μ of the system

$$\mathcal{G}_{ij}(\tau_{\mathrm{ir}}, \tau_{\mathrm{ma}}) := \langle \hat{T}_\tau \left[\hat{a}_{i,H}(\tau_{\mathrm{ir}}) \hat{a}_{j,H}^\dagger(\tau_{\mathrm{ma}}) \right] \rangle$$

$$= \frac{1}{Z} \mathrm{Tr} \left\{ e^{-\beta(\hat{H} - \mu\hat{N})} \hat{T}_\tau \left[\hat{a}_{i,H}(\tau_{\mathrm{ir}}) \hat{a}_{j,H}^\dagger(\tau_{\mathrm{ma}}) \right] \right\} ,$$

with the time arguments $\tau_{\mathrm{ir}}, \tau_{\mathrm{ma}} \in [0, \beta]$ and $\tau_{\mathrm{ir}} \neq \tau_{\mathrm{ma}}$. Further, Z denotes the grand canonical partition function

$$Z(\mu, V, \beta) = \mathrm{Tr}\, e^{-\beta(\hat{H} - \mu\hat{N})} .$$

The field operators are represented in the modified Heisenberg picture

$$\hat{A}_H(\tau) = e^{\tau(\hat{H} - \mu\hat{N})} \hat{A} e^{-\tau(\hat{H} - \mu\hat{N})} .$$

In the modified interaction picture

$$\hat{A}(\tau) = e^{\tau\hat{\tilde{D}}} \hat{A} e^{-\tau\hat{\tilde{D}}}$$

with respect to the diagonal part $\hat{\tilde{D}} := \hat{D} + \mu\hat{N}$ of the grand canonical Hamiltonian $\hat{H} = \hat{D} + \hat{Y} + \mu\hat{N}$, the MGF takes the form [31]

$$\mathcal{G}_{ij}(\tau_{\mathrm{ir}}, \tau_{\mathrm{ma}}) = \frac{1}{Z} \mathrm{Tr} \left\{ e^{-\beta\hat{\tilde{D}}} \hat{T}_\tau \left[e^{-\int_0^\beta \hat{Y}(\tau)\mathrm{d}\tau} \hat{a}_i(\tau_{\mathrm{ir}}) \hat{a}_j^\dagger(\tau_{\mathrm{ma}}) \right] \right\} .$$

For historical reasons, in terms of the WA, we call the annihilator *Ira* and the creator *Masha* [18]. We recall some important properties of the MGF: First, it is homogeneous in (imaginary) time, i.e,

$$\mathcal{G}_{ij}(\tau_{\text{ir}}, \tau_{\text{ma}}) = \mathcal{G}_{ij}(\tau = \tau_{\text{ir}} - \tau_{\text{ma}}, 0) = \langle \hat{T}_\tau \left[\hat{a}_{i,H}(\tau) \hat{a}^\dagger_{j,H}(0) \right] \rangle , \qquad (3.20)$$

where $\tau \in [-\beta, \beta] \backslash \{0\}$, i.e., the MGF has a discontinuity at $\tau = 0$. Second, for fermions, the MGF is anti-periodic under shifts of β

$$\begin{aligned} \mathcal{G}_{ij}(\tau - \beta) &= -\mathcal{G}_{ij}(\tau) \quad \tau \in (0, \beta] , \\ \mathcal{G}_{ij}(\tau + \beta) &= -\mathcal{G}_{ij}(\tau) \quad \tau \in [-\beta, 0) , \end{aligned} \qquad (3.21)$$

and third, it is related to the one-particle density matrix n_{ij} according to

$$\begin{aligned} \mathcal{G}_{ij}(0^-) &:= \lim_{\epsilon \to 0} \mathcal{G}_{ij}(0 - \epsilon) = - \langle \hat{a}^\dagger_j \hat{a}_i \rangle = -n_{ji} , \\ \mathcal{G}_{ij}(\beta^-) &:= \lim_{\epsilon \to 0} \mathcal{G}_{ij}(\beta - \epsilon) = + \langle \hat{a}^\dagger_j \hat{a}_i \rangle = +n_{ji} . \end{aligned} \qquad (3.22)$$

The grand canonical partition function

$$Z(\mu, V, \beta) = \text{Tr} \left\{ e^{-\beta \hat{\bar{D}}} \hat{T}_\tau e^{-\int_0^\beta \hat{Y}(\tau) d\tau} \right\}$$

obviously posses an expansion similar to that of the canonical partition function (cf. Eq. (3.18)). We only have to replace $\hat{D}$ by $\hat{\bar{D}}$ and drop the implied restriction of fixed particle number in the summation over $\{n\}$. Now, we investigate the quantity $\bar{\mathcal{G}}$ which is given by summation and integration over all MGFs multiplied by Z, i.e. ,it is

$$\begin{aligned} \bar{\mathcal{G}} :&= \sum_{ij} \int_0^\beta d\tau_{\text{ir}} \int_0^\beta d\tau_{\text{ma}} Z \cdot \mathcal{G}_{ij}(\tau_{\text{ir}}, \tau_{\text{ma}}) \\ &= \sum_{ij} \int_0^\beta d\tau_{\text{ir}} \int_0^\beta d\tau_{\text{ma}} \, \text{Tr} \left\{ e^{-\beta \hat{\bar{D}}} \hat{T}_\tau \left[e^{-\int_0^\beta \hat{Y}(\tau) d\tau} \hat{a}_i(\tau_{\text{ir}}) \hat{a}^\dagger_j(\tau_{\text{ma}}) \right] \right\} \\ &= \sum_{K=0}^\infty \sum_{\{n\}} \sum_{ij} \int_0^\beta d\tau_{\text{ir}} \int_0^\beta d\tau_{\text{ma}} \int' d^K \tau \\ & \qquad (-1)^K \langle \{n\} | e^{-\beta \hat{\bar{D}}} \hat{T}_\tau \left[\hat{Y}(\tau_K) \cdot \ldots \cdot \hat{Y}(\tau_1) \hat{a}_i(\tau_{\text{ir}}) \hat{a}^\dagger_j(\tau_{\text{ma}}) \right] | \{n\} \rangle , \end{aligned}$$

where in the last line, we have performed the trace in the basis of Fock states $|\{n\}\rangle$ and expanded the exponential according to Eq. (3.4). Inserting the expansion of the off-diagonal operators in terms of kink operators (cf. Eq. (3.15)) yields

$$\begin{aligned} \bar{\mathcal{G}} = \sum_{K=0}^\infty \sum_{\{n\}} \sum_{ij} \sum_{s_1} \cdots \sum_{s_K} \int_0^\beta d\tau_{\text{ir}} \int_0^\beta d\tau_{\text{ma}} \int' d^K \tau \\ (-1)^K \langle \{n\} | e^{-\beta \hat{\bar{D}}} \hat{T}_\tau \left[\hat{q}(s_K, \tau_K) \cdot \ldots \cdot \hat{q}(s_1, \tau_1) \hat{a}_i(\tau_{\text{ir}}) \hat{a}^\dagger_j(\tau_{\text{ma}}) \right] | \{n\} \rangle . \end{aligned}$$

3. Configuration path integral Monte Carlo

Due to the restrictions of the integrals over the kink times, the kink operators are already time ordered. However, we cannot drop the time-ordering operator since $\tau_{\mathrm{ir}}, \tau_{\mathrm{ma}} \in [0, \beta]$. Further, we have to be careful concerning the action of the time-ordering operator on a product of fermionic creation- and annihilation operators (with different time arguments). By definition it is

$$
\hat{T}_\tau \left[\hat{a}_i(\tau_{\mathrm{ir}}) \hat{a}_j^\dagger(\tau_{\mathrm{ma}}) \right] = \begin{cases} \hat{a}_i(\tau_{\mathrm{ir}}) \hat{a}_j^\dagger(\tau_{\mathrm{ma}}) & \text{if} \quad \tau_{\mathrm{ir}} > \tau_{\mathrm{ma}} \\ -\hat{a}_j^\dagger(\tau_{\mathrm{ma}}) \hat{a}_i(\tau_{\mathrm{ir}}) & \text{if} \quad \tau_{\mathrm{ir}} < \tau_{\mathrm{ma}} \end{cases} .
$$

Since the MGF is not defined for $\tau_{\mathrm{ir}} = \tau_{\mathrm{ma}}$, we have to make sure that this case is excluded in the integration over the times of Ira and Masha. We do that by adding a prime to the integral over τ_{ma}. Taking into account these aspects, we can produce a correctly time-ordered product as follows

$$
\bar{\mathcal{G}} = \sum_{K=0}^\infty \sum_{\{n\}} \int_0^\beta \mathrm{d}\tau_{\mathrm{ir}} \int_0'^\beta \mathrm{d}\tau_{\mathrm{ma}} \int' \mathrm{d}^K \tau \sum_{\pi \in \mathcal{S}_{k+2}} \sum_{\bar{s}_{\pi(1)}} \sum_{\bar{s}_{\pi(2)}} \cdots \sum_{\bar{s}_{\pi(K+2)}} \bar{\Theta}(\{\tau_{\pi(i)}\})
$$

$$
(-1)^{K+\Theta(\tau_{\mathrm{ma}}-\tau_{\mathrm{ir}})} \langle \{n\} | e^{-\beta \hat{D}} \hat{\bar{q}}(\bar{s}_{\pi(1)}, \tau_{\pi(1)}) \cdot \ldots \cdot \hat{\bar{q}}(\bar{s}_{\pi(K+2)}, \tau_{\pi(K+2)}) | \{n\} \rangle ,
$$
(3.23)

where it is $\tau_{K+1} = \tau_{\mathrm{ir}}$, $\tau_{K+2} = \tau_{\mathrm{ma}}$, $\bar{s}_{K+1} = i$ and $\bar{s}_{K+2} = j$. We sum over all permutations π of the permutation group $\mathcal{S}_{K+2}$ of $K + 2$ elements. Further, we have introduced the generalized theta function

$$
\bar{\Theta}(\{\tau_{\pi(i)}\}) := \Theta(\tau_{\pi(1)} - \tau_{\pi(2)}) \Theta(\tau_{\pi(2)} - \tau_{\pi(3)}) \cdot \ldots \cdot \Theta(\tau_{\pi(K+1)} - \tau_{\pi(K+2)}) ,
$$

which ensures that only the correct time-ordered product of *generalized kink operators* $\hat{\bar{q}}$ does not vanish. In accordance with the definition of the kink operators (3.12), these generalized kink operators are defined by

$$
\hat{\bar{q}}(\bar{s}_{\pi(i)}) := \begin{cases} \hat{a}_i & \text{if} \quad \bar{s}_{\pi(i)} = \bar{s}_{K+1} = i \in \mathbb{N} \\ \hat{a}_j^\dagger & \text{if} \quad \bar{s}_{\pi(i)} = \bar{s}_{K+2} = j \in \mathbb{N} \\ \left(h_{ik} + \sum_{\substack{j=0 \\ j \neq i,k}}^\infty w_{ijkj}^- \hat{n}_j \right) \hat{a}_i^\dagger \hat{a}_k & \text{if} \quad \bar{s}_{\pi(i)} = (i,k) \in A, \; \pi(i) \in \{1, \ldots, K\} \\ w_{ijkl}^- \hat{a}_i^\dagger \hat{a}_j^\dagger \hat{a}_l \hat{a}_k & \text{if} \quad \bar{s}_{\pi(i)} = (i,j,k,l) \in B, \; \pi(i) \in \{1, \ldots, K\} , \end{cases}
$$

and thus $\bar{s} \in A \cup B \cup \mathbb{N}$, but it is $\sum_{\bar{s}_{\pi(i)}} \neq \sum_{\bar{s} \in A \cup B \cup \mathbb{N}}$ because we have exactly one Ira and one Masha. We can ensure this by defining

$$
\sum_{\bar{s}_{\pi(i)}} \hat{\bar{q}}(\bar{s}_{\pi(i)}, \tau_{\pi(i)}) := \begin{cases} \sum_i \hat{a}_i(\tau_{\mathrm{ir}}) & \text{if} \quad \pi(i) = K+1 \\ \sum_j \hat{a}_j^\dagger(\tau_{\mathrm{ma}}) & \text{if} \quad \pi(i) = K+2 \\ \sum_{s_{\pi(i)} \in A \cup B} \hat{q}(s_{\pi(i)}, \tau_{\pi(i)}) & \text{if} \quad \pi(i) \in \{1, \ldots, K\} . \end{cases}
$$

Hence, we can simply interpret Ira and Masha as a *type 1* kink since these are given by only one creation or annihilation operator. Next, we insert $K + 1$ unit operators of the form $\hat{1} = \sum_{\{n^{(\pi(i))}\}} |\{n^{(\pi(i))}\}\rangle \langle\{n^{(\pi(i))}\}|$ between the generalized kink operators in Eq. (3.23), and with the matrix elements of the generalized kink operators

$$\hat{\bar{q}}_{\{n^{\pi(i)}\},\{n^{\pi(i-1)}\}}(\bar{s}_{\pi(i)}, \tau_{\pi(i)}) = e^{\tau_{\pi(i)}\bar{D}_{\{\pi(i)\}}} \bar{q}_{\{n^{\pi(i)}\},\{n^{\pi(i-1)}\}}(\bar{s}_{\pi(i)}) e^{-\tau_{\pi(i)}\bar{D}_{\{\pi(i)\}}}$$

(3.24)

we eventually find

$$\bar{\mathcal{G}} = \sum_{K=0}^{\infty} \sum_{\{n\}} \int_0^{\beta} \mathrm{d}\tau_{\mathrm{ir}} \int_0^{\prime\beta} \mathrm{d}\tau_{\mathrm{ma}} \int^{\prime} \mathrm{d}^K\tau \sum_{\pi\in\mathcal{S}_{k+2}} \sum_{\bar{s}_{\pi(1)}} \sum_{\bar{s}_{\pi(2)}} \cdots \sum_{\bar{s}_{\pi(K+1)}} \bar{\Theta}(\{\tau_{\pi(i)}\})$$

$$(-1)^{K+\Theta(\tau_{\mathrm{ma}}-\tau_{\mathrm{ir}})} e^{-\sum_{i=0}^{K+2} \hat{\bar{D}}_{\{n\}(\pi(i))}(\tau_{\pi(i+1)}-\tau_{\pi(i)})} \prod_{i=1}^{K+2} \bar{q}_{\{n^{(\pi(i))}\}\{n^{(\pi(i-1))}\}}(\bar{s}_{\pi(i)})$$

$$=: \oint_{C_{\mathrm{OP}}} W_{\mathrm{OP}}(C_{\mathrm{OP}}) \, ,$$

(3.25)

where we could drop the summation over the ONVs from the insertion of the $K+1$ unit operators since, in analogy to the kink operator, the matrix elements of the generalized kink operators (3.24) are completely defined by one state $|\{n^{\pi(i-1)}\}\rangle$ or $|\{n^{\pi(i)}\}\rangle$ and the type of the kink $\bar{s}_{\pi(i)}$. Due to the $\beta-$periodicity, we could also drop the summation over $\bar{s}_{\pi(K+2)}$.

This expansion of $\bar{\mathcal{G}}$ is very similar to that of the partition function (3.18). The only difference lies in the presence of two extra kinks, namely Ira and Masha. A contribution to $\bar{\mathcal{G}}$ is uniquely defined by the occupation numbers $\{n\}$ at $\tau = 0$, the kink times $\tau_1, \ldots, \tau_K$, the time of Ira τ_{ir} and Masha τ_{ma} determining the non-vanishing permutation π, the K kink types[11] $s_1, \ldots, s_K \in A \cup B$ (of type 2 or 4) and the orbital of Ira i and Masha j. Thus, a system configuration C_{OP} of $\bar{\mathcal{G}}$ is given by

$$C_{\mathrm{OP}} = \left((K), \{n\}, \underbrace{\tau_{\mathrm{ir}}, \tau_{\mathrm{ma}}, \tau_1, \ldots, \tau_K}_{\text{defines } \pi}, i, j, s_1, \ldots, s_K\right)$$

with the corresponding weight function

$$W_{\mathrm{OP}}(C_{\mathrm{OP}}) = (-1)^{K+\Theta(\tau_{\mathrm{ma}}-\tau_{\mathrm{ir}})} e^{-\sum_{i=0}^{K+2} \hat{\bar{D}}_{\{n\}(\pi(i))}(\tau_{\pi(i+1)}-\tau_{\pi(i)})}$$

$$\cdot \prod_{i=1}^{K+2} \hat{\bar{q}}_{\{n^{(\pi(i))}\}\{n^{(\pi(i-1))}\}}(\bar{s}_{\pi(i)}) \, .$$

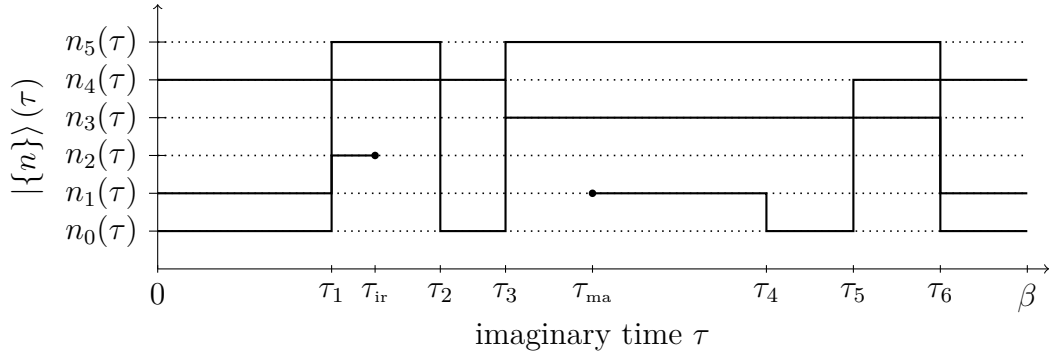[11]Actually, one of the kink types is also redundant due to the β-periodicity.

Figure 3.3.: Possible open path $\{n_0(\tau), n_1(\tau), \ldots, n_5(\tau)\}$ in imaginary time. In addition to the closed path (see Fig. 3.2), a particle is annihilated at time τ_{ir} and created at time τ_{ma}.

In analogy to the visualization of the closed path configurations (3.19) (see Fig. 3.2), these configurations can also be visualized as paths in imaginary time. An example is shown in Fig. 3.3. It is the same as the representation of closed paths, except that a particle is annihilated on the orbital i at time τ_{ir} and created on j at time τ_{ma}. Due to its appearance, we refer to these configurations as *open paths*, and interpret $\bar{\mathcal{G}}$ as the partition function of all open paths Z_{OP}.

Moreover, it is common to refer to Ira and Masha as the so called *Worm* that winds around the β-periodic paths. Actually, in the space of Fock states, there is no such thing as "the" worm, since in Fig. 3.3, there are many different ways to get from the tail (Masha) to the head (Ira) of the worm. For this reason, there also exists the notion *world line discontinuities* for Ira and Masha.

3.4. Total configuration space of the Worm algorithm

The general idea of the Worm algorithm is to sample not only closed but also open paths, i.e., we generate a Markov chain consisting of closed and open paths with suitable Monte Carlo steps (discussed in detail in Sec. 3.5). Not surprisingly, each closed path gives a contribution to the estimators of the standard thermodynamic observables that can be derived from the (grand) canonical partition function, whereas each open path contributes to the estimator(s) of the MGF. The estimators are derived in Chap. 4.

The total configuration space is defined by the sum of the grand canonical closed path partition function Z_{CP} (cf. Eq. (3.18) with $\hat{D} \to \hat{\bar{D}} = \hat{D} + \mu\hat{N}$) and the open path partition function Z_{OP} (cf. (3.25)). Due to the major importance for this thesis, the main equations of Sec. 3.2 and 3.3, which are required to define the total configuration space and which are necessary for the computation

of the weights, are summarized

$$
Z_{\text{Tot}} := Z_{\text{CP}}(\mu, \beta, V) + \bar{w} Z_{\text{OP}}(\mu, \beta, V) = \sum_{C_{\text{CP}}} \!\!\!\!\! \oint \; W_{\text{CP}}(C_{\text{CP}}) + \sum_{C_{\text{OP}}} \!\!\!\!\! \oint \; \bar{w} W_{\text{OP}}(C_{\text{OP}}) \; ,
$$

$$
Z_{\text{CP}} = \sum_{\substack{K=0, \\ K \neq 1}}^{\infty} \sum_{\{n\}} \sum_{s_1} \sum_{s_2} \cdots \sum_{s_{K-1}} \int' \mathrm{d}^K \tau
$$

$$
(-1)^K e^{-\sum_{i=0}^{K} \bar{D}_{\{n(i)\}}(\tau_{i+1} - \tau_i)} \prod_{i=1}^{K} \bar{q}_{\{n^{(i)}\}\{n^{(i-1)}\}}(s_i) \; ,
$$

$$
C_{\text{CP}} = \big((K), \{n\}, \tau_1, \tau_2, \ldots, \tau_K, s_1, s_2, \ldots, s_{K-1}\big) \; ,
$$

$$
Z_{\text{OP}} = \sum_{ij} \int_0^\beta \mathrm{d}\tau_{\text{ir}} \int_0^\beta \mathrm{d}\tau_{\text{ma}} Z_{\text{CP}} \cdot \mathcal{G}_{ij}(\tau_{\text{ir}}, \tau_{\text{ma}})
$$

$$
= \sum_{K=0}^{\infty} \sum_{\{n\}} \int_0^\beta \mathrm{d}\tau_{\text{ir}} \int_0'^\beta \mathrm{d}\tau_{\text{ma}} \int' \mathrm{d}^K \tau \sum_{\pi \in \mathcal{S}_{k+2}} \sum_{\bar{s}_{\pi(1)}} \sum_{\bar{s}_{\pi(2)}} \cdots \sum_{\bar{s}_{\pi(K+1)}} \bar{\Theta}(\{\tau_{\pi(i)}\})
$$

$$
(-1)^{K + \Theta(\tau_{\text{ma}} - \tau_{\text{ir}})} e^{-\sum_{i=0}^{K+2} \hat{\bar{D}}_{\{n\}(\pi(i))}(\tau_{\pi(i+1)} - \tau_{\pi(i)})} \prod_{i=1}^{K+2} \bar{q}_{\{n^{(\pi(i))}\}\{n^{(\pi(i-1))}\}}(\bar{s}_{\pi(i)}) \; ,
$$

$$
C_{\text{OP}} = \big((K), \{n\}, \underbrace{\tau_{\text{ir}}, \tau_{\text{ma}}, \tau_1, \ldots, \tau_K}_{\text{defines } \pi}, i, j, s_1, \ldots, s_K\big) \; , \tag{3.26}
$$

with the definitions

$$
\int' \mathrm{d}^K \tau := \int_0^\beta d\tau_1 \int_{\tau_1}^\beta d\tau_2 \ldots \int_{\tau_{K-1}}^\beta d\tau_K \; , \qquad \tau_{K+1} := \tau_{\text{ir}} \; , \quad \tau_{K+2} := \tau_{\text{ma}} \; ,
$$

$$
\bar{\Theta}(\{\tau_{\pi(i)}\}) := \Theta(\tau_{\pi(1)} - \tau_{\pi(2)}) \Theta(\tau_{\pi(2)} - \tau_{\pi(3)}) \cdot \ldots \cdot \Theta(\tau_{\pi(K+1)} - \tau_{\pi(K+2)}) \; ,
$$

$$
\hat{\bar{q}}(\bar{s}_{\pi(i)}) := \begin{cases} \hat{a}_i & \text{if} \quad \bar{s}_{\pi(i)} = \bar{s}_{K+1} = i \in \mathbb{N} \\ \hat{a}_j^\dagger & \text{if} \quad \bar{s}_{\pi(i)} = \bar{s}_{K+2} = j \in \mathbb{N} \\ \left(h_{ik} + \sum_{\substack{j=0 \\ j \neq i,k}}^{\infty} w_{ijkj}^- \hat{n}_j \right) \hat{a}_i^\dagger \hat{a}_k & \text{if} \quad \bar{s}_{\pi(i)} = (i,k) \in A, \; \pi(i) \in \{1, \ldots, K\} \\ w_{ijkl}^- \hat{a}_i^\dagger \hat{a}_j^\dagger \hat{a}_l \hat{a}_k & \text{if} \quad \bar{s}_{\pi(i)} = (i,j,k,l) \in B, \; \pi(i) \in \{1, \ldots, K\} \; , \end{cases}
$$

$$
\tag{3.27}
$$

$$\sum_{\bar{s}_{\pi(i)}} \hat{\bar{q}}(\bar{s}_{\pi(i)}, \tau_{\pi(i)}) := \begin{cases} \sum_i \hat{a}_i(\tau_{\mathrm{ir}}) & \text{if} \quad \pi(i) = K+1 \\ \sum_j \hat{a}_j^\dagger(\tau_{\mathrm{ma}}) & \text{if} \quad \pi(i) = K+2 \\ \sum_{s_{\pi(i)} \in A \cup B} \hat{q}(s_{\pi(i)}, \tau_{\pi(i)}) & \text{if} \quad \pi(i) \in \{1, \dots, K\}, \end{cases}$$
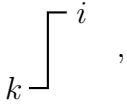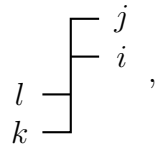
$$A := \left\{ (i,k) \in \mathbb{N}^2 \mid i \neq j \right\},$$

$$B := \left\{ (i,j,k,l) \in \mathbb{N}^4 \mid i < j, \ k < l, \ i \neq k, \ i \neq l, \ j \neq k, \ j \neq l \right\}.$$

As described in Sec. 2.1, since the weights of the total configuration space are both positive and negative, we have to apply the Metropolis algorithm to the partition sum that is given by the sum over the modulus weights

$$Z'_{\mathrm{Tot}} = Z'_{\mathrm{CP}}(\mu, \beta, V) + \bar{w} Z'_{\mathrm{OP}}(\mu, \beta, V) = \oint_{C_{\mathrm{CP}}} |W_{\mathrm{CP}}(C_{\mathrm{CP}})| + \oint_{C_{\mathrm{OP}}} \bar{w} |W_{\mathrm{OP}}(C_{\mathrm{OP}})|.$$

(3.28)

Thus, we sample closed paths C_{CP} with probability $\frac{|W_{\mathrm{CP}}(C_{\mathrm{CP}})|}{Z'_{\mathrm{Tot}}}$ and open paths C_{OP} with probability $\frac{\bar{w}|W_{\mathrm{OP}}(C_{\mathrm{OP}})|}{Z'_{\mathrm{Tot}}}$, where $\bar{w} \in \mathbb{R}_{>0}$ is some artificially introduced constant that will be used to determine the relative weight of open to closed paths, thereby optimizing the efficiency of the WA.

Graphically, the total configuration space consists of all possible β-periodic path $|n_0(\tau), n_1(\tau), \dots\rangle$ (see Fig. 3.2 and 3.3) that can be constructed with

- arbitrary number of type 2 kinks $s = (i,k) \in A$: ,

- arbitrary number of type 4 kinks $s = (i,j,k,l) \in B$: ,

- with or without Worm: Ira ⟶• and Masha •— ,

- and the connections of arbitrary length ——— .

Obviously, this configuration space has an infinite size even if we restrict the number of one-particle orbitals to some finite number N_B since the summation over the number of Kinks K goes up to infinity (cf. Eqs. (3.26)). However, only a small fraction of all these configurations gives a significant contribution to the total partition function, which makes the computation of observables via
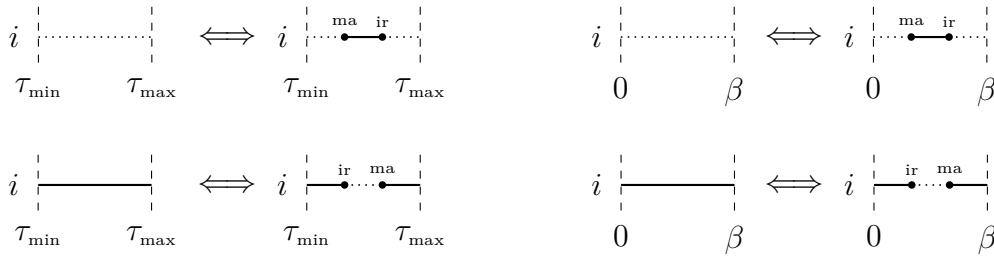
Figure 3.4.: Step 1 and 2: Left: Both possibilities to add and remove a worm with adjacent kinks on the orbital i at times $\tau_{\min}$ and $\tau_{\max}$. Right: Both possibilities to add a worm without kinks on the orbital i. When removing the worm in these two cases, the occupation of the orbital i is chosen randomly. Thereby, we either add or remove a whole particle from the path.

the Metropolis algorithm possible. To ensure ergodicity, we have to design a set of Monte Carlo steps that allow for the construction of all these possible configurations starting from any random paths with finite weight. Due to the $\beta-$periodicity, this task is much harder than one might expect. Moreover, if the two-particle integral w^-_{ijkl} is zero, then the corresponding kink operator and, consequently, the weight of all paths containing this kink vanish (cf. Eqs. (3.27)). Depending on the actual form of the Hamiltonian in the chosen one-particle basis, some of the one- and two-particle integrals can indeed be zero. This unfortunate circumstance makes the design of ergodic Monte Carlo steps even more complicated.

3.5. Monte Carlo steps

Since we can only work with a finite number of basis functions (or equivalently one-particle orbitals) N_B, the paths to be sampled are given by

$$\left| n_0(\tau), n_1(\tau), \ldots, n_{N_B-1}(\tau) \right\rangle \ .$$

In practice, we have to ensure that the calculated expectation values are converged for the used basis size N_B.

Further, in the following description of the Monte Carlo steps, all time intervals (τ_a, τ_b) with $\tau_a, \tau_b \in [0, \beta]$ are in fact $\beta-$periodic intervals, i.e., both $\tau_a < \tau_b$ or $\tau_b < \tau_a$ is possible, and hence, an ordering of times is not that trivial. We can only order times with respect to some reference time $\tau' \in [0, \beta]$. So for two times τ_a and τ_b, it is either τ_a or τ_b the next time point if we go around the beta cylinder clockwise starting from τ'. It is useful to define the length L_β of

such a β-periodic interval (τ_a, τ_b) as

$$L_\beta(\tau_a, \tau_b) := \begin{cases} \tau_b - \tau_a & \text{if} \quad \tau_a < \tau_b \\ \tau_b - \tau_a + \beta & \text{if} \quad \tau_a > \tau_b \, . \end{cases}$$

In the following description of the Monte Carlo steps, $L_{\beta,\tau}$ denotes the length of the $\beta-$periodic interval from which τ is chosen.

We will start with the two most important steps of the WA, which is to add and remove a worm in a given path, thereby switching between a closed or open path configuration. Fig. 3.4 shows the four possibilities to add and remove a worm.

Step 1: Add worm

I. Select a random orbital $i \in [0, N_B - 1]$.

II. Select a random time $\tau_{\text{ir}} \in (0, \beta)$.

III. Determine the times of adjacent kinks on i, i.e., left or right of τ_{ir} $\Rightarrow (\tau_{\text{min}}, \tau_{\text{max}})$. If there are no kinks on i, set $(\tau_{\text{min}}, \tau_{\text{max}}) = (0, \beta)$.

IV. Determine a time for Masha:

   a) If $(\tau_{\text{min}}, \tau_{\text{max}}) = (0, \beta)$, randomly select $\tau_{\text{ma}} \in (0, \beta)$.

   b) If i is unoccupied on $(\tau_{\text{min}}, \tau_{\text{max}})$, randomly select $\tau_{\text{ma}} \in (\tau_{\text{min}}, \tau_{\text{ir}})$.

   c) If i is occupied on $(\tau_{\text{min}}, \tau_{\text{max}})$, randomly select $\tau_{\text{ma}} \in (\tau_{\text{ir}}, \tau_{\text{max}})$.

Step 2: Remove worm

I. If Ira and Masha are not on the same orbital i, reject step.

II. If there is a kink between Ira and Masha on i, reject step.

III. Determine the times of adjacent kinks of Ira and Masha on $i \Rightarrow (\tau_{\text{min}}, \tau_{\text{max}})$.

IV. Determine the new occupation of the orbital i on the interval $(\tau_{\text{min}}, \tau_{\text{max}})$:

   a) If $(\tau_{\text{min}}, \tau_{\text{max}}) = (0, \beta)$, chose the occupation randomly. (Thereby a particle is added or removed.)

   b) If the ordering of times from left to right is $(\tau_{\text{min}}, \tau_{\text{ma}}, \tau_{\text{ir}}, \tau_{\text{max}})$, i will be unoccupied.

   c) If the ordering of times from left to right is $(\tau_{\text{min}}, \tau_{\text{ir}}, \tau_{\text{ma}}, \tau_{\text{max}})$, i will be occupied.

In the two right diagrams in Fig. 3.4, showing the case without kinks on the chosen orbital i, both configurations with worms are equivalent due to the β-periodicity. Therefore, we have to choose the occupation of the orbital randomly when removing the worm. To determine the acceptance probability A_{AW} for adding a worm, we have to set up the generalized detailed balance equation (cf. Eq. (2.4)) for the case that we first add a worm and in the next step remove it. If we denote the probability to chose the step x by P_{x}, it is

$$
P_{\mathrm{AW}} \frac{1}{N_B} \frac{1}{\beta} \frac{1}{L_{\beta,\tau_{\mathrm{ma}}}} A_{\mathrm{AW}}(C_{\mathrm{CP}} \to C'_{\mathrm{OP}}) |W_{\mathrm{CP}}(C_{\mathrm{CP}})|
$$
$$
= P_{\mathrm{RW}} O A_{\mathrm{RW}}(C'_{\mathrm{OP}} \to C_{\mathrm{CP}}) \bar{w} |W_{\mathrm{OP}}(C'_{\mathrm{OP}})| \,,
$$
(3.29)

where the prefactors of the l.h.s. represent the sampling probability to add one specific worm, whereas the prefactors on the r.h.s. determine the sampling probability to remove the worm in the next step in such a way that the configuration is exactly the original one without worm, i.e., C_{CP}. In Eq. (3.29), $L_{\beta,\tau_{\mathrm{ma}}}$ is the length of the interval from which the time of Masha is chosen. The factor O takes into account the random choice of the occupation in case the worm is removed from an orbital without kinks

$$
O = \begin{cases} \frac{1}{2} & \text{if } (\tau_{\min}, \tau_{\max}) = (0, \beta) \,, \\ 1 & \text{else.} \end{cases}
$$

According to Eq. (2.5), a possible solution of the detailed balance equation (3.29) is given by

$$
A_{\mathrm{AW}}(C_{\mathrm{CP}} \to C'_{\mathrm{OP}}) = \min\left\{ 1, \frac{P_{\mathrm{RW}}}{P_{\mathrm{AW}}} N_B \beta L_{\beta,\tau_{\mathrm{ma}}} O \bar{w} \left| \frac{W_{\mathrm{OP}}(C'_{\mathrm{OP}})}{W_{\mathrm{CP}}(C_{\mathrm{CP}})} \right| \right\} \,.
$$
(3.30)

Setting up the detailed balance for the inverse case of first removing and then adding a worm in the next step, we readily obtain

$$
A_{\mathrm{RW}}(C_{\mathrm{OP}} \to C'_{\mathrm{CP}}) = \min\left\{ 1, \frac{P_{\mathrm{AW}}}{P_{\mathrm{RW}}} \frac{1}{N_B \beta L_{\beta,\tau_{\mathrm{ma}}} O \bar{w}} \left| \frac{W_{\mathrm{CP}}(C'_{\mathrm{CP}})}{W_{\mathrm{OP}}(C_{\mathrm{OP}})} \right| \right\} \,,
$$
(3.31)

where we have to determine the correct length $L_{\beta,\tau_{\mathrm{ma}}}$ of the interval from which we would choose the time of Masha when proposing to add the same worm in the next step. In addition, it turns out that it is most efficient to adjust the constant $\bar{w}$ until the average acceptance probabilities to add and remove a worm are approximately equal, which results in an equal amount of open and closed paths in the Markov chain. The fraction of the modulus weights in (3.30) and (3.31) are calculated according to the Eqs. (3.26). To do this in an efficient way, i.e., only computing the factors that are actually changed by the
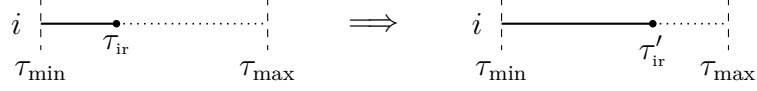
Figure 3.5.: Step 3: Moving Ira in time, where the new time τ'_{ir} can be between the adjacent kinks on that orbital with times τ_{min} and τ_{max}. If there is no kink on that orbital, then $\tau'_{\text{ir}} \in (0, \beta)$.

step, is quite involved and cannot be explained in detail for every step. Instead, the general aspects of the calculation of these weight fractions are discussed in detail in Sec. 3.5.1 after all steps have been introduced.

Once we have added a worm, i.e., we are in an open path configuration, we can move Ira either horizontally, by changing its time τ_{ir}, or vertically, by changing its orbital i, thereby a kink can be added, removed or changed. We proceed with the simplest step of shifting Ira in time as shown in Fig. 3.5.

Step 3: Move Ira in time

    I. Determine the kink times next to Ira $\Rightarrow (\tau_{\text{min}}, \tau_{\text{max}})$.
        If there is none, then it is $(\tau_{\text{min}}, \tau_{\text{max}}) = (0, \beta)$.

    II. Randomly select a new time $\tau'_{\text{ir}} \in (\tau_{\text{min}}, \tau_{\text{max}})$.

Since the inverse step is to shift Ira back from τ'_{ir} to the former time τ_{ir}, the sampling probability cancels in the detailed balance equation

$$P_{\text{MIT}} \frac{1}{L_{\beta, \tau'_{\text{ir}}}} A_{\text{MIT}}(C_{\text{OP}} \to C'_{\text{OP}}) |W_{\text{OP}}(C_{\text{OP}})|$$

$$= P_{\text{MIT}} \frac{1}{L_{\beta, \tau_{\text{ir}}}} A_{\text{MIT}}(C'_{\text{OP}} \to C_{\text{OP}}) |W_{\text{OP}}(C'_{\text{OP}})|$$

with the solution

$$A_{\text{MIT}}(C_{\text{OP}} \to C'_{\text{OP}}) = \min\left\{1, \left|\frac{W_{\text{OP}}(C'_{\text{OP}})}{W_{\text{OP}}(C_{\text{OP}})}\right|\right\} . \tag{3.32}$$

The next steps consists of changing the orbital of Ira, whereby a type 2 kink is added or removed (see Fig. 3.6)

Step 4: Add type 2 kink with Ira

    I. Select a random orbital $j \neq i$ for Ira (currently on i).

    II. Determine the times of the next left and right kink of Ira on the orbitals i and $j \Rightarrow (\tau_{\text{min}}, \tau_{\text{max}})$.

Figure 3.6.: Step 4 and 5: Add a type 2 kink with Ira. If the new orbital of Ira is unoccupied (occupied), than the new kink is added left (right) of Ira.

III. a) If j is unoccupied, then add a type 2 kink $s = (j, i)$ left of Ira, i.e. randomly select a new kink time $\tau_{new} \in (\tau_{\min}, \tau_{\mathrm{ir}})$.

   b) If j is occupied, then add a type 2 kink $s = (j, i)$ right of Ira, i.e. randomly select a new kink time $\tau_{new} \in (\tau_{\mathrm{ir}}, \tau_{\max})$.

Step 5: Remove type 2 kink with Ira

I. Suppose Ira is on orbital j as in Fig. 3.6. Randomly choose the next left or right kink s of Ira.

II. Reject the step if

   a) s is not of type 2, i.e., $s \neq (j, i)$.

   b) there is another kink s' on the orbital i or j in the interval $(\tau_s, \tau_{\mathrm{ir}})$ or $(\tau_{\mathrm{ir}}, \tau_s)$, respectively.

III. Remove $s = (j, i)$ by moving Ira to the orbital i. If s is left (right) of Ira, then j is unoccupied (occupied) afterwards.

We readily write down the detailed balance equation for adding a kink with Ira and in the next step remove exactly the same kink

$$P_{\mathrm{IAT2}} \frac{1}{N_B - 1} \frac{1}{L_{\beta, \tau_{\mathrm{new}}}} A_{\mathrm{IAT2}}(C_{\mathrm{OP}} \to C'_{\mathrm{OP}}) |W_{\mathrm{OP}}(C_{\mathrm{OP}})|$$

$$= P_{\mathrm{IRT2}} \frac{1}{2} A_{\mathrm{IRT2}}(C'_{\mathrm{OP}} \to C_{\mathrm{OP}}) |W_{\mathrm{OP}}(C'_{\mathrm{OP}})| \,,$$

which yields the acceptance probabilities for these steps

$$A_{\mathrm{IAT2}}(C'_{\mathrm{OP}} \to C_{\mathrm{OP}}) = \min \left\{ 1, \frac{P_{\mathrm{IRT2}}}{P_{\mathrm{IAT2}}} (N_B - 1) L_{\beta, \tau_{\mathrm{new}}} \frac{1}{2} \left| \frac{W_{\mathrm{OP}}(C'_{\mathrm{OP}})}{W_{\mathrm{OP}}(C_{\mathrm{OP}})} \right| \right\} \,,$$

$$A_{\mathrm{IRT2}}(C'_{\mathrm{OP}} \to C_{\mathrm{OP}}) = \min \left\{ 1, \frac{P_{\mathrm{IAT2}}}{P_{\mathrm{IRT2}}} \frac{1}{(N_B - 1) L_{\beta, \tau_{\mathrm{new}}}} 2 \left| \frac{W_{\mathrm{OP}}(C'_{\mathrm{OP}})}{W_{\mathrm{OP}}(C_{\mathrm{OP}})} \right| \right\} \,.$$

We can also place Ira on another orbital and change a nearby kink as described in the following.
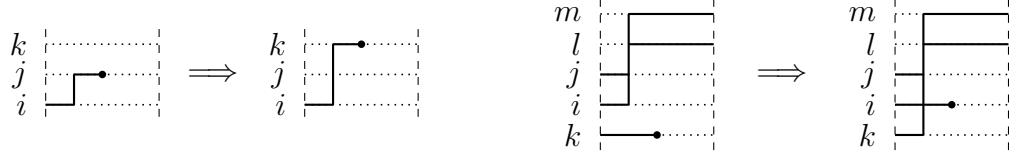
Step 6: Change kink with Ira

Figure 3.7.: Step 6: Two examples of changing a kink by placing Ira on another orbital. In total, there are 22 possible diagrams for a change kink with Ira. These are shown in Fig. A.1 and A.2.

I. Randomly select the next left or right kink s of τ_{ir}.

II. If s is left of Ira, randomly choose a new free orbital for Ira[12].

III. If s is right of Ira, randomly choose a new occupied orbital for Ira[13].

IV. Reject the step if s is of type 1 (Masha) or if s would be removed by the replacing of Ira[14].

V. Place Ira on the new orbital, whereby s is changed according to the 22 possibilities shown in Fig. A.1 and A.2.

Since the inverse step of changing a kink with Ira constitutes is to change the same kink such that it is again the original one, the sampling probability cancels in the detailed balance, and hence, the acceptance probability for this step is simply

$$A_{\mathrm{ICK}}(C_{\mathrm{OP}} \to C'_{\mathrm{OP}}) = \min\left\{1, \left|\frac{W_{\mathrm{OP}}(C'_{\mathrm{OP}})}{W_{\mathrm{OP}}(C_{\mathrm{OP}})}\right|\right\} \ ,$$

where each of the 22 diagrams corresponds to a different change in the weight.

The next steps can be proposed in both an open or closed path configuration. We begin with the addition or removal of a type 2 or 4 kink via a one- or two-particle excitation, and, at the same time, changing another kink. An example is shown in Fig. 3.8.

Step 7: Add T2 or T4 kink via one- or two-particle excitation

---

[12]In case s is of type 4 and the current orbital of Ira is not one of the two creators of s, then we can only place Ira on one of the two annihilator orbitals of s (see diagram in the third row and second column in Fig A.1).

[13]In case s is of type 4 and the current orbital of Ira is not one of the two annihilators of s, then we can only place Ira on one of the two creator orbitals of s (see diagram in the third row and second column in Fig A.2).

[14]Not including the remove kink step in the changing of a kink results in a higher acceptance probability for adding a kink with Ira.
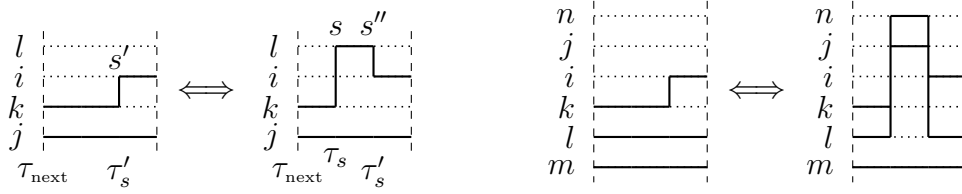
Figure 3.8.: Step 7: Left: A new type 2 kink $s = (l, k)$ is added via a one particle excitation from orbital k to l left of the kink $s' = (i, k)$. Thereby, $s' = (i, k)$ is changed to $s'' = (i, l)$. The time of s is randomly chosen from the interval $(\tau_{\text{next}}, \tau'_s)$, where τ_{next} is the time of the next kink left of s' that affects the orbital k and/or l. Right: In a similar way, we can add a type 4 kink $s = (j, n, l, k)$ via a two-particle excitation from k, l to j, n left of anther kink s' that will be changed. In the shown example, s' is of type 2 and is changed to a type 4 kink. All 48 possibilities to add a type 2 or 4 kink via a one- or two-particle excitation are shown in the Figs. A.3 - A.6.

   I. Randomly select one of the K kinks to be changed $\Rightarrow s'$. Reject the step if there are no kinks or if s' is of type 1 (Masha).

  II. Randomly choose a direction, left or right, for the new kink s to be added with respect to s'.

 III. Randomly choose if a type 2 or type 4 kink shall be added via one- or two-particle excitation, respectively.

 IV. Depending on the direction and the type to be added, randomly choose one occupied or two occupied orbital(s) left or right of s'.

  V. In case of a one-particle excitation, randomly choose a free orbital from those that would result in an excitation which is compatible with a proper changing of s'. In case of a two-particle excitation, randomly choose two free orbitals that are compatible with s'. The number of these possible orbitals compatible with a change[15] of s' depends on the chosen direction, the orbitals of s' and the already determined occupied orbital(s)[16]. All 48 different cases are shown in the Figs. A.3, A.4, A.5 and A.6.

 VI. Determine the time τ_{next} of the next kink left or right of s' affecting one of the orbitals that are involved in the excitation.

---

[15]The limited number of possible excitations simply lies in the fact that there are no type 6 kinks.

[16]Of course, we could simply select the orbitals randomly, and if the resulting excitation is not compatible with a changing of s', then just reject the step. This would result in a significantly smaller acceptance probability. In addition, for the calculation of the weight change, we have to distinguish between the 48 cases any way.

VII. Randomly choose a time τ_{new} for the new kink s from $(\tau_{\text{next}}, \tau_s')$ if the direction is left, or from $(\tau_s', \tau_{\text{next}})$ if the direction is right.

Step 8: Remove T2 or T4 kink via one- or two-particle excitation

I. Randomly choose a kink s to be removed. Reject the step if there are no kinks or if s is of type 1 (Masha).

II. Randomly choose a direction left or right.

III. Determine the excitation that removes s.

IV. Determine the time τ_{next} of the next kink left or right of s (depending on the chosen direction) affecting one or more orbitals of s.

V. Determine the number of kinks N_{CK} that can be changed. These are given by all kinks in the interval $(\tau_{\text{next}}, \tau_s)$ (if the direction is right) or in $(\tau_s, \tau_{\text{next}})$ (if the direction is left).

VI. Randomly choose a kink s' of the N_{CK} possible kinks to be changed.

VII. Check if s can actually be removed by changing s' according to one of the 48 possible diagrams shown in the Figs. A.3 - A.6, otherwise reject the step.

The detailed balance for first adding and then, in the next step, removing a kink with these two steps is given by

$$P_{AK} \frac{1}{K} \frac{1}{2} \frac{1}{2} \frac{1}{O_{\text{Ex}}} \frac{1}{L_{\beta,\tau_{\text{new}}}} A_{\text{AK}}(C_{\text{CP}\backslash\text{OP}} \to C'_{\text{CP}\backslash\text{OP}}) W_{\text{CP}\backslash\text{OP}}(C_{\text{CP}\backslash\text{OP}})$$

$$= P_{RK} \frac{1}{(K+1)} \frac{1}{2} \frac{1}{N_{\text{CK}}} A_{\text{RK}}(C'_{\text{CP}\backslash\text{OP}} \to C_{\text{CP}\backslash\text{OP}}) W_{\text{CP}\backslash\text{OP}}(C'_{\text{CP}\backslash\text{OP}}) \ ,$$

where O_{Ex} takes into account the number of possible excitations. It follows the acceptance probability of both steps

$$A_{\text{AK}}(C_{\text{CP}\backslash\text{OP}} \to C'_{\text{CP}\backslash\text{OP}}) = \min\left\{1, \frac{P_{\text{RK}}}{P_{\text{AK}}} \frac{2K O_{\text{Ex}} L_{\beta,\tau_{\text{new}}}}{(K+1)N_{\text{CK}}} \left|\frac{W_{\text{CP}\backslash\text{OP}}(C'_{\text{CP}\backslash\text{OP}})}{W_{\text{CP}\backslash\text{OP}}(C_{\text{CP}\backslash\text{OP}})}\right|\right\} ,$$

$$A_{\text{RK}}(C_{\text{CP}\backslash\text{OP}} \to C'_{\text{CP}\backslash\text{OP}}) = \min\left\{1, \frac{P_{\text{AK}}}{P_{\text{RK}}} \frac{K N_{\text{CK}}}{2(K-1)O_{\text{Ex}} L_{\beta,\tau_{\text{new}}}} \left|\frac{W_{\text{CP}\backslash\text{OP}}(C'_{\text{CP}\backslash\text{OP}})}{W_{\text{CP}\backslash\text{OP}}(C_{\text{CP}\backslash\text{OP}})}\right|\right\} .$$

These steps are the most elaborate of the algorithm. Only the implementation of the correct choice of the step parameters takes roughly a thousand lines of C++ code for these two steps. Distinguishing between all 48 cases for the
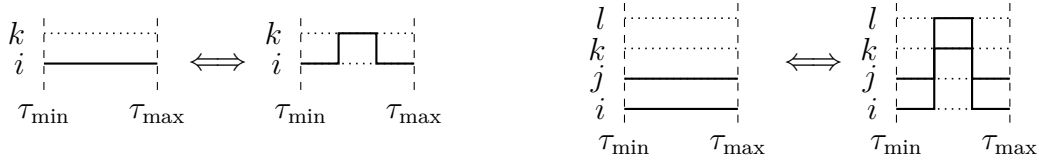
Figure 3.9.: Step 9 and 10: Left: A pair of type 2 kinks is added via a one-particle excitation. Right: A pair of type 4 kinks is added via a two-particle excitations.

computation of the weight fractions and, in case the step is accepted, realising the corresponding change in the path takes a couple of thousand lines.

The next two steps add or remove a pair of type 2 or 4 kinks via a one- or two-particle excitation as shown in Fig. 3.9.

Step 9: Add pair of type 2 kinks

   I. Randomly choose a time $\tau_1 \in (0, \beta)$ for the first kink to be added.

  II. Randomly choose one occupied (i) and one free orbital (k) at τ_1.

 III. Find the time τ_2 of the second kink to be added:

     a) If there are no kinks on i and k, randomly choose $\tau_2 \in (0, \beta)$.

     b) If there are kinks on i and k, randomly choose a direction, left or right, and determine the time τ_{next} of the next kink from τ_1 in the chosen direction affecting the orbitals i and k. Then, depending on the direction, randomly choose a time τ_2 from $(\tau_{\text{next}}, \tau_1)$ or $(\tau_1, \tau_{\text{next}})$.

 IV. Excite the orbital i to k on the interval (τ_2, τ_1) (if the direction is left) or (τ_1, τ_2) (if the direction is right) as shown in Fig. 3.9, whereby the kinks (i, k) and (k, i) are added.

Step 10: Add pair of type 4 kinks

   I. Randomly choose a time $\tau_1 \in (0, \beta)$ for the first kink to be added.

  II. Randomly choose two occupied (i, j) and two free orbitals (k, l) at τ_1.

 III. Find the time τ_2 of the second kink to be added:

     a) If there are no kinks on i, j and k, l, randomly choose $\tau_2 \in (0, \beta)$.

     b) If there are kinks on i, j and k, l, randomly choose a direction, left or right, and determine the time τ_{next} of the next kink from τ_1 in the chosen direction affecting the orbitals k, l and i, j. Then, depending on the direction, randomly choose a time τ_2 from $(\tau_{\text{next}}, \tau_1)$ or $(\tau_1, \tau_{\text{next}})$.

3. Configuration path integral Monte Carlo

IV. Excite the orbitals i and j to k and l on the interval (τ_2, τ_1) (if the direction is left) or (τ_1, τ_2) (if the direction is right) as shown in Fig. 3.9, whereby the kinks (i, j, k, l) and (k, l, i, j) are added.

Step 11: Remove pair of type 2 or 4 kinks

I. Randomly choose one of the K kinks (s_1). If there are no kinks or if s_1 is of type 1, reject the step.

II. If s_1 is of type 2, i.e., $s = (i, k)$, then

a) Randomly choose a direction left or right of s_1 and determine the next kink s_2 in that direction on one of the two orbitals i or j.

b) Reject the step if s_2 is not of type 2 with $s = (k, i)$.

c) Depending on the direction, excite the orbital i to k or k to i in such a way that s_1 and s_2 vanish (as shown in Fig. 3.9).

III. If s_1 is of type 4, i.e., $s = (i, j, k, l)$, then

a) Randomly choose a direction left or right of s_1 and determine the next kink s_2 in that direction on one of the four orbitals i, j, k and l.

b) Reject the step if s_2 is not of type 4 with $s = (k, l, i, j)$.

c) Depending on the direction, excite the orbitals i, j to k, l or k, l to i, j in such a way that s_1 and s_2 vanish (as shown in Fig. 3.9).

Setting up the detailed balance for these three steps as illustrated for the prior steps, we readily obtain the appropriate acceptance probabilities

$$A_{\text{A2T2(4)}}(C_{\text{CP}\backslash\text{OP}} \rightarrow C'_{\text{CP}\backslash\text{OP}}) = \min\left\{1, \frac{P_{\text{R2K}}}{P_{\text{A2T2(4)}}} \frac{\beta O_{\text{Ex}} L_{\beta,\tau_2}}{(K+2)} \left|\frac{W_{\text{CP}\backslash\text{OP}}(C'_{\text{CP}\backslash\text{OP}})}{W_{\text{CP}\backslash\text{OP}}(C_{\text{CP}\backslash\text{OP}})}\right|\right\},$$

$$A_{\text{R2K}}(C_{\text{CP}\backslash\text{OP}} \rightarrow C'_{\text{CP}\backslash\text{OP}}) = \min\left\{1, \frac{P_{\text{A2T2(4)}}}{P_{\text{R2K}}} \frac{K}{\beta O_{\text{Ex}} L_{\beta,\tau_2}} \left|\frac{W_{\text{CP}\backslash\text{OP}}(C'_{\text{CP}\backslash\text{OP}})}{W_{\text{CP}\backslash\text{OP}}(C_{\text{CP}\backslash\text{OP}})}\right|\right\}.$$

In case of removing two type 2 (4) kinks, we have to use P_{A2T2} (P_{A2T4}) for the computation of A_{R2K}. The factor O_{Ex} denotes the number of all possible excitations[17].

---

[17] Let N_{occ} be the number of occupied orbitals at τ_1. Then, for the adding of two type 2 kinks, we randomly choose one occupied and one free orbital, and hence, it is $O_{\text{Ex}} = N_{\text{occ}}(N_B - N_{\text{occ}})$. But, in case of type 4 kinks, we have to be careful as $O_{\text{Ex}} = N_{\text{occ}}(N_{\text{occ}} - 1)(N_B - N_{\text{occ}})(N_B - N_{\text{occ}} - 1)/4$. We have to divide by 4 since there are 4 different orders in which we can select the two occupied orbitals and two free orbitals resulting in the same excitation.
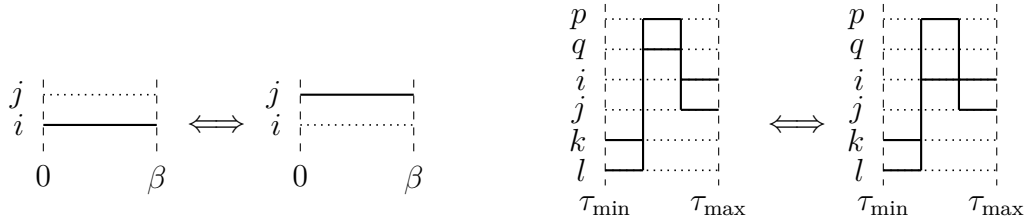
Figure 3.10.: Step 12: Left: If there are no kinks on the chosen orbital, then propose to excite the whole particle. Right: The orbital q is excited to the orbital i in between the two type 4 kinks.

The following step either proposes an excitation of a whole orbital from 0 to β to anther orbital or an excitation of an orbital between two kinks, whereby these are changed (see Fig. 3.10).

Step 12: One-particle excitation

I. Randomly choose between exciting a whole orbital or changing two kinks via a one-particle excitation. Excitation of a whole orbital is chosen with probability $\frac{1}{K}$ and changing two kinks with $\frac{K-1}{K}$, where K is the number of kinks in the path. If there are no kinks, then always propose to excite a whole orbital[18].

II. If exciting a whole orbital is chosen, then

   a) Randomly choose one of the occupied orbitals i and one of the free orbitals j without kinks from 0 to β.

   b) Propose to excite i to j (see Fig. 3.10).

III. If changing two kinks is chosen, then

   a) Randomly choose one of the K kinks (s_1). If s_1 is of type 1, reject the step.

   b) Randomly choose one occupied orbital i right of s_1.

   c) Randomly choose one free orbital j from those that allow for a correct changing of s_1. These orbitals are the same as in step 7 when adding a type 2 kink right of s_1 (cf. Fig. A.4).

   d) Determine the time τ_{next} of the next kink right of s_1 affecting i or j.

   e) Determine the number of kinks N_{s_2} in the interval $(\tau_{s_1}, \tau_{\text{next}}]$ and randomly choose one of them $\Rightarrow s_2$.

---

[18]Choosing the whole orbital excitation and the changing of two kinks with these probabilities is reasonable because accepting the excitation of a whole orbital is less likely the more kinks there are in the configuration.
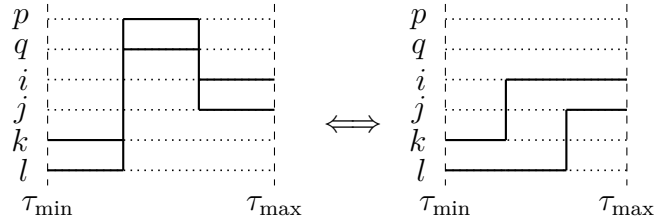
Figure 3.11.: Step 13: Two type 4 kinks are changed to two type 2 kinks via a two-particle excitation from p, q to i, l.

> f) Check if the excitation from i to j on the interval (τ_{s_1}, τ_{s_2}) allows for a proper changing of s_2, else reject the step.

Obviously, the inverse step of a one-particle excitation from orbital i to j is to propose an excitation from j to i on the same interval. Yet, the sampling probability does not cancel completely because the number of kinks N_{s_2} from which we choose the second kink s_2 changes after we have accepted an excitation and then again select step 12 proposing the inverse excitation. Therefore, we obtain the following acceptance probability for a one-particle excitation

$$
A_{\text{1PEx}}(C_{\text{CP}\backslash\text{OP}} \to C'_{\text{CP}\backslash\text{OP}}) =
\begin{cases}
\min\left\{1, \frac{N_{s_2}}{N'_{s_2}} \left| \frac{W_{\text{CP}\backslash\text{OP}}(C'_{\text{CP}\backslash\text{OP}})}{W_{\text{CP}\backslash\text{OP}}(C_{\text{CP}\backslash\text{OP}})} \right| \right\} & \text{if changing 2 kinks} \\
\min\left\{1, \left| \frac{W_{\text{CP}\backslash\text{OP}}(C'_{\text{CP}\backslash\text{OP}})}{W_{\text{CP}\backslash\text{OP}}(C_{\text{CP}\backslash\text{OP}})} \right| \right\} & \text{else.}
\end{cases}
$$

Similar to step 12, the last step to be discussed is a two-particle excitation, whereby two kinks are changed. We do not propose to excite two whole orbitals since this can always be achieved by exciting each orbital separately. An example for step 13 is shown in Fig. 3.11.

Step 13: Two-particle excitation

I. Randomly choose one of the K kinks s_1. If s_1 is of type 1, reject the step.

II. Randomly choose two occupied orbitals i and j right of s_1.

III. Randomly choose two free orbitals k and l from those that allow for a correct changing of s_1. These orbitals are the same as in step 7 when adding a type 4 kink right of s_1 (cf. Fig. A.6).

IV. Determine the time τ_{next} of the next kink right of s_1 affecting i, j, k or l.

V. Determine the number of kinks N_{s_2} in the interval $(\tau_{s_1}, \tau_{\text{next}}]$ and randomly choose one of them $\Rightarrow s_2$.
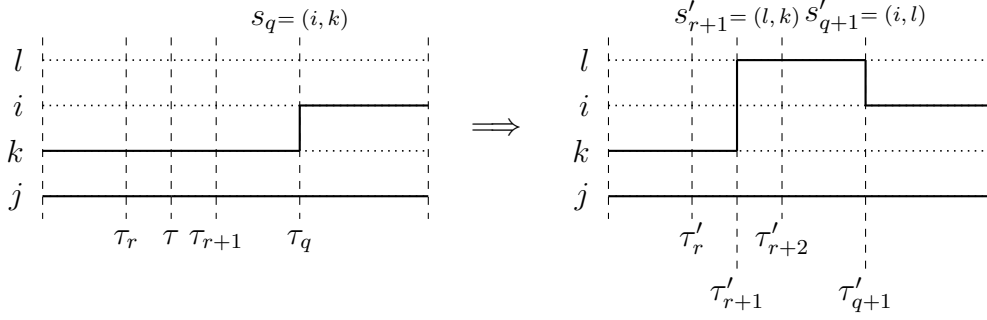
Figure 3.12.: Some part of a closed path that is changed by a one-particle excitation from the orbital k to l on the interval (τ, τ_q), whereby a type two kink $s'_{r+1} = (l, k)$ is added at τ and the kink $s_q = (i, k)$ at τ_q is changed to $s'_{q+1} = (i, l)$. The left diagram belongs to the configuration C_{CP}, in which the change is proposed, whereas the right diagram shows the configuration C'_{CP} if the proposed change is accepted. The next kink left (right) of τ that is somewhere in the path (concerning its orbitals) has the time τ_r (τ_{r+1}), i.e, we propose to add a kink in between the kinks at times τ_r and τ_{r+1}. Therefore, the indices of the kinks in the configuration C'_{CP} right of τ are shifted by one compared to C_{CP}. (It has to be $\tau_1 < \tau_2 < \ldots < \tau_K$ and $\tau'_1 < \tau'_2 < \ldots < \tau'_{K'}$ where $K' = K + 1$.)

VI. Check if the excitation from i, j to k, l on the interval (τ_{s_1}, τ_{s_2}) allows for a proper changing of s_2, else reject the step.

For a two-particle excitation, the number of kinks N_{s_2} from which we choose the second kink does not change in the inverse step, and thus, the acceptance probability is simply given by

$$A_{\text{2PEx}}(C_{\text{CP}\backslash\text{OP}} \to C'_{\text{CP}\backslash\text{OP}}) = \min\left\{1, \left|\frac{W_{\text{CP}\backslash\text{OP}}(C'_{\text{CP}\backslash\text{OP}})}{W_{\text{CP}\backslash\text{OP}}(C_{\text{CP}\backslash\text{OP}})}\right|\right\} .$$

Sure, in the steps 12 and 13, it would be more efficient to choose only from such excitations that are compatible with both kinks s_1 and s_2. This would require to draw the diagrams for each possible combination of kinks, which has not been done yet.

3.5.1. Calculation of weight differences

For the calculation of the acceptance probability of any step, we have to compute the fraction of the modulus weights $\left|\frac{W(C')}{W(C)}\right|$, where the proposed step changes the configuration C to C'. We could simply compute the total modulus weights of both configurations by evaluating the corresponding weight functions in the Eqs. (3.26). This is far too inefficient since we have to compute only those factors that do not cancel. The general procedure shall be explained for

3. Configuration path integral Monte Carlo

the example of step 7 in case we propose to add a type two kink via a one particle excitation in a closed path as shown in Fig. 3.12. According to the Eqs. (3.26), it is

$$\left| \frac{W_{\mathrm{CP}}(C'_{\mathrm{CP}})}{W_{\mathrm{CP}}(C_{\mathrm{CP}})} \right| = e^{-\beta \Delta E_D} |\Delta Q| \tag{3.33}$$

with the difference of the diagonal energy of both configurations ΔE_D and the fraction of all kink matrix elements ΔQ

$$\Delta E_D = E_D(C'_{\mathrm{CP}}) - E_D(C_{\mathrm{CP}})$$

$$:= \sum_{i=0}^{K'=K+1} D_{\{n^{(i)'}\}} \frac{(\tau'_{i+1} - \tau'_i)}{\beta} - \sum_{i=0}^{K} D_{\{n^{(i)}\}} \frac{(\tau_{i+1} - \tau_i)}{\beta}$$

$$\Delta Q = \frac{Q(C'_{\mathrm{CP}})}{Q(C_{\mathrm{CP}})} := \frac{\prod_{i=1}^{K'} \bar{q}_{\{n^{(i-1)'}\},\{n^{(i)'}\}}(s'_i)}{\prod_{i=1}^{K} \bar{q}_{\{n^{(i-1)}\},\{n^{(i)}\}}(s_i)} \ . \tag{3.34}$$

First, we simplify the difference of the diagonal energy. In Fig. 3.12, the occupation numbers of the path change only within the interval (τ, τ_q), where we excite the orbital k to l and add the kink at τ in between τ_r and τ_{r+1}. Thus, we can express the diagonal energy of the configuration C' in terms of the kink times and ONVs of C as follows:[19]

$$E_D(C'_{\mathrm{CP}}) = \sum_{i=0}^{K'=K+1} D_{\{n^{(i)'}\}} \frac{(\tau'_{i+1} - \tau'_i)}{\beta}$$

$$= \sum_{i=0}^{r-1} D_{\{n^{(i)}\}} \frac{(\tau_{i+1} - \tau_i)}{\beta} + D_{\{n^{(r)}\}} \frac{(\tau - \tau_r)}{\beta} + D_{\{n^{(r)}\}_k^l} \frac{(\tau_{r+1} - \tau)}{\beta}$$

$$+ \sum_{i=r+2}^{q-1} D_{\{n^{(i)}\}_k^l} \frac{(\tau_{i+1} - \tau_i)}{\beta} + \sum_{i=q}^{K} D_{\{n^{(i)}\}} \frac{(\tau_{i+1} - \tau_i)}{\beta} \ .$$

Obviously, we can split $E_D(C_{\mathrm{CP}})$ in summands for the same time intervals and immediately see that all summands cancel except for those in which the ONV has changed due to the excitation from k to l. Hence, we have

$$\Delta E_D = \left(D_{\{n^{(r)}\}_k^l} - D_{\{n^{(r)}\}} \right) \frac{\tau_{r+1} - \tau}{\beta} + \sum_{i=r+2}^{q-1} \left(D_{\{n^{(i)}\}_k^l} - D_{\{n^{(i)}\}} \right) \frac{(\tau_{i+1} - \tau_i)}{\beta} \ . \tag{3.35}$$

---

[19] As before, $\{n\}_k^l$ denotes the ONV that results from $\{n\}$ by exciting a particle from the orbital k to l. Analogously, $\{n\}_k$ denotes the ONV that is obtained by removing a particle from the orbital k in $\{n\}$.

According to Eq. (3.8), the diagonal matrix element $D_{\{n^{(r)}\}}$ is given by

$$D_{\{n^{(r)}\}} = \sum_i \left(h_{ii} + \sum_{j=i+1} w^-_{ijij} n^{(r)}_j \right) n^{(r)}_i$$

$$= \underbrace{\sum_{i\neq k} \left(h_{ii} + \sum_{\substack{j=i+1 \\ j\neq k}} w^-_{ijij} n^{(r)}_j \right) n^{(r)}_i}_{=D_{\{n^{(r)}\}_k}} + \underbrace{\left(h_{kk} + \sum_{j\neq k} w^-_{kjkj} n^{(r)}_j \right)}_{=:d_{k,\{n^{(r)}\}}},$$

where, in the second line, the contribution of the $k-$th orbital $d_{k,\{n^{(r)}\}}$ to the matrix element $D_{\{n^{(r)}\}}$ has been separated. Similarly, we find that

$$D_{\{n^{(r)}\}} = D_{\{n^{(r)}\}^l_k} + d_{k,\{n^{(r)}\}} - d_{l,\{n^{(r)}\}_k} \tag{3.36}$$

with

$$d_{l,\{n^r\}_k} = h_{ll} + \sum_{j\neq l,k} w^-_{ljlj} n^{(r)}_j .$$

Inserting Eq. (3.36) into (3.35), we see that the matrix elements of the excited ONVs $D_{\{n^{(i)}\}^l_k}$ cancel

$$\Delta E_D = \left(d_{l,\{n^{(r)}\}_k} - d_{k,\{n^{(r)}\}} \right) \frac{\tau_{r+1} - \tau}{\beta} + \sum_{i=r+2}^{q-1} \left(d_{l,\{n^{(i)}\}_k} - d_{k,\{n^{(i)}\}} \right) \frac{(\tau_{i+1} - \tau_i)}{\beta} . \tag{3.37}$$

Thereby, we have reduced the complexity of the computation of the diagonal energy difference from[20] $\mathcal{O}(K \cdot N^2)$ in (3.35) to $\mathcal{O}(K \cdot N)$ in (3.37). Since we have to calculate such diagonal energy differences for every Monte Carlo step, this matters a lot.

Next, we have to consider the contribution of the kinks in $|\Delta Q|$ (cf. Eq. (3.34)). According to the Eqs. (3.26), the modulus of the kink matrix elements is given by

$$\left| \bar{q}_{\{n^{(i-1)}\},\{n^{(i)}\}}(s_i) \right| = \begin{cases} h_{ik} + \sum_{j\neq i,k} w^-_{ijkj} n^{(i)}_j & \text{if} \quad \{n^{(i)}\} = \{n^{(i-1)}\}^i_k , \quad s_i = (i,k) \\ w^-_{ijkl} & \text{if} \quad \{n^{(i)}\} = \{n^{(i-1)}\}^{i<j}_{k<l} , \quad s_i = (i,j,k,l) . \end{cases} \tag{3.38}$$

Obviously, in $|\Delta Q|$, all matrix elements cancel, except for those type 2 kinks with times in the interval (τ, τ_q), because all ONVs $\{n^{(i)}\}$ in this interval change

---

[20] Of course, in practice, we only sum over the occupied orbitals in the computation of the diagonal energy of the orbitals (cf. Eq. 3.5.1). Besides, in standard CPIMC algorithm, the computation of the diagonal energy difference is of the order $\mathcal{O}(N_B^2)$ (due to the ONV picture).

according to $\{n^{(i)}\} \rightarrow \{n^{(i)}\}^l_k$. Further, the changed kink in C_{CP} and C'_{CP} and the added kink in C'_{CP} do not cancel. For a given type 2 kink $s = (i, k)$, we address the creator orbital with $s_{[1]} = i$ and the annihilator orbital with $s_{[2]} = k$. Having introduced this notation, the fraction of kink matrix elements simplifies to

$$
|\Delta Q| = \frac{\displaystyle\prod_{i=1}^{K'} |\bar{q}_{\{n^{(i-1)'}\},\{n^{(i)'}\}}(s'_i)|}{\displaystyle\prod_{i=1}^{K} |\bar{q}_{\{n^{(i-1)}\},\{n^{(i)}\}}(s_i)|}
$$

$$
= \frac{\displaystyle\prod_{\substack{i=r+1 \\ s_i \in A}}^{q-1} |\bar{q}_{\{n^{(i-1)}\},\{n^{(i)}\}}(s_i) - w^-_{s_i[1]k s_i[2]k} + w^-_{s_i[1]l s_i[2]l}|}{\displaystyle\prod_{\substack{i=r+1 \\ s_i \in A}}^{q-1} |\bar{q}_{\{n^{(i-1)}\},\{n^{(i)}\}}(s_i)|}
$$

$$
\cdot \frac{|\bar{q}_{\{n^{(q-1)}\}^l_k,\{n^{(q)}\}}((i,l))||\bar{q}_{\{n^{(r)}\},\{n^{(r)}\}^l_k}((l,k))|}{|\bar{q}_{\{n^{(q-1)}\},\{n^{(q)}\}}((i,k))|}
$$

$$(3.39)$$

Inserting the Eqs. (3.37) and (3.39) into (3.33) yields the modulus of the weight fraction that has to be computed when proposing to add a kink as shown in Fig. 3.12. In practice, we have implemented a set of functions that handles the change of the diagonal energy for arbitrary one- and two-particle excitations on arbitrary intervals. Another set of functions computes the change of the weights of the type 2 kinks due to an excitation, where, instead of each time calculating the weights $\bar{q}_{\{n^{(i-1)}\},\{n^{(i)}\}}(s_i)$ of the type 2 kinks according to (3.38), we store them for the whole configuration. Finally, we need functions that handle the change of an existing kink due to an excitation left or right of it. For the proper implementation of these functions it is necessary to perform similar considerations for the diagrams of all steps. There are 81 in total.

3.5.2. Development of the steps

The development of the presented Monte Carlo algorithm has been quite a challenging task. Despite the implementation and debugging of the steps, it took some time for T. Schoof and me to find those steps required to be ergodic. As such, it is worth to chronologically illustrate the development process, which will explain the necessity of each presented step that result in a program consisting of twenty thousand lines of C++ code. Remember that we refer to the *former or standard CPIMC algorithm* as the CPIMC method

in the ONV picture (cf. Sec. 3.1), which is in detail described in [10, 11] and which is without a WA.

Rewriting of the WA for bosonic lattice models into a WA for continuous fermionic systems - the ergodicity problem

As already mentioned, the WA in the occupation number representation has originally been applied to bosonic lattice models [12]. For such systems, the bosonic version of the simpler steps 1-4 is sufficient to be ergodic and obtain correct results[21]. At first, to get familiar with the algorithm, T. Schoof implemented the WA for the fermionic *Hubbard* model. In case of lattice models, there are no true two-particle operators in the Hamiltonian. Thus, w_{ijkl}^- is always zero, and there are no type 4 kinks in the paths at all. Consequently, for the fermionic *Hubbard model*, correct results could be obtained with the steps 1-4. After that, T. Schoof started with the implementation of the WA for the general Hamiltonian (3.7) and added step 5, i.e., the changing of a kink with Ira. With this step, a type 2 kink can be changed into a type 4 kink and vice versa (see Fig. A.1), and so, it might have been sufficient to only add this step. Unfortunately, this was not the case as the comparison of the obtained results with an exact diagonalization method revealed a very small but significant error on the fourth decimal place in the energy. In addition, the average number of kinks in the sampled configurations turned out to be slightly smaller than that of configurations sampled with the standard CPIMC algorithm (explained in [10]). From the theory, the average number of kinks in both algorithms should be equal. Since for systems only containing type 2 kinks the average number of kinks was equal in both algorithms, most likely some type 4 kinks were missing. Indeed, suppose a certain type 4 kink can be constructed from a certain number of type 2 kinks by changing them with step 5. If all these type 2 kinks have a vanishing matrix element, then we will never sample a path containing this type 4 kink. Therefore, a step that directly proposes to add a type 4 kink, is necessary.

First attempt: Introduction of a second worm

A type two kink can be added by changing the orbital of Ira (step 4). Adding a type 4 kink with a similar step requires a second worm. Then, we can consider adding a type 4 kink as adding two type 2 kinks at the same time by moving both Iras as shown in Fig. 3.13. Formally, we have to extend the total configuration space with open paths containing two worms by performing

---

[21]In fact, for bosons, the only difference in the configurations is that in the paths the occupation numbers can be greater than 1, i.e., $n_i(\tau) \in \mathbb{N}$. Consequently, it is always possible to add the worm everywhere in the path and then move the worm in any direction, e.g., n times around the $\beta-$cylinder on the orbital i, whereby n particles are added.
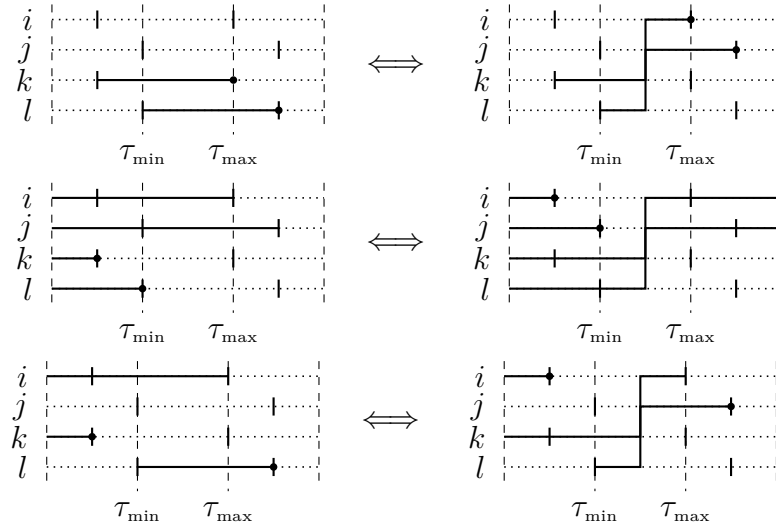
Figure 3.13.: Adding a type 4 kink by changing the orbital of both Iras can be considered as adding two type 2 kinks at the same time. The time of the new kink can be left, right or in between the times of both Iras.

a similar expansion for the two-particle MGF as shown for the one-particle MGF in Sec. 3.3. By that time, I joined in the development of the algorithm. Having properly implemented the addition and removal of a second worm and the addition and removal of type 4 kinks in those two worm configurations, we would still obtain a slightly too small average number of kinks. So the set of steps still was not ergodic.

Second attempt: Introduction of virtual kinks

Next, we utilized the concept of so called *virtual weights* or *virtual kinks*, which has already been useful in the development of the standard CPIMC algorithm by T. Schoof (see [11]). The basic idea is fairly simple. Since kinks that have a vanishing matrix element do not occur in any path, we refer to those as *forbidden kinks*. In the simulation, we can artificially assign the same, very small but finite matrix element to every forbidden kink, e.g., 10^{-10}. Then, in some configurations of the Markov chain, generated with our Monte Carlo steps, the former forbidden kinks are realized, and we refer to them as *virtual kinks* with a virtual matrix element. Configurations containing one or more virtual kinks are called virtual configurations. When ignoring all these virtual configurations of the Markov chain in the sampling of observables, the obtained results are still correct since sequences of virtual configurations in the Markov chain can be considered as macro updates for the non-virtual configurations.

The implementation of virtual kinks made the WA ergodic, and the obtained results were correct. Surprisingly, the average number of kinks of the WA with
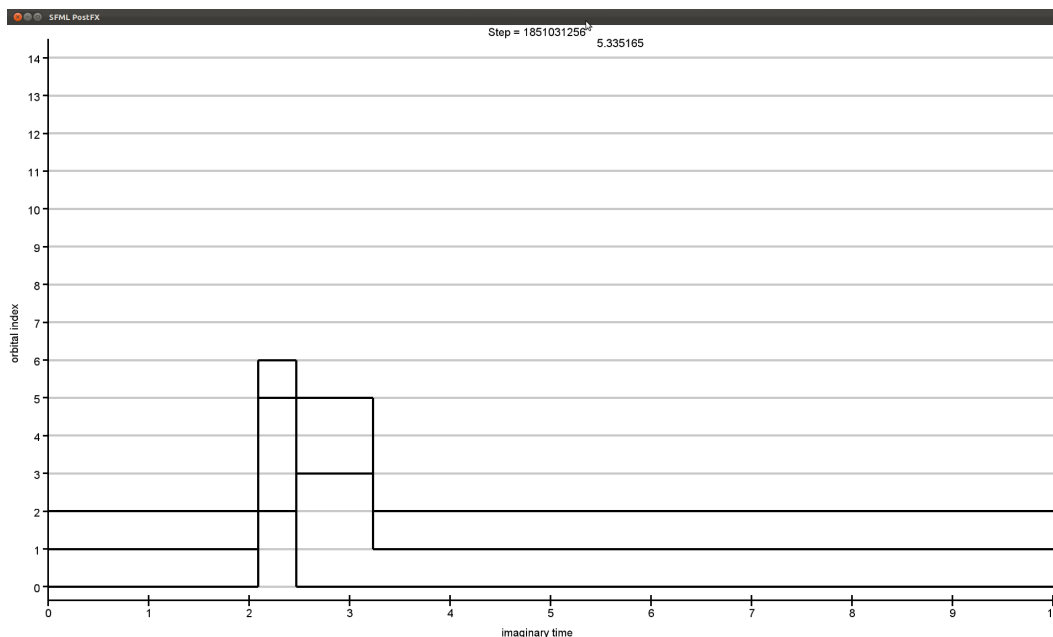
Figure 3.14.: Graphical output of the program: Missing configuration for a simulation (without virtual kinks) of 3 particles in 15 basis functions at an inverse temperature of $\beta = 10$. The y-axis denotes the orbitals (0-14), whereas the x-axis represents the imaginary time $\tau \in [0, \beta]$. Since there are three particles, at each time of the path, exactly three orbitals are occupied.

virtual kinks perfectly coincided with that of the standard CPIMC algorithm without virtual kinks. Hence, the Monte Carlo steps of the former algorithm allow for the construction of single kinks or combinations of these that were missing in the WA without virtual kinks. Unfortunately, simulations with virtual weights are likely to become unstable and inefficient when spending too long times in virtual configurations since these do not count for the sampling process. Therefore, the missing paths in the WA had to be found, and then, appropriate steps that allow for the construction of those configurations had to be designed.

Solution: Rewrite the steps of the standard CPIMC algorithm

Since we knew the problem was connected to the type 4 kinks only, we used a test Hamiltonian only consisting of type 4 kinks. First, we checked if all non-forbidden kinks would be realized in simulations without virtual kinks. This was the case, and hence, we were missing some more complex constructions of kinks. Then, we did simulations for a very small system, i.e., three particles in 15 basis functions, and restricted the maximum number of kinks to 3. For this small system, a unique number could be assigned to every possible path.

We first performed a long simulation with virtual weights and then without, where, for both simulations, all occurring, pairwise different configurations were stored. After comparing these configurations, we could eventually find those that were missing in simulations without virtual kinks. Fig. 3.14 shows the graphical output of the program for such a missing configuration. As expected, it turned out that these could only be constructed by first adding a virtual type 4 kink, then doing some intermediate steps, and afterwards removing the virtual kink. We could not find a simple step that would fix this problem, and thus, we transformed the steps of the standard CPIMC algorithm into the kink picture. After implementing the steps 7 and 8 of adding and removing a kink via a one- or two-particle excitation, we finally obtained correct results for the observables and the average kink number even without the second worm. Therefore, the steps 1-8 are sufficient to be ergodic. For simulations in the closed path only, i.e., without worm, we additionally had to implement the steps 9-13. In that case, especially adding a pair of type 2 or 4 kinks is required since there are no closed paths with only one kink. Further, the excitation of a whole orbital in step 12 is necessary if there are orbitals that are not part of any type 2 kink. Finally, the changing of two kinks via a one- or two-particle excitations (step 12 and 13) has been implemented since we could reuse a lot of code from step 7 and, in the majority of cases, more different Monte Carlo steps reduce the auto-correlation time of the samples. Thus, the steps 7-12 can be used for the simulation of systems in the canonical ensemble.

Due to the more sophisticated choice of the proposed excitations in the CPIMC WA, the acceptance probabilities could be improved by a factor 2 to 4 compared to that of the standard CPIMC algorithm (without WA). In combination with a more efficient programming, this leads to a speed up at least of the order $\mathcal{O}(10)$, which strongly increases with the system size, i.e., with the number of basis function N_B. However, the acceptance probabilities are still small so that we have to perform 10^3 to $4 \cdot 10^3$ Monte Carlo steps (cycles) to obtain a sufficiently small auto-correlation time.

4. Estimators

After we have defined the configuration space to be sampled and explained the Monte Carlo steps, it remains to derive the estimators[1] for the quantities of interest. Before, some general remarks on the sampling of quantities should be made: Performing Metropolis Monte Carlo with the steps described in Sec 3.5, generates a Markov chain consisting of closed and open paths of varying particle number. According to the partition function of the total configuration space Z'_{Tot} (see Eq. (3.28)), the sampled closed paths are distributed with the probability $\frac{|W_{\mathrm{CP}}(C_{\mathrm{CP}})|}{Z'_{\mathrm{Tot}}}$, whereas open paths are distributed with $\bar{w}\frac{|W_{\mathrm{OP}}(C_{\mathrm{OP}})|}{Z'_{\mathrm{Tot}}}$ in the Markov chain. However, we can also ignore all closed paths in this Markov chain and interpret these as a macro Monte Carlo update for the open paths. Then, the remaining Markov chain consists of open paths distributed with $\frac{|W_{\mathrm{OP}}(C_{\mathrm{OP}})|}{Z'_{\mathrm{OP}}}$, regardless of the actual value of the constant[2] $\bar{w}$. Similarly, ignoring the open paths, the sampled closed paths are distributed with $\frac{|W_{\mathrm{CP}}(C_{\mathrm{CP}})|}{Z'_{\mathrm{CP}}}$. Moreover, the same holds true for closed paths with a certain particle number N'. When only taking into account those closed paths with particle number N', these are distributed with $\frac{|W_{\mathrm{CP}}(C_{\mathrm{CP}})|}{Z'_{\mathrm{CP}}(N=N')}$. For that reason, we can use a different length of Monte Carlo cycles N_{cycle} (see Sec. 2.1) for quantities that either receive a contribution from closed paths, open paths, or closed paths with a given particle number. In other words, we sample canonical quantities, grand canonical quantities and the MGF in one simulation.

4.1. Estimators of thermodynamic observables

To find an estimator for an observable, we have to write its expectation value in the form of Eq. (2.1), where, for the partition function, we use the expansion (3.18). It is straightforward to do this by utilizing the standard relations of statistical physics between expectation values and the partition function. For the expectation value of the total energy of a system in the canonical ensemble, we have to differentiate the canonical partition function with respect to the inverse temperature β, i.e., $\langle \hat{H} \rangle = -\frac{1}{Z_{\mathrm{CP}}}\frac{\partial Z_{\mathrm{CP}}}{\partial \beta}$. To perform the differentiation,

---

[1]The notion estimator has been introduced in Sec. 2.1.

[2]Of course, for extremely large or small values of $\bar{w}$, we (practically) either sample only closed or open paths.

4. Estimators

we substitute $\tau_i = \beta t_i$ and $\mathrm{d}\tau_i = \beta \mathrm{d}t_i$ in the closed path partition function (3.18) and obtain

$$Z_{\mathrm{CP}} = \sum_{\substack{K=0, \\ K \neq 1}}^{\infty} \sum_{\{n\}} \sum_{s_1} \sum_{s_2} \cdots \sum_{s_{K-1}} \int_0^1 \mathrm{d}t_1 \int_{t_1}^1 \mathrm{d}t_2 \cdots \int_{t_{K-1}}^1 \mathrm{d}t_K$$

$$(-\beta)^K \exp\left\{-\beta \sum_{i=0}^K D_{\{n^{(i)}\}}(t_{i+1} - t_i)\right\} \prod_{i=1}^K \bar{q}_{\{n^{(i)}\}\{n^{(i-1)}\}}(s_i) \ .$$

Computing the partial derivative of this expression with respect to β and then back substituting, yields

$$\langle \hat{H} \rangle = \frac{1}{Z_{\mathrm{CP}}} \sum_{\substack{K=0, \\ K \neq 1}}^{\infty} \sum_{\{n\}} \sum_{s_1} \sum_{s_2} \cdots \sum_{s_{K-1}} \int_0^\beta \mathrm{d}\tau_1 \int_{\tau_1}^\beta \mathrm{d}\tau_2 \cdots \int_{\tau_{K-1}}^\beta \mathrm{d}\tau_K$$

$$\left(\frac{-K}{\beta} + \sum_{i=0}^K D_{\{n^{(i)}\}} \frac{(\tau_{i+1} - \tau_i)}{\beta}\right)$$

$$\cdot (-1)^K \exp\left\{-\sum_{i=0}^K D_{\{n^{(i)}\}}(\tau_{i+1} - \tau_i)\right\} \prod_{i=1}^K \bar{q}_{\{n^{(i)}\}\{n^{(i-1)}\}}(s_i)$$

$$= \oint_{C_{\mathrm{CP}}} \left(\frac{-K}{\beta} + \sum_{i=0}^K D_{\{n^{(i)}\}} \frac{(\tau_{i+1} - \tau_i)}{\beta}\right) \frac{W_{\mathrm{CP}}(C_{\mathrm{CP}})}{Z_{\mathrm{CP}}} \ ,$$

which is the desired form (2.1). We can identify the corresponding estimator of the total energy

$$E(C_{\mathrm{CP}}) = \frac{-K}{\beta} + \sum_{i=0}^K D_{\{n^{(i)}\}} \frac{(\tau_{i+1} - \tau_i)}{\beta} \ . \tag{4.1}$$

Thus, the energy of a closed path C_{CP} is given by $E(C_{\mathrm{CP}})$, where all realized ONVs $\{n^{(i)}\}$ contribute with their corresponding diagonal matrix element weighted with the relative (time) length of the ONV in the path. Interestingly, the off-diagonal contribution is only given by the number of kinks in the path divided by the inverse temperature β, i.e., the actual values of the kink matrix elements do not enter directly in the total energy of the path.

In case of the grand canonical closed path partition function (3.26), where $D_{\{n^{(i)}\}}$ is replaced by $\bar{D}_{\{n^i\}} = D_{\{n^{(i)}\}} + \mu N_{\{n^{(i)}\}}$ and the summation over the first ONV is not restricted to a fixed particle number, we obtain exactly the same estimator (4.1) for the total energy because the partial differentiation with respect to β is carried out for $\mu\beta =$ const.

Next, we consider the expectation value of the one-particle density matrix in the canonical ensemble

$$n_{pq} = \langle \hat{a}_p^\dagger \hat{a}_q \rangle = \frac{1}{Z} \mathrm{Tr}\left\{\hat{a}_p^\dagger \hat{a}_q e^{-\beta \hat{H}}\right\} \ .$$

After inserting the general second quantized Hamiltonian (3.7), we can express this expectation value in terms of a partial derivative of the partition function with respect to the one-particle integrals

$$n_{pq} = \frac{1}{Z} \text{Tr} \left\{ \hat{a}_p^\dagger \hat{a}_q e^{-\beta \left(\sum_{i,j} h_{ij} \hat{a}_i^\dagger \hat{a}_j + \sum_{i<j,k<l} w_{ijkl}^- \hat{a}_i^\dagger \hat{a}_j^\dagger \hat{a}_l \hat{a}_k \right)} \right\}$$

$$= -\frac{1}{\beta} \frac{1}{Z} \frac{\partial Z}{\partial h_{pq}} \ .$$

Carrying out the differentiation for the closed path partition function (3.18) for $p = q$, we obtain the estimator of the average occupation number of the $p-$th one-particle orbital

$$\langle \hat{n}_p \rangle = d_{pp} = \oint\limits_{C_{\text{CP}}} \underbrace{\left(\sum_{i=0}^{K} n_p^{(i)} \frac{(\tau_{i+1} - \tau_i)}{\beta} \right)}_{n_p(C_{\text{CP}})} \frac{W_{\text{CP}}(C_{\text{CP}})}{Z_{\text{CP}}} \ ,$$

where the estimator can be rewritten as

$$n_p(C_{\text{CP}}) = \frac{1}{\beta} \int_0^\beta n_p(\tau) \mathrm{d}\tau \ , \tag{4.2}$$

which is the average occupation of the $p-$th orbital in the closed path C_{CP}. For the off-diagonal elements of the one-particle density matrix, the differentiation leads to the estimator

$$n_{pq}(C_{\text{CP}}) = -\frac{1}{\beta} \sum_{i=1}^{K} \frac{1}{h_{pq} + \sum_{j \neq p,q} w_{pjqj}^- n_j^{(i)}} \delta_{s_i,(p,q)} \ . \tag{4.3}$$

That means, we get a contribution of one over the corresponding kink matrix element without phase factor for all type 2 kinks s_i in the path with $s_i = (p,q)$.

Obviously, for the grand canonical ensemble, where we sum over closed paths of all particle numbers, the estimators for the elements of the one-particle density matrix are also given by Eq. (4.2) and (4.3).

Note that, as described in Sec 2.1, we can only sample closed paths distributed with $\frac{|W_{\text{CP}}(C_{\text{CP}})|}{Z'_{\text{CP}}}$ and then calculate the expectation values according to Eq. (2.7).

4.2. Estimators of the MGF

After having developed an ergodic set of the Monte Carlo steps, the next major part of this work consists of finding a sufficiently fast converging estimator for the MGF.

At first, we derive the trivial estimator for the MGF and explicitly take into account the sign of the sampled paths. Apart from some other disadvantages,

this estimator, in practice, introduces a discretization error. Therefore, we developed an estimator that does not require a discretization. Unfortunately, this estimator produces poor results due to a bad convergence with the number of samples. To speed up the convergence, we utilized an idea that significantly improves the estimator of the MGF in the DPIMC method [17]. In the case of CPIMC, the improvement turns out to be insignificant. Eventually, from the obtained results of the first two estimators (without a discretization error), the ideas can be combined yielding an estimator with a much better convergence.

4.2.1. The trivial estimator

From the definition of the open path partition function (cf. Eqs. (3.26)), it directly follows that the MGF $Z_{\mathrm{CP}}\mathcal{G}_{i'j'}(\tau'_{\mathrm{ir}}, \tau'_{\mathrm{ma}})$ is given by the summation over all weights of open paths with Ira on the orbital i' at time τ'_{ir} and Masha on the orbital j' at time τ'_{ma}

$$Z_{CP}\mathcal{G}_{i'j'}(\tau'_{\mathrm{ir}}, \tau'_{\mathrm{ma}}) = \sum_{C_{\mathrm{CP}}} \!\!\!\!\!\!\!\!\diagdown\,\, W_{\mathrm{OP}}(C_{\mathrm{CP}}, i', j', \tau'_{\mathrm{ir}}, \tau'_{\mathrm{ma}}) \qquad (4.4)$$

where

$$\left(C_{\mathrm{CP}}, i', j', \tau'_{\mathrm{ir}}, \tau'_{\mathrm{ma}}\right) = \left(\{n\}, \tau'_{\mathrm{ir}}, \tau'_{\mathrm{ma}}, \tau_1, \ldots, \tau_K, i', j', s_1, \ldots, s_K\right),$$

In other words, the summation only goes over the closed path degree of freedom of the open paths since the worm ends are fixed to the arguments of the MGF. Therefore, we easily obtain an estimator for the MGF by adding the summation over the worm ends and compensate this with delta functions[3] and Kronecker deltas

$$\mathcal{G}_{i'j'}(\tau'_{\mathrm{ir}}, \tau'_{\mathrm{ma}}) = \frac{1}{Z_{\mathrm{CP}}} \sum_{C_{\mathrm{CP}}} \!\!\!\!\!\!\!\!\diagdown\,\, \sum_{i,j} \int_0^\beta \mathrm{d}\tau_{\mathrm{ir}} \int_0^{'\beta} \mathrm{d}\tau_{\mathrm{ma}} \delta_{i,i'}\delta_{j,j'}\delta(\tau_{\mathrm{ir}}, \tau'_{\mathrm{ir}})\delta(\tau_{\mathrm{ma}}, \tau'_{\mathrm{ma}})W_{\mathrm{OP}}(C_{\mathrm{OP}})$$

$$= \frac{Z_{\mathrm{OP}}}{Z_{\mathrm{CP}}} \sum_{C_{\mathrm{OP}}} \!\!\!\!\!\!\!\!\diagdown\,\, \left(\delta_{i,i'}\delta_{j,j'}\delta(\tau_{\mathrm{ir}}, \tau'_{\mathrm{ir}})\delta(\tau_{\mathrm{ma}}, \tau'_{\mathrm{ma}})\right) \frac{W_{\mathrm{OP}}(C_{\mathrm{OP}})}{Z_{\mathrm{OP}}}$$

$$= \langle \delta_{i,i'}\delta_{j,j'}\delta(\tau_{\mathrm{ir}}, \tau'_{\mathrm{ir}})\delta(\tau_{\mathrm{ma}}, \tau'_{\mathrm{ma}})\rangle_{\mathrm{OP}} \ .$$

In analogy to the closed paths, we can sample only open paths distributed with $\frac{|W_{\mathrm{OP}}(C_{\mathrm{OP}})|}{Z'_{\mathrm{OP}}}$ (cf. Eq. (3.28)), and hence, we have to rewrite the expectation value

---

[3]To shorten the notation, we write the delta functions as $\delta(x, x') := \delta(x - x')$.

of the MGF analog to Eq. (2.7)

$$
\mathcal{G}_{i'j'}(\tau'_{\mathrm{ir}}, \tau'_{\mathrm{ma}}) = \frac{Z_{\mathrm{OP}}}{Z_{\mathrm{CP}}} \frac{\displaystyle\sum_{C_{\mathrm{OP}}} (\delta_{i,i'}\delta_{j,j'}\delta(\tau_{\mathrm{ir}}, \tau'_{\mathrm{ir}})\delta(\tau_{\mathrm{ma}}, \tau'_{\mathrm{ma}})S_{\mathrm{OP}}(C_{\mathrm{OP}}))) \frac{|W_{\mathrm{OP}}(C_{\mathrm{OP}})|}{Z'_{\mathrm{OP}}}}{\displaystyle\sum_{C_{\mathrm{OP}}} S_{\mathrm{OP}}(C_{\mathrm{OP}}) \frac{|W_{\mathrm{OP}}(C_{\mathrm{OP}})|}{Z'_{\mathrm{OP}}}}
$$

$$
= \frac{Z_{\mathrm{OP}}}{Z_{\mathrm{CP}}} \frac{\langle \delta_{i,i'}\delta_{j,j'}\delta(\tau_{\mathrm{ir}}, \tau'_{\mathrm{ir}})\delta(\tau_{\mathrm{ma}}, \tau'_{\mathrm{ma}})S_{\mathrm{OP}}\rangle'_{\mathrm{OP}}}{\langle S_{\mathrm{OP}}\rangle'_{\mathrm{OP}}} \ , \tag{4.5}
$$

where $S_{\mathrm{OP}}(C_{\mathrm{OP}}) = \mathrm{sgn}(W_{\mathrm{OP}}(C_{\mathrm{OP}}))$ is the sign of the open path weight function $W_{\mathrm{OP}}(C_{\mathrm{OP}})$. The prefactor consisting of the fraction of the open and closed path partition functions has to be sampled separately[4]. For that purpose, we express it in terms of averages over the actually sampled paths

$$
\frac{Z_{\mathrm{OP}}}{Z_{\mathrm{CP}}} = \frac{\displaystyle\sum_{C_{\mathrm{OP}}} W_{\mathrm{OP}}(C_{\mathrm{OP}})}{\displaystyle\sum_{C_{\mathrm{CP}}} W_{\mathrm{CP}}(C_{\mathrm{CP}})} = \frac{Z'_{\mathrm{OP}}}{Z'_{\mathrm{CP}}} \frac{\displaystyle\sum_{C_{\mathrm{OP}}} S_{\mathrm{OP}}(C_{\mathrm{OP}}) \frac{|W_{\mathrm{OP}}(C_{\mathrm{OP}})|}{Z'_{\mathrm{OP}}}}{\displaystyle\sum_{C_{\mathrm{CP}}} S_{\mathrm{CP}}(C_{\mathrm{CP}}) \frac{|W_{\mathrm{CP}}(C_{\mathrm{CP}})|}{Z'_{\mathrm{CP}}}} = \frac{Z'_{\mathrm{OP}}}{Z'_{\mathrm{CP}}} \frac{\langle S_{\mathrm{OP}}\rangle'_{\mathrm{OP}}}{\langle S_{\mathrm{CP}}\rangle'_{\mathrm{CP}}} \ .
$$
$$
\tag{4.6}
$$

The fraction of the primed partition functions can be further rewritten as

$$
\frac{Z'_{\mathrm{OP}}}{Z'_{\mathrm{CP}}} = \frac{\displaystyle\sum_{C_{\mathrm{OP}}} |W_{\mathrm{OP}}(C_{\mathrm{OP}})|}{\displaystyle\sum_{C_{\mathrm{CP}}} |W_{\mathrm{CP}}(C_{\mathrm{CP}})|} = \frac{\displaystyle\sum_{C_{\mathrm{Tot}}} \delta_{\mathrm{OP}}(C_{\mathrm{Tot}}) \frac{1}{\bar{w}} \frac{|W_{\mathrm{Tot}}(C_{\mathrm{Tot}})|}{Z'_{\mathrm{Tot}}}}{\displaystyle\sum_{C_{\mathrm{Tot}}} \delta_{\mathrm{CP}}(C_{\mathrm{Tot}}) \frac{|W_{\mathrm{Tot}}(C_{\mathrm{Tot}})|}{Z'_{\mathrm{Tot}}}} = \frac{1}{\bar{w}} \frac{\langle \delta_{\mathrm{OP}}\rangle'_{\mathrm{Tot}}}{\langle \delta_{CP}\rangle'_{\mathrm{Tot}}} \ ,
$$
$$
\tag{4.7}
$$

where $C_{\mathrm{Tot}} \in \{C_{\mathrm{CP}}\} \cup \{C_{\mathrm{OP}}\}$, i.e., the summation goes over all closed and open paths, and we used the following notations

$$
W_{\mathrm{Tot}}(C_{\mathrm{Tot}}) = \begin{cases} \bar{w} W_{\mathrm{OP}}(C_{\mathrm{Tot}}) & \text{if} \quad C_{\mathrm{Tot}} \in \{C_{\mathrm{OP}}\} \\ W_{\mathrm{CP}}(C_{\mathrm{Tot}}) & \text{if} \quad C_{\mathrm{Tot}} \in \{C_{\mathrm{CP}}\} \end{cases} \ ,
$$

$$
\delta_{\mathrm{CP}}(C_{\mathrm{Tot}}) = \begin{cases} 1 & \text{if} \quad C_{\mathrm{Tot}} \in \{C_{\mathrm{CP}}\} \\ 0 & \text{else} \end{cases} \ , \quad \delta_{\mathrm{OP}}(C_{\mathrm{Tot}}) = \begin{cases} 1 & \text{if} \quad C_{\mathrm{Tot}} \in \{C_{\mathrm{OP}}\} \\ 0 & \text{else} \end{cases} \ .
$$

Hence, $\frac{\langle \delta_{\mathrm{OP}}\rangle'_{\mathrm{Tot}}}{\langle \delta_{CP}\rangle'_{\mathrm{Tot}}}$ is estimated by the fraction of the total number of open to the total number of closed paths in the sampled Markov chain. Inserting Eqs. (4.6) and (4.7) into Eq. (4.5), we obtain an estimator for the MGF that can actually be sampled

$$
\mathcal{G}_{i'j'}(\tau'_{\mathrm{ir}}, \tau'_{\mathrm{ma}}) = \frac{1}{\bar{w}} \frac{\langle \delta_{\mathrm{OP}}\rangle'_{\mathrm{Tot}}}{\langle \delta_{CP}\rangle'_{\mathrm{Tot}}} \frac{\langle \delta_{i,i'}\delta_{j,j'}\delta(\tau_{\mathrm{ir}}, \tau'_{\mathrm{ir}})\delta(\tau_{\mathrm{ma}}, \tau'_{\mathrm{ma}})S_{\mathrm{OP}}\rangle'_{\mathrm{OP}}}{\langle S_{\mathrm{CP}}\rangle'_{\mathrm{CP}}} \ , \tag{4.8}
$$

---

[4] In the DPIMC WA for bosons, the normalization of the MGF is automatically included when interpreting the MGF as a quantity in the total configuration space. For fermions, where paths can only be sampled according to the modulus weights, this is not correct, and the normalization has to be sampled in terms of a total configuration quantity, both, in the DPIMC and CPIMC WA.

where we notice that, instead of dividing by the average sign of the open paths, we now divide by the average sign of the closed paths[5]. This cancellation is the reason for explicitly taking into account the sign in the derivation of the MGF estimator (in contrast to the derivation of the estimators for the thermodynamic observables in the previous Sec. 4.1). Strictly speaking, Eq. (4.8) is not one estimator but consists of four estimators. However, it has an obvious drawback: In practice, we have to replace the delta functions for the continuous times by

$$\delta(\tau, \tau') \to \delta_B(\tau, \tau') = \begin{cases} \frac{1}{B} & \text{if} \quad \tau \in [\tau' - \frac{B}{2}, \tau' + \frac{B}{2}] \\ 0 & \text{else.} \end{cases}$$

Otherwise, we would never get a contribution to the estimator in the numerator (4.8). This introduces a discretization error, which can be reduced by minimizing B (the bin width). Thereby, the number of samples for that time point is reduced, which, in turn, enhances the statistical error. In addition, due to the exponential time dependence of the MGF, an exponential rather than an equidistant grid should be used for the time points at which the MGF is sampled. Further, in Eq. (4.8), we have not taken advantage of the MGF being homogeneous in time (cf. Eq. (3.20)). Hence, we actually want to sample the MGF $\mathcal{G}_{i'j'}(\tau_p, 0)$ at time points τ_p with $p = 0 \dots N_p$. Due to the anti-periodicity with respect to shifts of β (cf. Eq. (3.21)), we only have to sample the MGF at time points $\tau_p \in (0, \beta]$.

4.2.2. First estimator without discretization error

Next, an estimator for $\mathcal{G}_{i'j'}(\tau_p, 0)$ without a discretization is derived. Utilizing Eq. (3.20), it is

$$\mathcal{G}_{i'j'}(\tau_p, 0) = \mathcal{G}_{i'j'}(\tau_p + \tau', \tau') \quad \text{with} \quad \tau_p, \tau' \in [0, \beta]. \tag{4.9}$$

Since $\mathcal{G}_{i'j'}(\tau, 0)$ is only defined for $\tau \in (0, \beta]$, the r.h.s. is defined by

$$\mathcal{G}_{i'j'}(\tau_p + \tau', \tau') := \begin{cases} \mathcal{G}_{i'j'}(\tau_p + \tau', \tau') & \text{if} \quad (\tau_p + \tau') \leq \beta \\ -\mathcal{G}_{i'j'}(\tau_p + \tau' - \beta, \tau') & \text{if} \quad (\tau_p + \tau') > \beta \,. \end{cases}$$

---

[5]Actually, this is surprising since the MGF represents an open path quantity and as such, we would expect that we have to divide by the average sign of the open paths as in Eq. (4.5), thereby enhancing the statistical error of the nominator by one over the average open path sign. Fortunately, it is always $\langle S_{\text{CP}} \rangle'_{\text{CP}} \geq \langle S_{\text{OP}} \rangle'_{\text{OP}}$, for in the open paths there are always two more kinks, namely Ira and Masha, each contributing with a sign changing phase factor.

The r.h.s. in Eq. (4.9) does not depend on τ', and it follows

$$
\begin{aligned}
\mathcal{G}_{i'j'}(\tau_p, 0) &= \frac{1}{\beta} \int_0^\beta \mathrm{d}\tau_{\mathrm{ma}} \mathcal{G}_{i'j'}(\tau_p + \tau_{\mathrm{ma}}, \tau_{\mathrm{ma}}) \\
&= \frac{1}{Z_{\mathrm{CP}}} \frac{1}{\beta} \oint_{C_{\mathrm{CP}}} \sum_{i,j} \int_0^\beta \mathrm{d}\tau_{\mathrm{ma}} \delta_{i,i'} \delta_{j,j'} W_{\mathrm{OP}}(C_{\mathrm{CP}}, i, j, \tau_p + \tau_{\mathrm{ma}}, \tau_{\mathrm{ma}}) \,,
\end{aligned}
$$

$$(4.10)$$

where in the second line Eq. (4.4) has been inserted for the integrand. Now we employ the simple fact that for $a \neq 0$ it is $a = \frac{a}{b}b$ if $b \neq 0$. Using the abbreviation $\widetilde{C} = (C_{\mathrm{CP}}, i, j)$, it is

$$
W_{\mathrm{OP}}(\widetilde{C}, \tau_p + \tau_{\mathrm{ma}}, \tau_{\mathrm{ma}}) = \frac{1}{L_{\mathrm{ir}}(\widetilde{C}, \tau_{\mathrm{ma}})} \int_0^\beta \mathrm{d}\tau_{\mathrm{ir}} \frac{W_{\mathrm{OP}}(\widetilde{C}, \tau_p + \tau_{\mathrm{ma}}, \tau_{\mathrm{ma}})}{W_{\mathrm{OP}}(\widetilde{C}, \tau_{\mathrm{ir}}, \tau_{\mathrm{ma}})} W_{\mathrm{OP}}(\widetilde{C}, \tau_{\mathrm{ir}}, \tau_{\mathrm{ma}}),
$$

where

$$
L_{\mathrm{ir}}(\widetilde{C}, \tau_{\mathrm{ma}}) = \int_0^\beta \mathrm{d}\tau_{\mathrm{ir}} \Theta_0(|W_{\mathrm{OP}}(\widetilde{C}, \tau_{\mathrm{ir}}, \tau_{\mathrm{ma}})|) \,, \tag{4.11}
$$

$$
\Theta_0(x) := \begin{cases} 1 & \text{if } x > 0 \\ 0 & \text{else,} \end{cases}
$$

i.e., in a given open path $(C_{\mathrm{CP}}, i, j, \tau_{\mathrm{ir}}, \tau_{\mathrm{ma}})$, we can interpret $L_{\mathrm{ir}}(C_{\mathrm{CP}}, i, j, \tau_{\mathrm{ma}})$ as the length of the interval where Ira can be shifted without vanishing of the resulting weight. This interval is determined by the time of the next left and right kink on the orbital i with respect to τ_{ir}. Inserting Eq. (4.11) into (4.10), yields

$$
\begin{aligned}
\mathcal{G}_{i'j'}(\tau_p, 0) &= \frac{1}{\beta} \frac{1}{Z_{\mathrm{CP}}} \sum_{C_{\mathrm{CP}}} \sum_{i,j} \int_0^\beta \mathrm{d}\tau_{\mathrm{ir}} \int_0^\beta \mathrm{d}\tau_{\mathrm{ma}} \frac{\delta_{i,i'} \delta_{j,j'}}{L_{\mathrm{ir}}(\widetilde{C}, \tau_{\mathrm{ma}})} \\
&\qquad\qquad\qquad\qquad \cdot \frac{W_{\mathrm{OP}}(\widetilde{C}, \tau_p + \tau_{\mathrm{ma}}, \tau_{\mathrm{ma}})}{W_{\mathrm{OP}}(\widetilde{C}, \tau_{\mathrm{ir}}, \tau_{\mathrm{ma}})} W_{\mathrm{OP}}(\widetilde{C}, \tau_{\mathrm{ir}}, \tau_{\mathrm{ma}}) \\
&= \frac{1}{\beta} \frac{Z_{\mathrm{OP}}}{Z_{\mathrm{CP}}} \oint_{C_{\mathrm{OP}}} \left(\frac{\delta_{i,i'} \delta_{j,j'}}{L_{\mathrm{ir}}(\widetilde{C}, \tau_{\mathrm{ma}})} \frac{W_{\mathrm{OP}}(\widetilde{C}, \tau_p + \tau_{\mathrm{ma}}, \tau_{\mathrm{ma}})}{W_{\mathrm{OP}}(\widetilde{C}, \tau_{\mathrm{ir}}, \tau_{\mathrm{ma}})} \right) \frac{W_{\mathrm{OP}}(\widetilde{C}, \tau_{\mathrm{ir}}, \tau_{\mathrm{ma}})}{Z_{\mathrm{OP}}} \\
&= \frac{1}{\beta} \frac{Z_{\mathrm{OP}}}{Z_{\mathrm{CP}}} \left\langle \frac{\delta_{i,i'} \delta_{j,j'}}{L_{\mathrm{ir}}(\widetilde{C}, \tau_{\mathrm{ma}})} \frac{W_{\mathrm{OP}}(\widetilde{C}, \tau_p + \tau_{\mathrm{ma}}, \tau_{\mathrm{ma}})}{W_{\mathrm{OP}}(\widetilde{C}, \tau_{\mathrm{ir}}, \tau_{\mathrm{ma}})} \right\rangle_{\mathrm{OP}} \,.
\end{aligned}
$$

Obviously, the fraction of weights in the estimator is related to the acceptance probability of moving Ira in time (cf. Eq. (3.32)) in the sampled closed path

4. Estimators

$C_{\mathrm{OP}} = (C_{\mathrm{CP}}, i, j, \tau_{\mathrm{ir}}, \tau_{\mathrm{ma}})$ to $C'_{\mathrm{OP}} = (C_{\mathrm{CP}}, i, j, \tau_p + \tau_{\mathrm{ma}}, \tau_{\mathrm{ma}})$ according to

$$A_{\mathrm{MIT}}\Big(C_{\mathrm{OP}} \to C'_{\mathrm{OP}} = (\widetilde{C}, \tau_p + \tau_{\mathrm{ma}}, \tau_{\mathrm{ma}})\Big) = \min\left\{1, \left|\frac{W_{\mathrm{OP}}(\widetilde{C}, \tau_p + \tau_{\mathrm{ma}}, \tau_{\mathrm{ma}})}{W_{\mathrm{OP}}(\widetilde{C}, \tau_{\mathrm{ir}}, \tau_{\mathrm{ma}})}\right|\right\}$$

$$=: \min\left\{1, \left|\widetilde{A}_{\mathrm{MIT}, C_{\mathrm{OP}}}\Big(\tau_{\mathrm{ir}} \to \tau_p + \tau_{\mathrm{ma}}\Big)\right|\right\} \;,$$

whereby the notation $\widetilde{A}_{\mathrm{MIT}, C_{\mathrm{OP}}}$ is introduced for the fraction of weights corresponding to shifting Ira from τ_{ir} to $\tau_p + \tau_{\mathrm{ma}}$ in the open path C_{OP}. In fact, the length $L_{\mathrm{ir}}(\widetilde{C}, \tau_{\mathrm{ma}})$ of the interval where Ira is allowed to be shifted is nothing but the length $L_{\widetilde{A}_{\mathrm{MIT}, C_{\mathrm{OP}}}}$ of the interval where $\widetilde{A}_{\mathrm{MIT}, C_{\mathrm{OP}}}$ does not vanish. Thus, we have

$$\mathcal{G}_{i'j'}(\tau_p, 0) = \frac{1}{\beta}\frac{Z_{\mathrm{OP}}}{Z_{\mathrm{CP}}}\left\langle \frac{\delta_{i,i'}\delta_{j,j'}}{L_{\widetilde{A}_{\mathrm{MIT}, C_{\mathrm{OP}}}}} \widetilde{A}_{\mathrm{MIT}, C_{\mathrm{OP}}}\Big(\tau_{\mathrm{ir}} \to \tau_p + \tau_{\mathrm{ma}}\Big)\right\rangle_{\mathrm{OP}} .$$

$$(4.12)$$

Inserting relation (4.6) for the fraction of the closed to the open path partition function and rewriting Eq. (4.12) for the sampling of open paths according to the modulus weights, we finally end up with

$$\mathcal{G}_{i'j'}(\tau_p, 0) = \underbrace{\frac{1}{\bar{w}\beta\,\langle S_{\mathrm{CP}}\rangle'_{\mathrm{CP}}}\frac{\langle \delta_{\mathrm{OP}}\rangle'_{\mathrm{Tot}}}{\langle \delta_{CP}\rangle'_{\mathrm{Tot}}}}_{=:\,\mathcal{N}_{\mathcal{G}}}\left\langle \underbrace{\frac{\delta_{i,i'}\delta_{j,j'}}{L_{\widetilde{A}_{\mathrm{MIT}, C_{\mathrm{OP}}}}}\widetilde{A}_{\mathrm{MIT}, C_{\mathrm{OP}}}(\tau_{\mathrm{ir}} \to \tau_p + \tau_{\mathrm{ma}})S_{\mathrm{OP}}}_{=:\,\mathcal{G}^{[\mathrm{est}\,1]}_{i',j',\tau_p}(C_{\mathrm{OP}})}\right\rangle'_{\mathrm{OP}}$$

$$= \mathcal{N}_{\mathcal{G}}\left\langle \mathcal{G}^{[\mathrm{est}\,1]}_{i',j',\tau_p}(C_{\mathrm{OP}})\right\rangle'_{\mathrm{OP}} . \tag{4.13}$$

In contrast to (4.8), this estimator has no discretization error. Assuming we have generated a Markov chain of open paths $\{C_{\mathrm{OP},m}\}$ of length $N_{\mathrm{MC,OP}}$ distributed with $\frac{|W_{\mathrm{OP}}(C_{\mathrm{OP}})|}{Z'_{\mathrm{OP}}}$, then (4.13) is estimated according to

$$\mathcal{G}_{i'j'}(\tau_p, 0) \approx \mathcal{N}_{\mathcal{G},\mathrm{MC}}\frac{1}{N_{\mathrm{MC,OP}}}\sum_{m=1}^{N_{\mathrm{MC,OP}}} \mathcal{G}^{[\mathrm{est}\,1]}_{i',j',\tau_p}(C_{\mathrm{OP},m}) = \mathcal{N}_{\mathcal{G},\mathrm{MC}}\left\langle \mathcal{G}^{[\mathrm{est}\,1]}_{i',j',\tau_p}(C_{\mathrm{OP}})\right\rangle'_{\mathrm{OP,MC}}$$

with

$$\mathcal{N}_{\mathcal{G}} \approx \mathcal{N}_{\mathcal{G},\mathrm{MC}} = \frac{1}{\bar{w}\beta\,\langle S_{\mathrm{CP}}\rangle'_{\mathrm{CP,MC}}}\frac{\langle \delta_{\mathrm{OP}}\rangle'_{\mathrm{Tot,MC}}}{\langle \delta_{CP}\rangle'_{\mathrm{Tot,MC}}} .$$

Thus, for each sampled open path $C_{\mathrm{OP},m}$ with Ira on the orbital i and Masha on j, we get a non-vanishing contribution of $\mathcal{G}^{[\mathrm{est}\,1]}_{i,j,\tau_p}(C_{\mathrm{OP},m})$ for all times τ_p
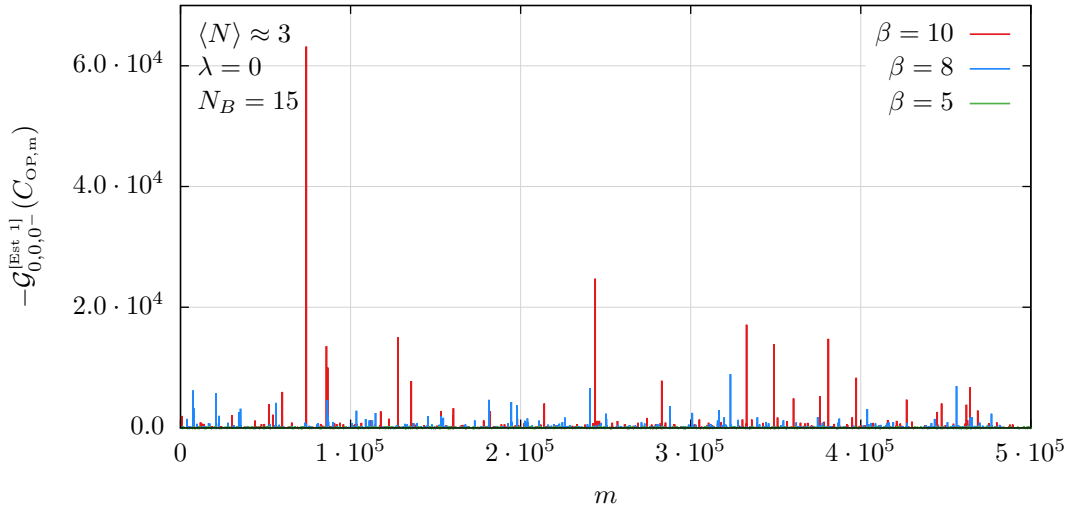
Figure 4.1.: Complete sample history of the MGF estimator $\mathcal{G}^{[\text{est 1}]}_{j'=0,j'=0,\tau_p=\beta^-}(C_{\text{OP},m})$ (without normalization factor $\mathcal{N}_{\mathcal{G},\text{MC}}$) for $N_{\text{MC,OP}} = 5 \cdot 10^5$ samples. The paths are sampled for a test system of $N = 3$ ideal particles ($\lambda = 0$) in $N_B = 15$ basis functions at three different temperatures. The actual test system is defined in Sec. 6.1 and is of no relevance for the interpretation of this graphic.

with a non-vanishing acceptance probability $A_{\text{MIT},C_{\text{OP}}}(\tau_{\text{ir}} \rightarrow \tau_p + \tau_{\text{ma}})$. This strongly improves the statistics of $\mathcal{G}_{ij}(\tau_p, 0)$ for each $i, j \in \{0, \ldots, N_B - 1\}$ and $p \in \{0, \ldots, N_p - 1\}$ in contrast to the estimator (4.8), where we only get a single non-vanishing contribution to $\mathcal{G}_{ij}(\tau_{\text{ir}}, \tau_{\text{ma}})$ for each sampled open path. Nevertheless, we could not obtain sufficiently good results with the estimator (4.13) since, according to Eq. (3.33), it is

$$|\widetilde{A}_{\text{MIT},C_{\text{OP}}}(\tau_{\text{ir}} \rightarrow \tau_p + \tau_{\text{ma}})| \propto e^{-\beta \Delta E_D} \ ,$$

and thus, if the shift of Ira from τ_{ir} to $\tau_p + \tau_{\text{ma}}$ in the sampled path C_{OP} corresponds to a strongly negative change in the diagonal energy ΔE_D, then the values of $|\widetilde{A}_{\text{MIT},C_{\text{OP}}}(\tau_{\text{ir}} \rightarrow \tau_p + \tau_{\text{ma}})|$ can become extremely large. This, of course, becomes worse for lower temperatures. As an example for the severity of this problem, Fig. 4.1 shows the values of $\mathcal{G}^{[\text{est 1}]}_{0,0,\beta^-}(C_{\text{OP},m})$ for all $m = 1 \ldots N_{\text{MC,OP}}$ open path samples for three different temperatures, where $N_{\text{MC,OP}} = 5 \cdot 10^5$. While for $\beta = 5$, the sample history behaves smoothly, corresponding to a small variance, for $\beta = 10$, there are a few extremely large peaks of the order $\mathcal{O}(10^4)$. Obviously, the samples for $\beta = 10$ are not even Gaussian distributed, and the mean value strongly depends on how many peaks we have in the samples; or in other words, how many samples we generated. Consequently, it is not possible to compute a statistical error of the mean value. In addition, the samples in Fig. 4.1 are generated for an ideal system, i.e., there are no kinks at all in the

paths so that Ira can always be shifted to any time in the path. Consequently, in Eq. (4.13) it is always $L_{\widetilde{A}_{\mathrm{MIT},C_{\mathrm{OP}}}} = \beta$. For an interacting system, i.e., with kinks in the sampled paths, $L_{\widetilde{A}_{\mathrm{MIT},C_{\mathrm{OP}}}}$ can become very small. Thereby, the discussed problem of the estimator is significantly enhanced, i.e., the peaks in the samples are even much larger for an interacting system. However, an estimator with such a behavior is unemployable, and a better one had to be found.

4.2.3. Second estimator: Utilizing the idea of the DPIMC estimator

Employing the idea of the MGF estimator in the DPIMC method [17], we rewrite Eq. (4.13) as

$$
\mathcal{G}_{i'j'}(\tau_p, 0) = \mathcal{N}_{\mathcal{G}} \int_0^\beta \mathrm{d}\tau_{\mathrm{trial}} P(\tau_{\mathrm{trial}})
$$
$$
\left\langle \frac{\delta_{i,i'}\delta_{j,j'}}{L_{\widetilde{A}_{\mathrm{MIT},C_{\mathrm{OP}}}}} \frac{\delta_{\tau_{\mathrm{trial}},\tau_p}^{\Delta\beta}}{\Delta\beta} \frac{\widetilde{A}_{\mathrm{MIT},C_{\mathrm{OP}}}(\tau_{\mathrm{ir}} \to \tau_p + \tau_{\mathrm{ma}})}{P(\tau_{\mathrm{trial}})} S_{\mathrm{OP}} \right\rangle'_{\mathrm{OP}}
$$
$$
= \mathcal{N}_{\mathcal{G}} \underbrace{\left\langle \frac{\delta_{i,i'}\delta_{j,j'}}{L_{\widetilde{A}_{\mathrm{MIT},C_{\mathrm{OP}}}}} \frac{\delta_{\tau_{\mathrm{trial}},\tau_p}^{\Delta\beta}}{\Delta\beta} \frac{\widetilde{A}_{\mathrm{MIT},C_{\mathrm{OP}}}(\tau_{\mathrm{ir}} \to \tau_p + \tau_{\mathrm{ma}})}{P(\tau_{\mathrm{trial}})} S_{\mathrm{OP}} \right\rangle'_{\mathrm{OP},\tau_{\mathrm{trial}}}}_{=:\mathcal{G}_{i',j',\tau_p}^{[\mathrm{est}\ 2]}(C_{\mathrm{OP}},\tau_{\mathrm{trial}})},
$$

(4.14)

where

$$
\delta_{\tau_{\mathrm{trial}},\tau_p}^{\Delta\beta} := \begin{cases} 1 \text{ if } \tau_p \in [\tau_{\mathrm{trial}} - \tau_{\mathrm{ma}} - \frac{\Delta\beta}{2}, \tau_{\mathrm{trial}} - \tau_{\mathrm{ma}} + \frac{\Delta\beta}{2}] \\ 0 \text{ else} \end{cases}, \qquad (4.15)
$$

and $P(\tau)$ is some arbitrary, normalized probability density, i.e., $\int_0^\beta \mathrm{d}\tau P(\tau) = 1$. Thus, from Eq. (4.13) to Eq. (4.14) we only added

$$
1 = \frac{1}{\Delta\beta} \int_0^\beta \mathrm{d}\tau_{\mathrm{trial}} \delta_{\tau_{\mathrm{trial}},\tau_p}^{\Delta\beta} = \int_0^\beta \mathrm{d}\tau_{\mathrm{trial}} P(\tau_{\mathrm{trial}}) \frac{\delta_{\tau_{\mathrm{trial}},\tau_p}^{\Delta\beta}}{\Delta\beta} \frac{1}{P(\tau_{\mathrm{trial}})}
$$

for some arbitrary $\Delta\beta \in (0, \beta]$. In fact, for a chosen $\Delta\beta$, the integral over the Kronecker delta is not always $\Delta\beta$, in particular, if $\tau_p \pm \frac{\Delta\beta}{2} \notin [-\beta, \beta]$ since $\tau_{\mathrm{ir}} - \tau_{\mathrm{ma}} \in [-\beta, \beta] \backslash \{0\}$. For simplicity, we neglect this as it is not necessary for the understanding of the main idea. In practice, of course, this has to be taken into account. For the evaluation of the estimator (4.14), we not only have to sample an open path C_{OP} but also another variable τ_{trial} distributed
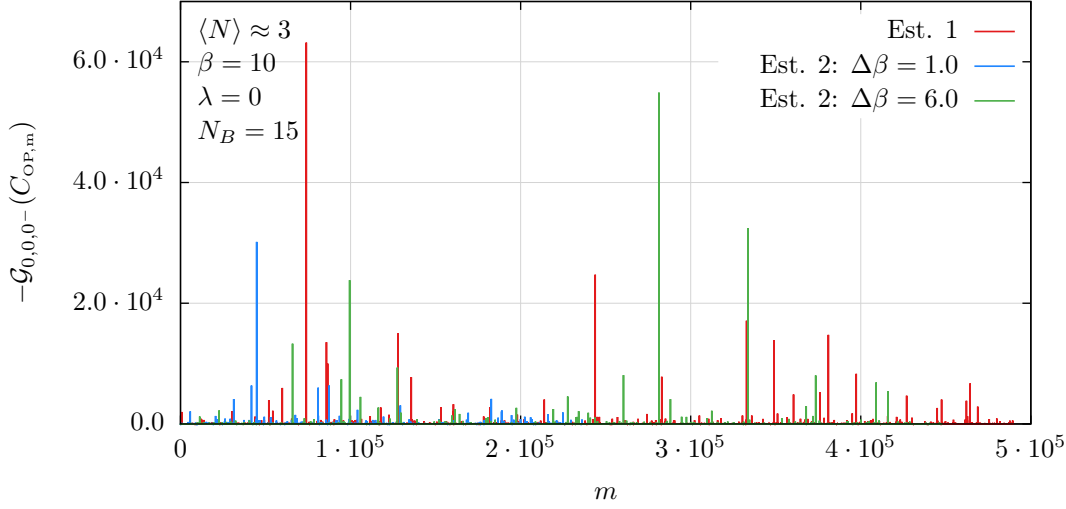
Figure 4.2.: Same as Fig. 4.1 but for the estimator $\mathcal{G}_{i',j',\tau_p}^{[\text{est } 1]}(C_{\text{OP}})$ (cf. Eq. (4.13)) (red curve) and $\mathcal{G}_{i',j',\tau_p}^{[\text{est } 2]}(C_{\text{OP}}, \tau_{\text{trial}})$ (cf. Eq. (4.14)) (blue and green curve) for two different $\Delta\beta$.

with $P(\tau_{\text{trial}})$. Then, we get a contribution to all $\mathcal{G}_{i,j}(\tau_p)$ for which $\delta_{\tau_{\text{trial}},\tau_p}^{\Delta\beta} = 1$ and $\widetilde{A}_{\text{MIT},C_{\text{OP}}}(\tau_{\text{ir}} \to \tau_p + \tau_{\text{ma}}) \neq 0$. If we choose

$$P(\tau_{\text{trial}}) = \frac{|\widetilde{A}_{\text{MIT},C_{\text{OP}}}(\tau_{\text{ir}} \to \tau_{\text{trial}})|}{\int_0^\beta \mathrm{d}\tau |\widetilde{A}_{\text{MIT},C_{\text{OP}}}(\tau_{\text{ir}} \to \tau)|} =: \frac{|\widetilde{A}_{\text{MIT},C_{\text{OP}}}(\tau_{\text{ir}} \to \tau_{\text{trial}})|}{\mathcal{N}_{\widetilde{A}}} , \quad (4.16)$$

then it is

$$\mathcal{G}_{i',j',\tau_p}^{[\text{est } 2]}(C_{\text{OP}}, \tau_{\text{trial}}) = \frac{\delta_{i,i'}\delta_{j,j'}}{L_{\widetilde{A}_{\text{MIT},C_{\text{OP}}}}} \frac{\delta_{\tau_{\text{trial}},\tau_p}^{\Delta\beta}}{\Delta\beta} \mathcal{N}_{\widetilde{A}} \frac{\widetilde{A}_{\text{MIT},C_{\text{OP}}}(\tau_{\text{ir}} \to \tau_p + \tau_{\text{ma}})}{|\widetilde{A}_{\text{MIT},C_{\text{OP}}}(\tau_{\text{ir}} \to \tau_{\text{trial}})|} S_{\text{OP}}$$

Due to the Kronecker delta (4.15), we only update those τ_p's with $\tau_p \approx \tau_{\text{trial}} - \tau_{\text{ma}}$ if $\Delta\beta$ is chosen sufficiently small, i.e., for each non-vanishing contribution, it is approximately

$$\frac{|\widetilde{A}_{\text{MIT},C_{\text{OP}}}(\tau_{\text{ir}} \to \tau_p + \tau_{\text{ma}})|}{|\widetilde{A}_{\text{MIT},C_{\text{OP}}}(\tau_{\text{ir}} \to \tau_{\text{trial}})|} \approx 1 .$$

Hence, the introduction of an additional variable τ_{trial} that is sampled according to the probability density (4.16), replaces the exponential factor $|\widetilde{A}_{\text{MIT},C_{\text{OP}}}|$ that causes the huge peaks in the estimator (4.13) by the normalization factor $\mathcal{N}_{\widetilde{A}}$ in Eq. (4.14). If $|\widetilde{A}_{\text{MIT},C_{\text{OP}}}|$ is some peaked function, then this should reduce the peak height in the samples. In Fig. 4.2, the sample history of the first estimator (4.13) is compared to that of the second estimator (4.14) with two

different choices of $\Delta\beta$. Obviously, the peak height and at the same time the number of samples is reduced for $\Delta\beta = \beta/10 = 1$ (blue curve) by roughly a factor of two in comparison to the first estimator (red curve), while for $\Delta\beta = 6$ (green curve) there are no significant changes compared to the first estimator. However, these peaks are still far too large to obtain good results, and further reducing $\Delta\beta$ does not help since we divide each sample by $\Delta\beta$. Besides, too small $\Delta\beta$ leads to very few samples in the same computation time. We tried some other choices for $P(\tau_{\mathrm{trial}})$ but without success concerning the peaks in the samples.

4.2.4. Combining the first and the second estimator

The idea of extending the sampling process by an additional variable has sufficiently improved the estimator of the MGF in the DPIMC WA[17]. Unfortunately, for CPIMC, this is not the case. Nevertheless, from the results of the first and second estimator, we conclude that an estimator which contains the factor

$$\frac{\widetilde{A}_{\mathrm{MIT},C_{\mathrm{OP}}}(\tau_{\mathrm{ir}} \to \tau_p + \tau_{\mathrm{ma}})|}{\int_0^\beta \mathrm{d}\tau |\widetilde{A}_{\mathrm{MIT},C_{\mathrm{OP}}}(\tau_{\mathrm{ir}} \to \tau)|}$$

instead of only $|\widetilde{A}_{\mathrm{MIT},C_{\mathrm{OP}}}(\tau_{\mathrm{ir}} \to \tau_p + \tau_{\mathrm{ma}})|$, most likely produces much better results (provided we do not additionally divide by some small interval). And indeed, it is possible to rewrite the estimator such that this desired factor is obtained. For that purpose, we return to Eq. (4.10)

$$\mathcal{G}_{i'j'}(\tau_p, 0) = \frac{Z_{\mathrm{OP}}}{Z_{\mathrm{CP}}} \frac{1}{\beta} \sum_{C_{\mathrm{CP}}} \sum_{i,j} \int_0^\beta \mathrm{d}\tau_{\mathrm{ma}} \delta_{i,i'} \delta_{j,j'} \frac{W_{\mathrm{OP}}(C_{\mathrm{CP}}, i, j, \tau_p + \tau_{\mathrm{ma}}, \tau_{\mathrm{ma}})}{Z_{\mathrm{OP}}} \;.$$

$$(4.17)$$

Dropping all arguments of the open path weight function except that for the time of Ira, it is

$$
\begin{aligned}
\int_0^\beta d\tau_{\mathrm{ma}} W_{\mathrm{OP}}(\tau_p + \tau_{\mathrm{ma}}) &= \int_0^\beta d\tau_{\mathrm{ma}} \frac{\int_0^{\prime\beta} d\tau_{\mathrm{ir}} |W_{\mathrm{OP}}(\tau_{\mathrm{ir}})|}{\int_0^{\prime\beta} d\tau |W_{\mathrm{OP}}(\tau)|} W_{\mathrm{OP}}(\tau_p + \tau_{\mathrm{ma}}) \\
&= \int_0^\beta d\tau_{\mathrm{ma}} \int_0^{\prime\beta} d\tau_{\mathrm{ir}} \frac{\frac{W_{\mathrm{OP}}(\tau_p+\tau_{\mathrm{ma}})}{|W_{\mathrm{OP}}(\tau_{\mathrm{ir}})|}}{\int_0^{\prime\beta} d\tau \left|\frac{W_{\mathrm{OP}}(\tau)}{W_{\mathrm{OP}}(\tau_{\mathrm{ir}})}\right|} |W_{\mathrm{OP}}(\tau_{\mathrm{ir}})| \\
&= \int_0^\beta d\tau_{\mathrm{ma}} \int_0^{\prime\beta} d\tau_{\mathrm{ir}} \frac{\frac{W_{\mathrm{OP}}(\tau_p+\tau_{\mathrm{ma}})}{W_{\mathrm{OP}}(\tau_{\mathrm{ir}})}}{\int_0^{\prime\beta} d\tau \left|\frac{W_{\mathrm{OP}}(\tau)}{W_{\mathrm{OP}}(\tau_{\mathrm{ir}})}\right|} W_{\mathrm{OP}}(\tau_{\mathrm{ir}}) \\
&= \int_0^\beta d\tau_{\mathrm{ma}} \int_0^{\prime\beta} d\tau_{\mathrm{ir}} \frac{\widetilde{A}_{\mathrm{MIT},C_{\mathrm{OP}}}(\tau_{\mathrm{ir}} \to \tau_p + \tau_{\mathrm{ma}})}{\int_0^{\prime\beta} d\tau |\widetilde{A}_{\mathrm{MIT},C_{\mathrm{OP}}}(\tau_{\mathrm{ir}} \to \tau)|} W_{\mathrm{OP}}(\tau_{\mathrm{ir}}) ,
\end{aligned}
$$

(4.18)

where from the second to the third line, we have multiplied and divided by the sign of $W_{\mathrm{OP}}(\tau_{\mathrm{ir}})$. The integration of τ_{ir} has to be restricted to such times where $W_{\mathrm{OP}}(\tau_{\mathrm{ir}}) \neq 0$, which is indicated by the prime. We insert this into Eq. (4.17) and obtain[6]

$$
\mathcal{G}_{i'j'}(\tau_p, 0) = \frac{Z_{\mathrm{OP}}}{Z_{\mathrm{CP}}} \frac{1}{\beta} \oint_{C_{\mathrm{OP}}} \left(\delta_{i,i'} \delta_{j,j'} \frac{\widetilde{A}_{\mathrm{MIT},C_{\mathrm{OP}}}(\tau_{\mathrm{ir}} \to \tau_p + \tau_{\mathrm{ma}})}{\int_0^\beta d\tau |\widetilde{A}_{\mathrm{MIT},C_{\mathrm{OP}}}(\tau_{\mathrm{ir}} \to \tau)|} \right) \frac{W_{\mathrm{OP}}(C_{\mathrm{CP}}, i, j, \tau_{\mathrm{ir}}, \tau_{\mathrm{ma}})}{Z_{\mathrm{OP}}}
$$

Again explicitly taking into account the sign and utilizing relation (4.6), we end up with

$$
\mathcal{G}_{i'j'}(\tau_p, 0) = \mathcal{N}_{\mathcal{G}} \Big\langle \underbrace{\delta_{i,i'} \delta_{j,j'} S_{\widetilde{A}} P_{\mathrm{ir}}(\tau_{\mathrm{ma}} + \tau_p) S_{\mathrm{OP}}}_{=\mathcal{G}_{i',j',\tau_p}^{\mathrm{Est}\ 3}(C_{\mathrm{OP}})} \Big\rangle_{\mathrm{OP}}^{\prime} ,
\tag{4.19}
$$

$$
P_{\mathrm{ir}}(\tau_{\mathrm{ma}} + \tau_p) := \frac{|\widetilde{A}_{\mathrm{MIT},C_{\mathrm{OP}}}(\tau_{\mathrm{ir}} \to \tau_{\mathrm{ma}} + \tau_p)|}{\int_0^\beta d\bar{\tau} |\widetilde{A}_{\mathrm{MIT},C_{\mathrm{OP}}}(\tau_{\mathrm{ir}} \to \bar{\tau})|} ,
$$

where $S_{\widetilde{A}}$ denotes the sign of $\widetilde{A}_{\mathrm{MIT},C_{\mathrm{OP}}}(\tau_{\mathrm{ir}} \to \tau_{\mathrm{ma}} + \tau_p)$. Now, $P_{\mathrm{ir}}(\tau_{\mathrm{ma}} + \tau_p)$ is the probability density to find Ira at $\tau_{\mathrm{ma}} + \tau_p$ if all other parameters of the sampled paths, i.e., times and types of the kinks, remain fixed. According to Eq. (4.18), $P_{\mathrm{ir}}(\tau_{\mathrm{ma}} + \tau_p)$ is independent of the time of Ira (τ_{ir}) in the sampled open path C_{OP}. Fig. 4.3 shows the sample history of the final estimator (4.19) for the same test system as in Fig. 4.2 but for three different coupling parameters (for its Def. see Sec. 6.1). For the ideal system (green curve), we always get the

---

[6]In Eq. (4.17), $W_{\mathrm{OP}}(\tau_{\mathrm{ir}}) \neq 0$ is ensured since we sample open paths with Ira at τ_{ir}.
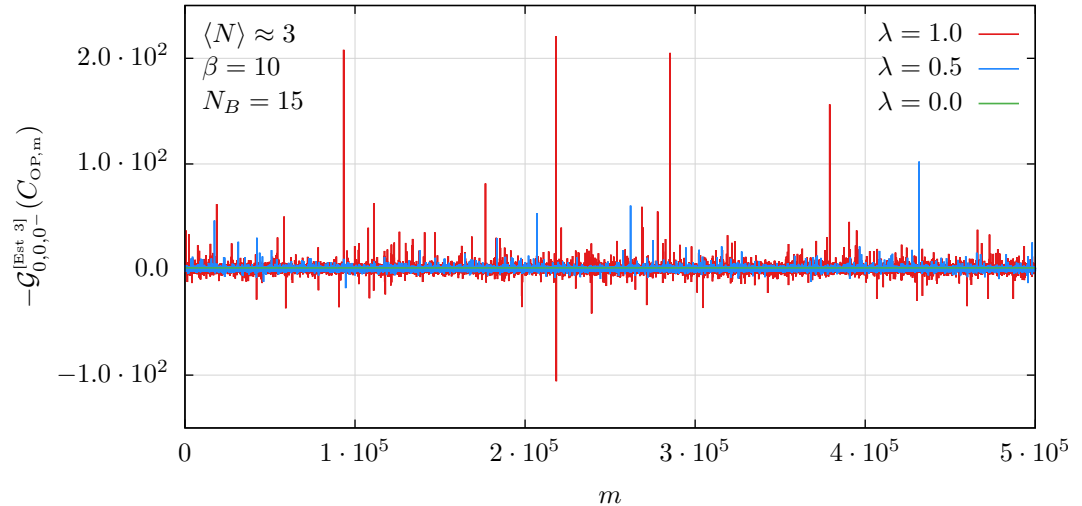
Figure 4.3.: Same as Fig. 4.1 but for the estimator $\mathcal{G}^{[\text{est 3}]}_{i',j',\tau_p}$ and for three different coupling parameters of the test system defined in Sec. 6.1.

same contribution for each sampled path, i.e., in that case the estimator (4.19) reduces the height of the peaks by almost five orders of magnitude (see Fig. 4.2). For the interacting system (blue curve), the kinks in the paths can result in very small intervals on which $\tilde{A}_{\text{MIT},C_{\text{OP}}}(\tau_{\text{ir}} \to \tau)$ does not vanish since we can move Ira only to times τ that are in between the left and the right kink of τ_{ir} on Ira's orbital. Consequently, in such cases, $P_{\text{ir}}(\tau)$ is a peaked distribution leading to large values in the samples for $P_{\text{ir}}(\tau_{\text{ma}} + \tau_p)$. This problem is enhanced for increasing coupling (red curve) since this means, on average, more kinks in the paths. Nevertheless, doubling the coupling from 0.5 to 1.0 only doubles the peak height, which is still three orders of magnitudes smaller than that of the other estimators. Besides, for the interacting system, the peaks are positive and negative since the weights of the paths can be positive and negative. Hence, most of them cancel in the mean value of the samples. For that reason, it requires many samples to obtain a good value of the true mean value. Moreover, the normalization factor is inversely proportional to the average sign of the closed paths which tends to zero for stronger coupling. That means, a very precise mean value of $\mathcal{G}^{\text{Est 3}}_{i',j',\tau_p}(C_{\text{OP}})$ is required. The just said is nothing but the manifestation of the fermion sign problem in the sampling of the MGF.

It should be mentioned that the existence of various estimators for the same physical quantity is not unusual. Another example is the estimator for the energy in the DPIMC method. There, the standard estimator obtained from the differentiation of the partition function is also numerically unstable, while another estimator obtained by employing the viral theorem is stable. Yet, in the limit of an infinite number of samples, the mean value of these different

estimators is of course the same, but the number of samples required for the convergence up to a given error can be very different.

Furthermore, in terms of computation time, we do not get a better estimator for free. For the trivial estimator (4.8), only delta functions have to be evaluated. For the first estimator without discretization error (Eq. (4.13)), $\widetilde{A}_{\mathrm{MIT}}$ has to be computed, which is of the same complexity as the computation of the acceptance probability for moving Ira in time. And for the evaluation of the final estimator (4.19), the normalization of the probability density $P_{\mathrm{ir}}(\tau)$ has to be computed, which is, in theory, quite complex and requires roughly two thousand lines of C++ code. Yet, due to the much smaller variance of this estimator, the additional effort definitely pays off. Certainly, there exist estimators for the MGF that converge even faster. For example, in addition to analytically taking into account the time of Ira by the computation of $P_{\mathrm{ir}}(\tau)$, it should be possible to analogously treat the times of the left and right kink of Ira analytically, whereby the height of the peaks in the samples and thus the variance of the estimator would be further reduced. There are many other things that can be done, but, of course, if the evaluation of the estimator becomes too expensive, then it might be more efficient to use an estimator that can be evaluated fast and generate more samples in the same computation time.

Finally, some remarks on the calculation of the statistical errors have to be made. A proper error estimation of the MGF according to Eq. (2.8) requires the storing of the complete sample history[7] for each $\mathcal{G}^{\mathrm{Est\ 3}}_{i,j,\tau_p}(C_{\mathrm{OP}})$ with $i,j = 1 \ldots N_B$ and $p = 1 \ldots N_p$, i.e., we have to store $N_B^2 \cdot N_p \cdot N_{\mathrm{MC,OP}}$ numbers of type double. For the investigated system, the maximum values of these parameters are $N_B = 96, N_p = 100$ and $N_{\mathrm{MC,OP}} \approx 10^8$ which corresponds to $5 \cdot 10^3$GB of hard disc space. This is far too much and therefore, we only perform a Gaussian error propagation to estimate the error of $\mathcal{G}_{i',j'}(\tau_p)$ (cf. Eq. (4.19)), which is computed from four mean values[8] all entering with a statistical error. In doing so, we completely neglect all auto- and cross correlations of these four mean values. We can check if the auto-correlation is sufficiently small by computing it for a couple of elements of the MGF. To make sure that the statistical error is not underestimated, we also double the computed value from the Gaussian error propagation. This, in most cases, overestimates the error.

---

[7]And, as already mentioned in Sec. 2.1, binning analysis can not be applied due to the required treatment of the sign. Moreover, it is not possible to only store the non-vanishing samples because for the calculation of the cross- and auto-correlation the actual position in the sample history has to be known. Quite some time has been spent on this problem but even with the use of an HDF5 library, which has been written by the group member Chritopher Hinz for in- and output of large data sets, no efficient solution could be found.
[8]Note the Def. of the normalization factor $\mathcal{N}_{\mathcal{G}}$ in Eq. (4.13).

5. Finite temperature Hartree-Fock

For this work, the Hartree-Fock (HF) approximation at zero and also at finite temperature (FTHF) is of central meaning for two reasons. First, it represents an approximation concerning the interaction with a vanishing error for ideal systems. In other words, the quality of HF calculations tends to become better for higher degeneracy of the system[1]. Since this is the regime where CPIMC can be applied to compute exact results, a comparison of both methods has to be made. Moreover, within the HF approximation, much larger systems can be simulated because there is no fermion sign problem (like in the exact CPIMC approach). Second, if the one- and two-electron integrals (cf. Eq. (2.28) and (2.39)), which serve as input data for the CPIMC program, are computed in the HF one-particle basis, then the sign problem is significantly reduced compared to that in the ideal one-particle basis. This reduction of the sign problem within the HF basis has been observed even before the development of a WA, i.e., within the standard CPIMC method [9]. The explanation for this behavior will be given later on in Sec. 6.3.

This chapter is not considered as being a general introduction into the HF approximation. Rather, we focus only on those aspects relevant for this work.

For an interacting, fermionic N-particle system at zero temperature, the HF approximation consists in the assumption that the ground state is given by a single Slater-determinant (cf. Eq. (2.17)), or equivalently, by a single ONV. Since the true ground state minimizes the expectation value of the energy, the energy must be stationary under variation of the occupied one-particle orbitals that form the Slater determinant. Carrying out the variation leads to the HF equation at zero temperature [27, 19]

$$\hat{f}_\alpha \left|i\right\rangle_\alpha = \epsilon_i \left|i\right\rangle_\alpha$$

$$\hat{f}_\alpha = \hat{h}_\alpha + \sum_{j=0}^{N-1} \left\langle j\right|_\beta \hat{w}_{\alpha,\beta}(1 - \hat{P}_{\alpha,\beta}) \left|j\right\rangle_\beta \ , \tag{5.1}$$

where $\hat{f}_\alpha$ is the so called Fock-operator acting on the particle α. The single particle Hamiltonian $\hat{h}_\alpha$, the two-particle interaction operator $\hat{w}_{\alpha,\beta}$ and the

---

[1] Also FTHF is better at lower temperatures since one needs fewer basis functions to describe the system.

two-particle exchange operator are defined in the Secs. 2.2.1 and 2.2.5. Further, in this work, we only consider spin polarized systems and thus, we neglect the spin projections. Assuming the eigenstates $\{|i\rangle_\alpha\}$ of the Fock-operator to be ordered according to the eigenvalues ϵ_i, i.e., it is $\epsilon_i \leq \epsilon_{i+1}$, the ground state determinant in the HF approximation is constructed from the first N eigenstates. Since the Fock-operator is Hermitian, its eigenstates form a basis in the one-particle Hilbert space. This basis is the Hartree-Fock basis.

For finite temperatures, e.g. in the grand canonical ensemble, the N-particle state is not given by a single determinant. Instead the system is described by the N-particle density operator and a corresponding ensemble of Slater determinants or ONVs. The HF approximation at finite temperatures consists in the assumption that the N-particle density operator $\hat{\rho}_{1,2,\ldots,N}$ is given by a product of one-particle density operators $\hat{\rho}_\alpha$, i.e.,

$$\hat{\rho}_{1,2,\ldots,N} = \hat{\rho}_1 \hat{\rho}_2 \cdot \ldots \cdot \hat{\rho}_N \ .$$

Minimizing the grand canonical potential under this assumption leads to the FTHF equation [21]

$$\hat{f}_\alpha |i\rangle_\alpha = \epsilon_i |i\rangle_\alpha \tag{5.2}$$

$$\hat{f}_\alpha = \hat{h}_\alpha + \sum_{j=0}^{\infty} \langle j|_\beta \, \hat{w}_{\alpha,\beta}(1 - \hat{P}_{\alpha,\beta}) \, |j\rangle_\beta \, \langle \hat{n}_j \rangle$$

$$\langle \hat{n}_j \rangle = \frac{1}{e^{\beta(\epsilon_j - \mu)} + 1} \ .$$

Obviously, in the limit of $\beta \to \infty$, this is equivalent to the zero temperature HF equation for the particle number that corresponds to the chemical potential μ. Note that the FT Fock-operator depends on both all eigenstates and eigenvalues so that Eq. (5.2) is a non-linear eigenvalue problem[2]. To solve the FTHF equation, we can formally expand the first N_B HF orbitals into some known one-particle basis $\{|\nu\rangle\}$ (we now drop the indices for the particle)

$$|i\rangle = \sum_{\nu=0}^{N_B-1} \underbrace{\langle \nu|i\rangle}_{=C_{\nu i}} |\nu\rangle \ , \quad i = 0, 1, \ldots, N_B \ , \tag{5.3}$$

where the overlap matrix $S_{\nu\mu} = \langle \nu|\mu \rangle$ not necessarily has to be zero, i.e., $\{|\nu\rangle\}$ can be a non-orthonormal basis. The expansion coefficients are referred to as the *Roothann coefficients*. Inserting the expansion (5.3) into the HF equation (5.2) and multiplying from the left with $\langle \tau|$, we obtain

$$\sum_{\nu=0}^{N_B-1} \langle \tau|\hat{f}|\nu\rangle C_{\nu i} = \epsilon_i \sum_{\nu=0}^{N_B-1} S_{\tau\nu}C_{\nu i} \quad \text{for all} \quad i, \tau = 0 \ldots N_B - 1 \ ,$$

---

[2]Of course, the ground state HF equation (5.1) is non-linear, too.

which is a generalized eigenvalue problem of the form

$$\underline{\underline{f}} \cdot \underline{C}_i = \epsilon_i \underline{\underline{S}} \cdot \underline{C}_i \;, \qquad \underline{C}_i = (C_{1i} \ldots C_{N_B i})^T \;, \qquad i = 0 \ldots N_B - 1 \;. \tag{5.4}$$

The elements of the Fock matrix in this basis are given by

$$f_{\tau\nu} = h_{\tau\nu} + \sum_{\eta,\mu=0}^{N_B-1} \rho_{\mu\eta} \underbrace{(w_{\tau\eta\nu\mu} - w_{\tau\eta\mu\nu})}_{=w_{\tau\eta\nu\mu}^-} \tag{5.5}$$

with the one-particle density matrix

$$\rho_{\mu\eta} = \sum_{j=0}^{N_B-1} C_{\mu j} \langle n_j \rangle C_{\eta j}^* \;. \tag{5.6}$$

The non-linear, generalized eigenvalue problem (5.4) is called the *Roothann equation.* It can be solved iteratively according to the following algorithm:

1. Compute the one- and two-particle integrals in the known representation of the basis $\{|\nu\rangle\}$. In most cases this is the coordinate representation $\langle \underline{r}|\nu\rangle = \phi_\nu(\underline{r})$, i.e., one has solve the integrals

$$h_{\tau\nu} = \int \mathrm{d}\underline{r} \phi_\tau^* \underline{r} \left(-\frac{1}{2}\nabla^2 + v(\underline{r}) \right) \phi_\nu(\underline{r})$$

$$w_{\tau\eta\nu\mu} = \int \mathrm{d}\underline{r} \int \mathrm{d}\underline{r}' \, \phi_\tau^*(\underline{r})\phi_\eta^*(\underline{r}')w(\underline{r},\underline{r}')\phi_\mu(\underline{r})\phi_\nu(\underline{r}') \;. \tag{5.7}$$

   Due to the symmetries of the two-electron integrals (cf. Eq. (2.40)), only $\mathcal{O}(\frac{N_B^4}{8})$ integrals have to be computed.

2. Calculate the elements of the Fock-matrix according to Eq. (5.5) (The first time with an arbitrary initial density matrix $\rho_{\mu\eta}(0)$).

3. Solve the generalized eigenvalue problem[3] $\underline{\underline{f}} \cdot \underline{C}_i = \epsilon_i \underline{\underline{S}} \cdot \underline{C}_i$.

4. Compute the new occupation numbers corresponding to the eigenvalues ϵ_i and the new density matrix according to (5.6) with the new occupation numbers and eigenvectors $\underline{C}_i$.

5. Proceed with step 2 until the chosen convergence criterion is fulfilled.

---

[3]This can be done with standard libraries like e.g. *Lapack.*

The iteration is usually stopped if both the HF energy and the density matrix are converged scientifically well. The HF energy is given by

$$E_{HF} = \text{Tr}\left\{\hat{\rho}\hat{h}\right\} + \frac{1}{2}\text{Tr}\left\{\hat{\rho}(\hat{f} - \hat{h})\right\},$$

which is easily evaluated by performing the trace in the utilized basis $\{|\nu\rangle\}$. If $E_{HF}(i)$ and $\rho(i)$ denote the energy and the one-particle density matrix in the i-the iteration, we stop the HF iteration when the following inequalities are both satisfied:

$$|E_{HF}(i) - E_{HF}(i-1)| < \Delta E_{\max} ,$$

$$\frac{1}{N_B^2}\sum_{\mu\eta}|\rho_{\mu\eta}(i) - \rho_{\mu\eta}(i-1)| < \Delta\rho_{\max} . \tag{5.8}$$

However, even if both energy and the density matrix are converged, the obtained solution may not be the true HF solution since the grand canonical potential can have local minima. Consequently, the solution can depend on the initial choice of the one-particle density matrix. Moreover, in some cases, the energy converges, while the density matrix shows oscillatory behavior. To stabilize the convergence, it is common to introduce a damping-parameter d, and then use

$$\bar{\rho}_{\mu\eta}(i+1) = d \cdot \rho_{\mu\eta}(i) + (1-d)\rho_{\mu\eta}(i+1) \tag{5.9}$$

for the next iteration instead of $\rho_{\mu\eta}(i+1)$. Sure, this does not solve the problem of possibly false solutions. However, since the Fock-operator is Hermitian, any solution for the eigenstates form a basis regardless whether it is the true HF solution or not. Hence, if we have some self-consistent solution of the Roothaan equation (5.4), according to the expansion of the eigenstates (5.3), we can transform the computed one- and two-electron integrals (5.7) into the HF basis[4]

$$h_{ij} = \sum_{\tau\nu}^{N_B} C_{\tau i}^* h_{\tau\nu} C_{\nu j}$$

$$w_{ijkl} = \sum_{\tau\nu\mu\eta}^{N_B} C_{\tau i}^* C_{\nu j}^* w_{\tau\nu\mu\eta} C_{\mu k} C_{\eta l} .$$

Further, instead of fixing the chemical potential in the grand canonical HF calculation, we can also fix the average particle number $\langle N \rangle$ to some desired value. This can be achieved by changing the chemical potential in each iteration such that

$$\langle \hat{N} \rangle (\beta, \{\epsilon_i\}, \mu) - N = \sum_{i=1}^{N_B} \langle \hat{n}_i \rangle (\epsilon_i, \beta, \mu) - N \stackrel{!}{=} 0 ,$$

---

[4]We refer to the eigenstates of the Fock-operator as the HF basis even if it is not the true HF solution.

and then use the corresponding average occupation numbers $\langle \hat{n}_i \rangle$ to compute the new density matrix.

It is also possible to perform HF calculations in the canonical ensemble for N particles by computing the average occupation numbers in each iteration according to

$$\langle \hat{n}_i \rangle (\beta) = \sum_{\{n\}} \delta_{N, \sum_p n_p} n_i e^{-\beta \sum_{p=0}^{N_B-1} \epsilon_p n_p} \,,$$

which consists of $\binom{N_B}{N}$ summands, and thus, the complexity for the computation of all occupation numbers in each iteration is of the order $\mathcal{O}(N_B \binom{N_B}{N})$. Of course, this can only be performed for smaller systems, e.g., $N = 8$ and $N_B = 66$ is not possible. There also exist recursive formulas for the calculation of the canonical occupation numbers with much less complexity [32], but for fermions, these are numerically unstable due to cancellation effects. Obviously, for ground state HF, we only replace the average occupation numbers by

$$\langle \hat{n}_i \rangle = \begin{cases} 1 & \text{if} \quad i < N_B \\ 0 & \text{else.} \end{cases}$$

Finally, it shall be mentioned that, due to the finite basis size, the choice of the known basis $\{|\nu\rangle\}$ can strongly influence the quality of the HF results. However, in many cases, one has to choose a basis in which the one- and two-electron integrals can be solved fast and numerically stable, rather than a physically reasonable basis. For the investigated test system in this work (see Sec. 6.1), the eigenstates $|i\rangle_{\text{ideal}}$ of the ideal one-particle Hamiltonian $\hat{h}$ can be used as the "reference" basis, i.e., we use $\{|\nu\rangle\} = \{|i\rangle_{\text{ideal}}\}$.

6. Numerical results

In this chapter, first, the test system is specified. Next, the ground state HF and the FTHF method is applied to the test system and investigated concerning the different solutions of the HF equation. Afterwards, the fermion sign problem in the CPIMC calculation is explored for different HF basis sets. Then, the MGF in the limit of the density is compared to CI and HF calculations. It follows the presentation of the results for the time-dependent MGF, which are compared to the HF approximation. Finally, the fermion sing problem for the test system is discussed in general.

6.1. Test system

The developed CPIMC WA is applied to the fairly general two-dimensional test system of spin polarized, Coulomb interacting fermions in a harmonic trap, where we focus on the investigation of the results for the MGF. For N particles, the Hamiltonian of this system in dimensionless (oscillator) units is given by

$$\hat{H} = \underbrace{\sum_{\alpha=1}^{N} \frac{1}{2} \left(\hat{p}_\alpha^{\,2} + \hat{r}_\alpha^{\,2} \right)}_{\hat{H}_0} + \underbrace{\sum_{\alpha<\beta}^{N} \frac{\lambda}{|\hat{r}_\alpha - \hat{r}_\beta|}}_{\hat{W}} \,, \tag{6.1}$$

where $\lambda = \frac{e^2}{r_0 \omega}$ with $r_0 = \frac{1}{\sqrt{m\omega}}$ is the coupling parameter that determines the ratio of the Coulomb to the trap energy, i.e., $\lambda = 0$ corresponds to the ideal system of N non-interacting fermions in a harmonic trap. In the units of Eq. (6.1), energy is given by $\frac{E}{\omega}$, chemical potential by $\frac{\mu}{\omega}$ and the inverse temperature by $\beta\omega = \frac{\omega}{T}$.

The one- and two-particle integrals of the corresponding Hamiltonian in second quantization (cf. Eq. (3.7)) can be computed in the well-known ideal basis $\{|i\rangle_{\text{ideal}}\}$ of the 2D harmonic oscillator. Instead of using the Cartesian coordinate representation $\Phi_i(x, y)$ for the evaluation of the integrals, it is advantageous to switch to polar coordinates $\Phi_i(r, \phi)$ since then the integrals can be solved much faster [33]. Further, these functions are per definition radial symmetric. The computed one- and two-electron integrals can be used directly for CPIMC calculations or as input for the HF algorithm as in detail described in Chap. 5. After a self-consistent solution of the HF equation has

been found, the integrals are transformed from the ideal into the HF basis (cf. Eq. 5), which are then used for the CPIMC calculations. We also refer to this as performing CPIMC in the ideal or HF basis since it corresponds to a second quantized Hamiltonian with respect to the ideal or HF basis. The HF basis has to be computed for each coupling parameter λ and the parameters depending on the type of the HF calculation: For ground state HF the particle number N, for HF in the canonical ensemble the inverse temperature β and the particle number N and for HF in the grand canonical ensemble the inverse temperature β and the chemical potential μ or the HF expectation value of the particle number $\langle N \rangle$. The utilized program for the evaluation of the one- and two-electron integrals and the HF program have originally been written by the former group member Dr. D. Hochstuhl and modified by me and T. Schoof.

For the choice of the particle numbers and basis sizes in this chapter, the shell structure of the 2D harmonic oscillator plays an important role. In the ideal case, the $i-$th orbital energy ϵ_i is $(i+1)$ fold degenerate, i.e., we have closed shells for $N_B = 1, 3, 6, 10, 15, 21, 28, 36, 45, 55, 66, 78, 91 \ldots$. Due to the radial symmetry, the most orbital energies of the interacting system are still 2-fold degenerate.

6.2. Investigation of the Hartree-Fock basis

The reduction of the fermion sign problem for CPIMC calculations in the HF basis compared to the ideal basis has been observed by T. Schoof almost three years ago [11]. In his diploma, thesis he applied the standard CPIMC method without the WA to the same test system (cf. Eq. (6.1)) but in one-dimension only. For the utilized range of parameters, the canonical HF basis always resulted in a larger average sign compared to the ideal basis. Surprisingly, the grand canonical basis significantly enhanced the sign problem, making calculations impossible in that basis. This even applied at very low temperatures where the canonical and the grand canonical HF solution are expected to be approximately equal. Moreover, after switching to the two-dimensional system and investigating larger systems, the fact that the canonical HF basis can only be computed for smaller systems (as explained in Sec. 5) became a serious problem. Therefore, the behavior of the CPIMC method in different basis sets had to be analysed in detail. For the understanding, it is advantageous to first explore the different HF basis sets and especially, the convergence behaviour of the HF algorithm.

For that purpose, we define two quantities

$$\Sigma_{\text{T2}}^{|\{n_p\}\rangle_{\text{HF}}} := \sum_{i\neq k}^{N_B} |f_{ik}| = h_{ik} + \sum_{p\neq i,k}^{N_B} w_{ipkp}^{-} \langle n_p \rangle \ ,$$

$$\Sigma_{\text{T4}} := \sum_{\substack{i,j,k,l=0 \\ i<j,k<l, \\ i\neq k,i\neq l,j\neq k,j\neq l}}^{N_B} |w_{ijkl}^{-}| \ , \tag{6.2}$$

i.e., $\Sigma_{\text{T2}}^{|\{n_p\}\rangle_{\text{HF}}}$ is the modulus sum over the off-diagonal matrix elements of the Fock-operator (cf. Eq. (5.2)) in the HF basis $\{|i\rangle\}$. As this basis self-consistently solves the HF equation (5.2), $\Sigma_{\text{T2}}^{|\{n_p\}\rangle_{\text{HF}}}$ is zero. However, if we define $\Sigma_{\text{T2}}^{|\{n_p\}\rangle_{\text{HF}}}(i)$ to be the modulus sum over the off-diagonal elements of the Fock-operator in the $i-$th HF iteration, then the vanishing of $\Sigma_{\text{T2}}^{|\{n_p\}\rangle_{\text{HF}}}(i)$ can serve as another convergence criterion. Similarly, $\Sigma_{\text{T4}}(i)$ denotes the modulus sum of all off-diagonal elements of the two-particle integrals computed in the HF basis of the $i-$th iteration. The choice of the symbol already indicates that Σ_{T4} is nothing but the modulus sum over all possible kink matrix elements of type 4 (cf. Eqs. (3.27)) when using the corresponding HF basis for the CPIMC WA. On the other hand, $\Sigma_{\text{T2}}^{|\{n_p\}\rangle_{\text{HF}}}$ is only strongly related to the modulus sum over all possible kink matrix elements of type 2 since the modulus weight of a type 2 kink depends on the actual occupation numbers at the time of the kink in the path (cf. Eqs. (3.27)). This will be discussed in detail in the next section. Nevertheless, we simply refer to $\Sigma_{\text{T2}}^{|\{n_p\}\rangle_{\text{HF}}}$ (Σ_{T4}) as the sum of type 2 (4) kinks.

Fig. 6.1 shows the relative convergence of the HF energy and the sum of type 2 and 4 kinks for 100 iterations of a ground state HF calculation. The test system consists of $N = 5$ and 6 particles in $N_B = 45$ basis functions with a coupling parameter of $\lambda = 0.8$. The energy and the sum of type 2 kinks in Fig. 6.1 are converged after roughly 15 iterations for both particle numbers. In contrast to that, the sum of type 4 kinks seems to be constant for $N = 5$ particles while for 6 particles it performs (quasi) chaotic oscillations. In Fig. 6.2, the same quantities are pictured but for 10^4 iterations and only 5 particles. After about 500 iterations, the energy suddenly drops by approximately 0.25%. This change is recorded by the sum of type 2 kinks which shows a peak around 500 iterations, i.e., the HF equation is momentarily not self-consistently solved. Interestingly, after the energy has dropped, the sum of type 4 kinks first strongly increases and then also starts to heavily oscillate, while it never returns to the lowest value corresponding to the higher energy. One might suppose that this behavior can be explained by some numerical problem, e.g., small errors caused by the finite precision summing up in each iteration. This question will be answered later on in this section.
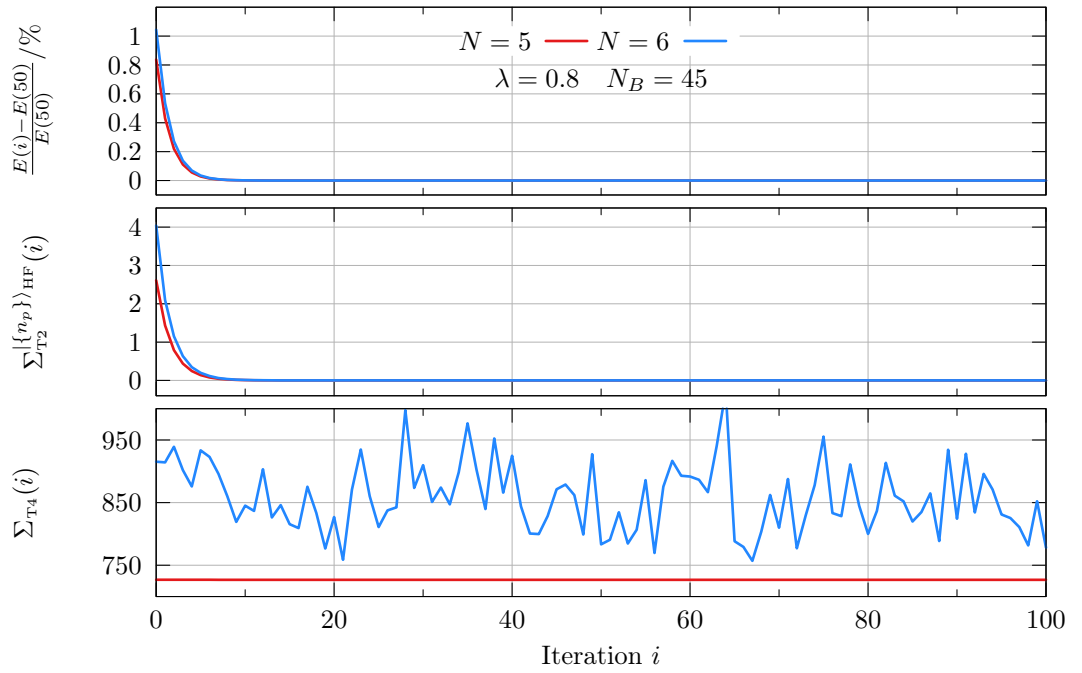
Figure 6.1.: Ground state HF: Relative convergence of the HF energy and the sum of type 2 and 4 kinks for $N = 5$ (red curve) and 6 (blue curve) particles in $N_B = 45$ basis functions at a coupling of $\lambda = 0.8$ for 100 iterations.
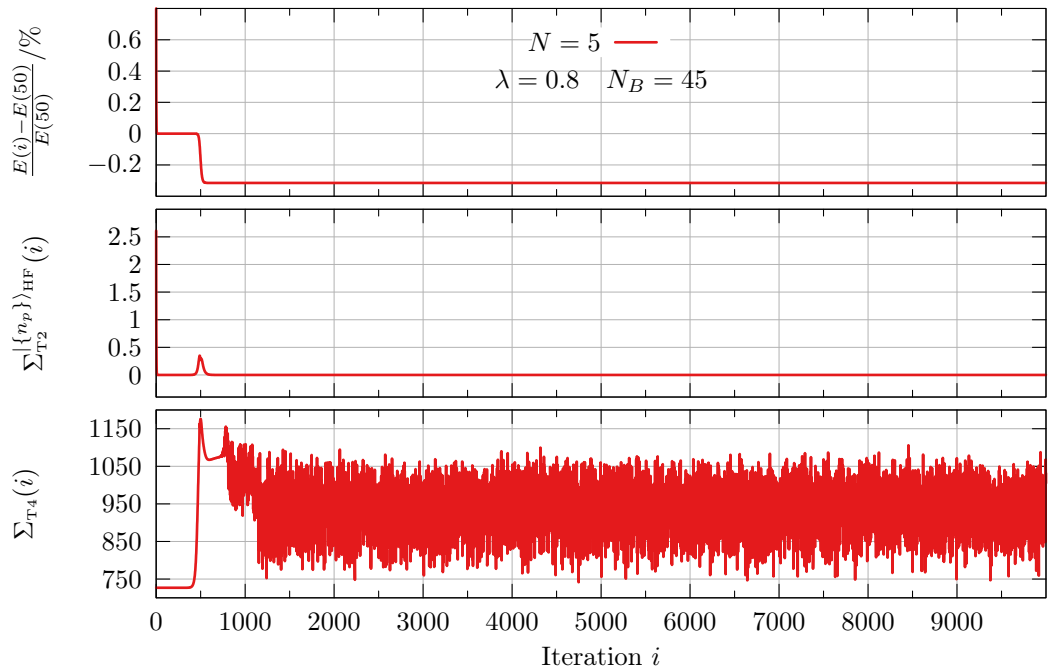
Figure 6.2.: Same as Fig. 6.1 but for 10^4 iterations and only $N = 5$ particles.
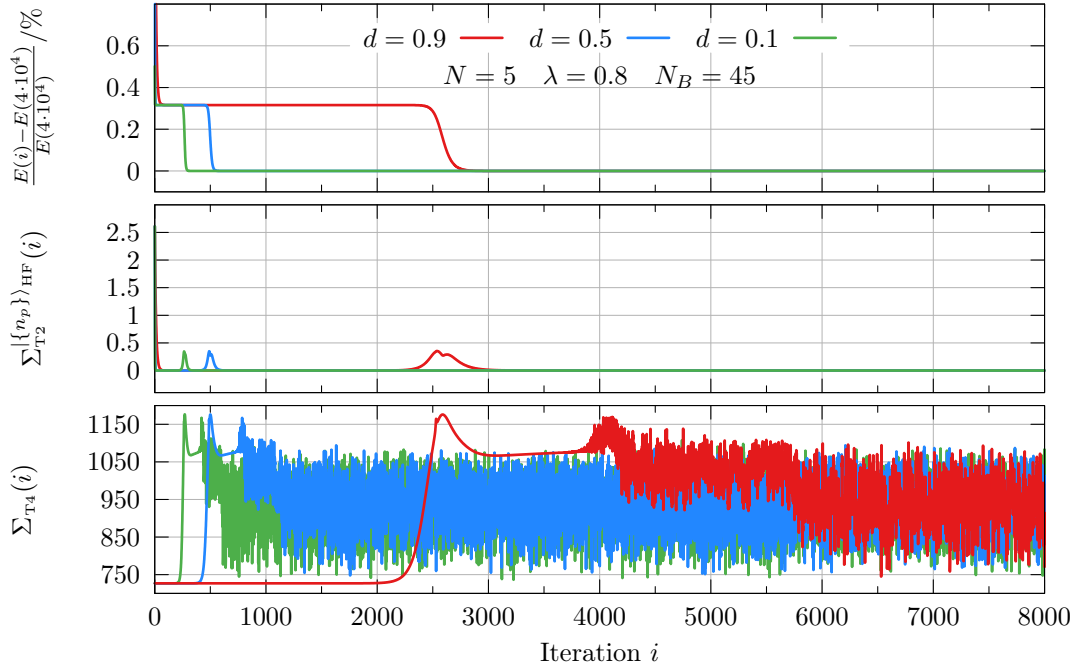
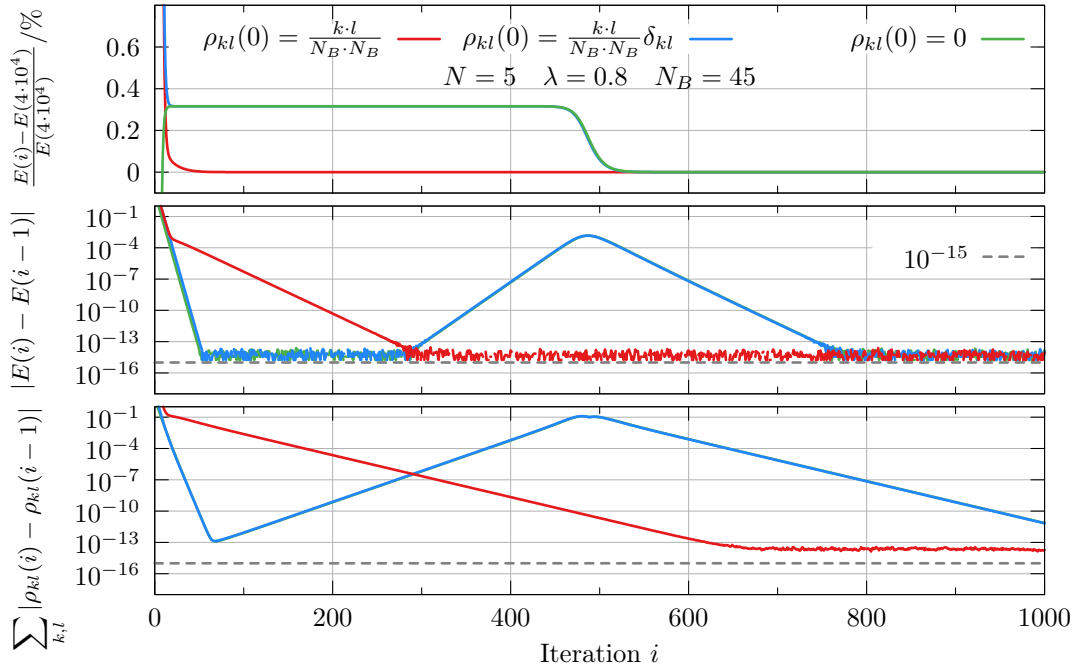**Figure 6.3.:** Ground state HF: Relative convergence of the energy and the sum of type 2 and 4 kinks for three different damping parameters.
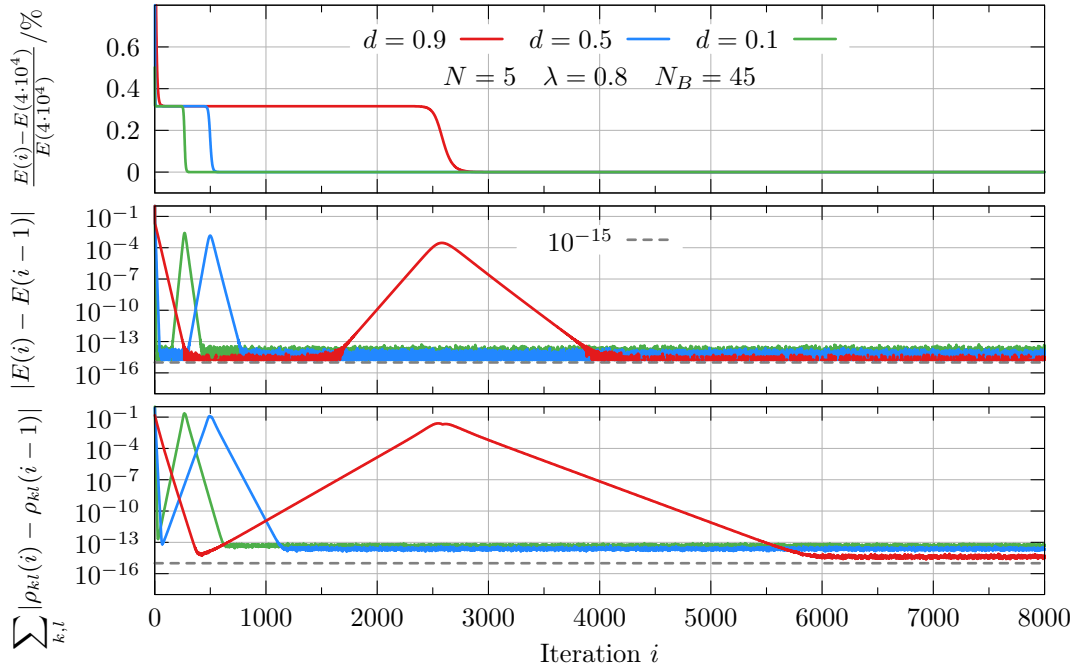
Figure 6.4.: Ground state HF: Relative convergence of the energy and change of the energy and the density matrix to the previous iteration for three different damping parameters in the ground state HF method (Note the logarithmic scale for the latter two).

85

For the moment, we focus on examining the sudden drop in the energy while the HF equation has already been self-consistently solved. To obtain more information on this behaviour, the same ground state HF calculations have been performed for three different damping parameters[1]. In addition to the sum of the type 2 and 4 kinks (Fig. 6.3), we also investigate the change of the energy and the density matrix compared to the previous iteration (Fig. 6.4), which are commonly used as convergence criteria (see Eq. (5.8)). As expected, for larger damping (red curve in Fig. 6.3), the onset of the dropping in the energy and the start of the oscillations in the sum of the type 4 kinks occurs later with respect to the number of iterations. Further, more iterations are required to again obtain a self-consistent solution, which can be seen in the larger width of the peak in the sum of type 2 kinks. In Fig. 6.4, for a damping of $d = 0.9$ (red curve), the energy converges up to $\Delta E = 10^{-15}$ after approximately 200 iterations and then starts to slightly oscillate. Since the energy of this system is roughly 15, this is not surprising because the maximum number of significant digits of double precision[2] is 17. The oscillations continue for about 1500 iterations. After that, we see an increase followed by a decrease to maximum precision around the iteration numbers in which the drop of the energy occurs. On the other hand, the total difference of all elements of the density matrix (graph at the bottom of Fig. 6.4) converges to maximum precision[3] and right after that starts to increase again. The maximum is reached at the drop of the energy. Eventually, it slowly decreases to maximum precision and also starts to slightly oscillate.

In my opinion, the most likely explanation for the observed drop in the energy is the following: Apparently, the higher energy corresponds to a local minimum concerning the solution of the HF equation. When the elements of the density matrix reach double precision, then the correct iteration chain is interrupted or disturbed since the correct computation of the next Fock-matrix from the new density matrix would require a higher precision. This slight disturbance helps to escape the local minimum in which the iteration chain was stuck. Comparing the energy of both solutions with the exact ground state energy reveals that the lower energy is indeed closer to the exact but still slightly larger, which is due to the neglecting of the correlation energy in the HF approximation (the correlation energy is negative). Both solutions will be explored in more detail concerning the resulting particle density in Sec. 6.4.1.

---

[1]The damping parameter in the HF method has been introduced in Eq. (5.9).

[2]That means if the energies of the $i-$the and $(i+1)$-th iteration $E(i)$ and $E(i+1)$ are equal up to th 17-the digit, then $\Delta E = |E(i) - E(i+1)|$ is zero in terms of double precision. Due to the logarithmic scale, only the non-vanishing energy differences are shown in Fig. 6.4.

[3]Since $\Delta\rho = \sum_{kl} |\rho_{kl}(i) - \rho_{kl}(i-1)|$ is the modulus sum of all differences of all elements, $\Delta\rho$ itself is larger than the maximum precision.
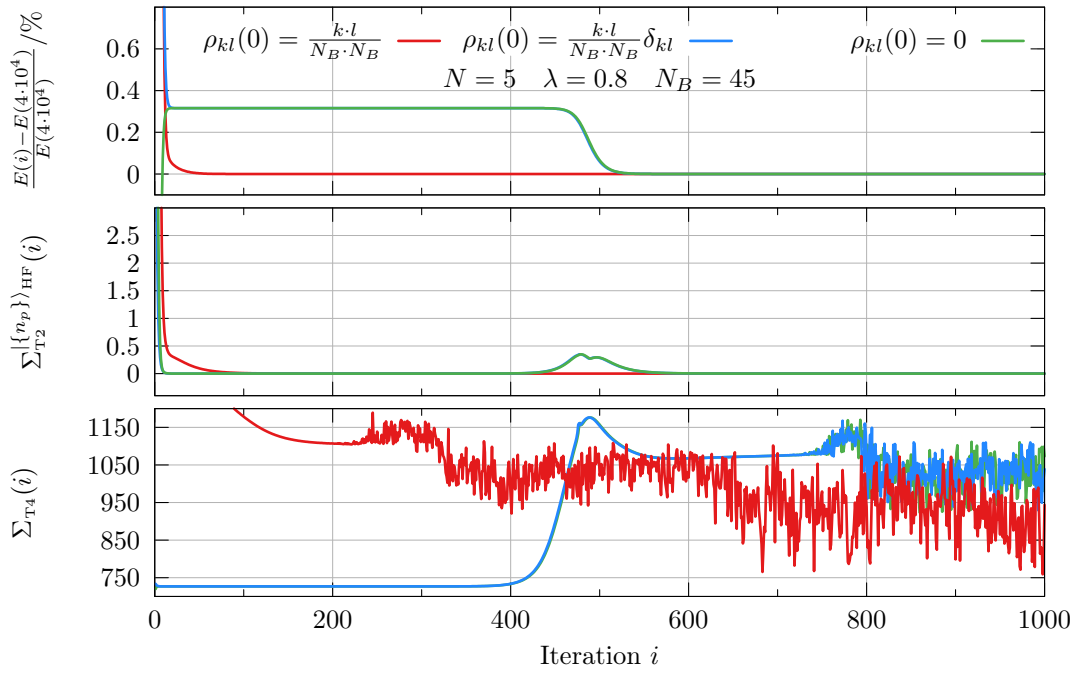
Figure 6.5.: Ground state HF: Relative convergence of the energy and the sum of type 2 and 4 kinks for three different initial density matrices.

Figure 6.6.: Ground state HF: Relative convergence of the energy and change of the energy and the density matrix to the previous iteration for three different initial density matrices (Note the logarithmic scale for the latter two).

6. Numerical results

In addition, by choosing a different initial density matrix for the HF iteration, it is possible to directly converge to the solution with the lower energy as is demonstrated by the red curve in Fig. 6.5. For that reason, it is obvious that the second solution is indeed a true solution of the HF equation and not just one that is obtained due to numerical problems occurring in the continuing iteration after convergence. Further, performing calculations with the off-diagonal elements of the initial density matrix set to zero, results in the convergence to the higher energy solution first (blue and green curve in Fig. 6.5). For the previous calculations, the initial density matrix has been chosen such that the first N diagonal entries equal one while all other elements are set to zero. Since we start in the ideal basis, an initial density matrix with vanishing off-diagonal elements corresponds to a start from an ideal system, while setting the off-diagonal elements to large values corresponds to a start in a strongly interacting system. This is in agreement to the particle density of both solutions shown and discussed in Sec. 6.4.1.

For completion, Fig. 6.6 also shows the evolution of the convergence criteria for the energy and the density matrix for the three different initial density matrices whose courses are in agreement with the explanations given above.

So far, the presented data has been obtained from ground state HF calculations only. Before considering the oscillations in the sum of the type 4 kinks, the convergence behaviour of the canonical and grand canonical HF calculations should be explored. Fig. 6.7 and 6.8 picture the convergence of the energy, sum of type 2 and 4 kinks, and the course of the convergence criteria for the energy and the density matrix for a canonical HF calculation. The system parameters are the same as for the ground state calculations (cf. Fig. 6.1) but for two inverse temperatures $\beta = 10$ and $\beta = 2$. Fig. 6.9 and 6.10 show the same but for grand canonical HF calculations, where the absolute particle numbers are replaced by their HF expectation value.

In the canonical ensemble, we observe another drop in the energy of 0.4% only for 5 particles at $\beta = 10$ after about 400 iterations (red curve in Fig. 6.7). This is also recorded by the courses of the convergence criteria in Fig. 6.8. Like in the ground state HF calculation (cf. Fig. 6.1), for six particles, the sum of type 4 kinks heavily oscillates right from the start of the iterations (green and violet curve in Fig. 6.7). We also notice that the minima in the oscillations of the type 4 kink sums are larger for $\beta = 2$ (violet curve) than for $\beta = 10$ (green curve). Further, for $N = 5$ particles, the behaviour of the type 4 kink sums is very similar for both temperatures. For $\beta = 2$ (blue curve), the oscillations start right after the density matrix and the energy are converged to double precision. The same is observed for $\beta = 10$ (red curve) after the drop of the energy has occurred. And yet, there is a difference in the behaviour of the convergence criteria (blue and red curve in Fig. 6.8). While at the beginning, both, the energy and the density matrix converge equally fast for
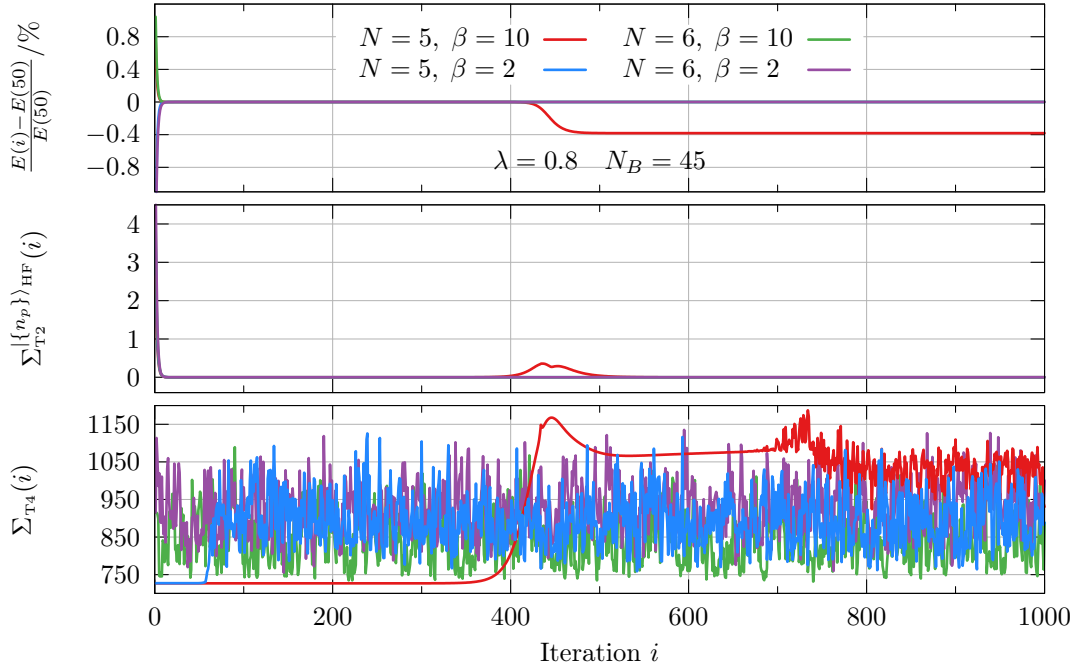
Figure 6.7.: Canonical HF: Relative convergence of the HF energy and the sum of type 2 and 4 kinks for $N = 5$ (red, blue curve) and 6 (green, violet curve) particles in $N_B = 45$ basis functions with a coupling of $\lambda = 0.8$ for two different inverse temperatures.
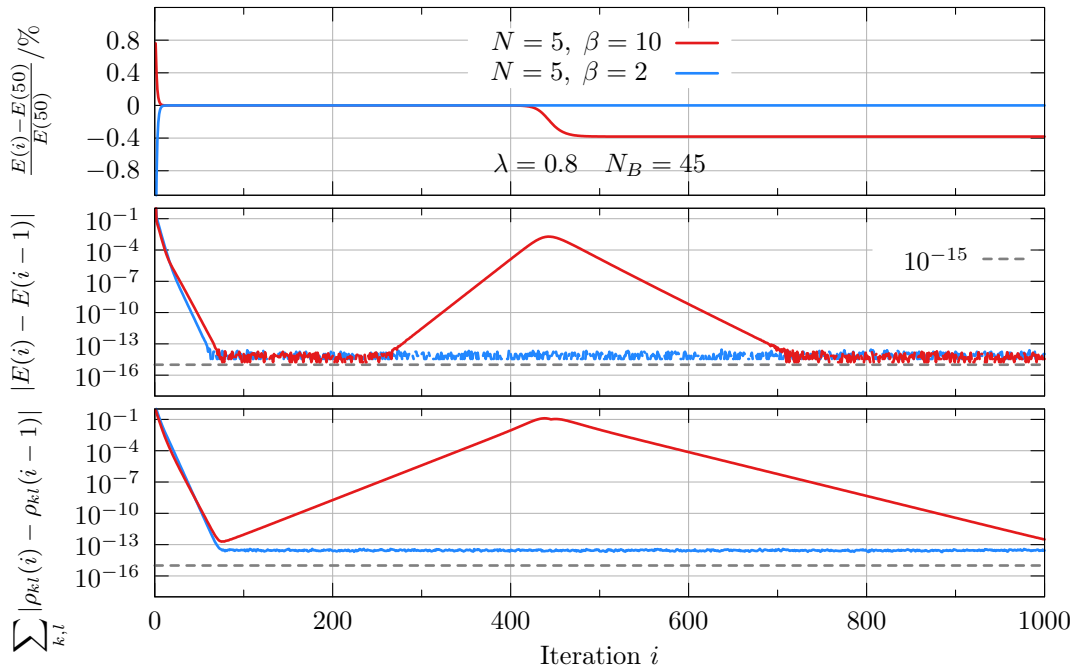
Figure 6.8.: Canonical HF: Course of the energy and density matrix convergence criteria for the same system (only 5 particles) as in Fig. 6.7.
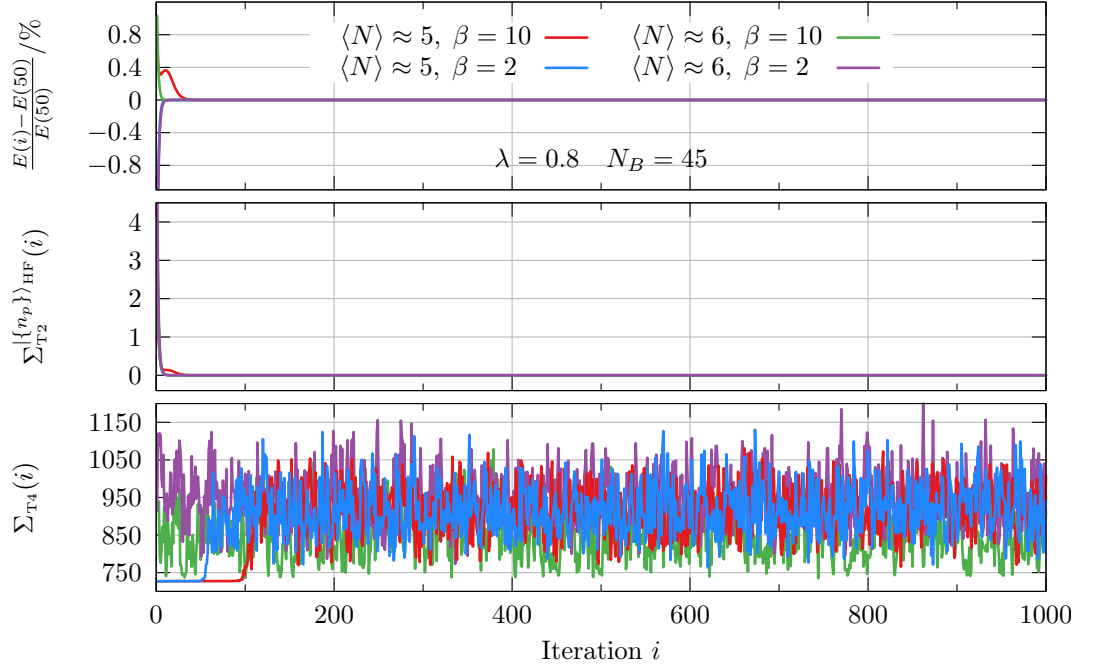
Figure 6.9.: Grand canonical HF: Relative convergence of the HF energy and the sum of type 2 and 4 kinks for $\langle N \rangle \approx 5$ (red, blue curve) and 6 (green, violet curve) particles in $N_B = 45$ basis functions with a coupling of $\lambda = 0.8$ for two different inverse temperatures.
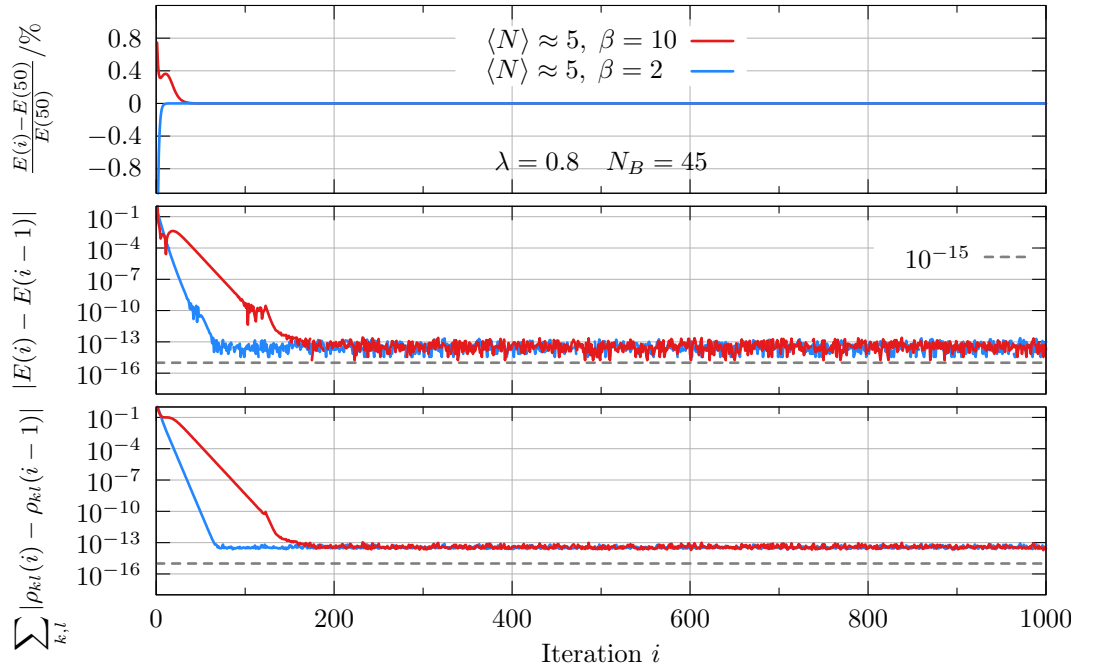
Figure 6.10.: Grand canonical HF: Course of the energy and density matrix convergence criteria for the same system (only 5 particles) as in Fig. 6.9).

both temperatures, this is not the case after the drop of the energy for $\beta = 10$. There, the energy converges significantly faster than the density matrix and even after 1000 iterations the density matrix is not completely converged to double precision. At the same time, we observe that the oscillation in the type 4 kink sum (red curve in Fig. 6.7) has not reached its full amplitude after 1000 iterations.

For the grand canonical HF calculations, we might also expect an additional drop in the energy for $\langle N \rangle \approx 5$ particles at an inverse temperature $\beta = 10$ but this does not happen (see red curve in Fig. 6.9 an 6.10). Instead, in contrast to ground state and canonical HF, we observe a non-monotonic convergence of the energy at about 0.4% (red curve in Fig. 6.9). Since the energy in the canonical HF calculation also drops by 0.4% (see Fig. 6.7), the grand canonical HF iteration seems to be attracted by a very similar self-consistent solution that belongs to the higher energy. But, unlike in the canonical HF, it does not get stuck in this solution. The behavior of the type 4 kink sums is consistent to what we have observed for ground state and canonical HF. For 6 particles, there are heavy oscillations right from the first iteration, while for 5 particles, the oscillations start after the convergence of the energy and the density matrix to double precision.

Finally, we have to discuss the unusual or unexpected behavior of the type 4 kink sums. For that purpose, we summarize the important observations of this section. First, independent from the ensemble, for $N = 6$ particles, the sum of type 4 kinks oscillates right from the beginning, while for $N = 5$ particles, the oscillations start when the energy and the density matrix are converged to double precision; regardless whether there exist a metastable solution or not. We remember that $N = 6$ ($N = 5$) particles corresponds to a closed (open) shell configuration of the 2D harmonic oscillator. Indeed, it turned out that this behavior of the type 4 kink sums is the general case for open or closed shell configurations. Moreover, once the true[4] HF solution has been reached, in addition to the vanishing of the modulus sum over all off-diagonal elements of the Fock-operator, further investigation revealed that the eigenvalues ϵ_i of the Fock-operator, i.e., the orbital energies of the HF orbitals, also remain constant when further iterating. Consequently, the average occupation numbers $\langle \hat{n}_i \rangle$ remain constant, too. Otherwise the HF energy would change. Since the basis that diagonalizes a Hermitian matrix is unique up to a constant factor, I expect the (normalized) HF basis to be uniquely defined. In that case, the sum of type four kinks should be uniquely defined as well. Obviously, the fact that each element of the Fock-operator depends on all basis functions (cf. Eq. (5.2)), allows for a self-consistent solution for different basis sets. This might

---

[4]Of course, we never know if there exist no other solution with an even lower energy. We can only perform the iteration for many initial density matrices to minimize the possibility for that.

be connected to the rotational invariance of the system. Even though the onset of the oscillations seems to be triggered by the convergence of the density matrix for open shells, in my opinion, it is most unlikely that the oscillations are caused by the evolution of some numerical noise when further iterating the solution. If this were the case, then we should not observe heavy oscillations for closed shell configurations right from the first iteration. In addition, further iterations should then lead to completely wrong results which could not be observed even after 10^5 iterations.

Properly analysing the non-uniqueness of the HF basis from a mathematical point of view is beyond the scope of this work. For the utilization of the HF basis in CPIMC calculations, it is only important that all self-consistent solutions correspond to a complete basis set[5]. From the studies of this section and the fact that the results computed in different basis sets (also in the ideal basis) perfectly agree with each other, it is most likely that all these basis sets are indeed (nearly) complete.

---

[5]Sure, it is always just a nearly complete basis since we work with a finite basis size.

Figure 6.11.: Dependence of the average (canonical) sign $\langle s \rangle$ (in CPIMC WA calculations) on the sum of type 4 kinks Σ_{T4} for different ground state [a)] and grand canonical [b)] HF basis sets. Each point corresponds to a two hour CPIMC calculation of $N = 6$ particles in $N_B = 45$ basis functions at an inverse temperature $\beta = 10$. The coupling parameter is distinguished by the color of the points. For each coupling parameter, 300 different HF basis sets have been used for the CPIMC calculations, which are obtained from further iteration of the self-consistent solution of an HF calculation for the same parameters (for grand canonical HF with $\langle N \rangle \approx 6$). The statistical errors are smaller than the points.

6.3. Dependence of the average sign on different Hartree-Fock basis sets

In this section, the dependence of the average sign in CPIMC WA calculations on different HF basis sets is investigated. In Sec. 6.2 it has been shown that the HF basis is not unique. Especially the sum of type 4 kinks, defined in Eq. (6.2), can vary massively for different self-consistent solutions of the HF equation.

Fig. 6.11 shows the average sign of CPIMC WA calculations for $N = 6$ particles in $N_B = 45$ basis functions at $\beta = 10$ for different coupling parameters (indicated by the color). For each coupling parameter, 300 different ground state (left graphic) and grand canonical (right graphic) HF basis sets have been used. These are obtained by further iteration of the self-consistent HF solution, where the same parameters as for the CPIMC calculations are used. Obviously, the average sign strongly depends on the value of the sum of type 4 kinks of the utilized basis. For a coupling of $\lambda = 0.7$ (red points), the average sign varies from 0 to 0.8. The largest values for the average sign are realized for the
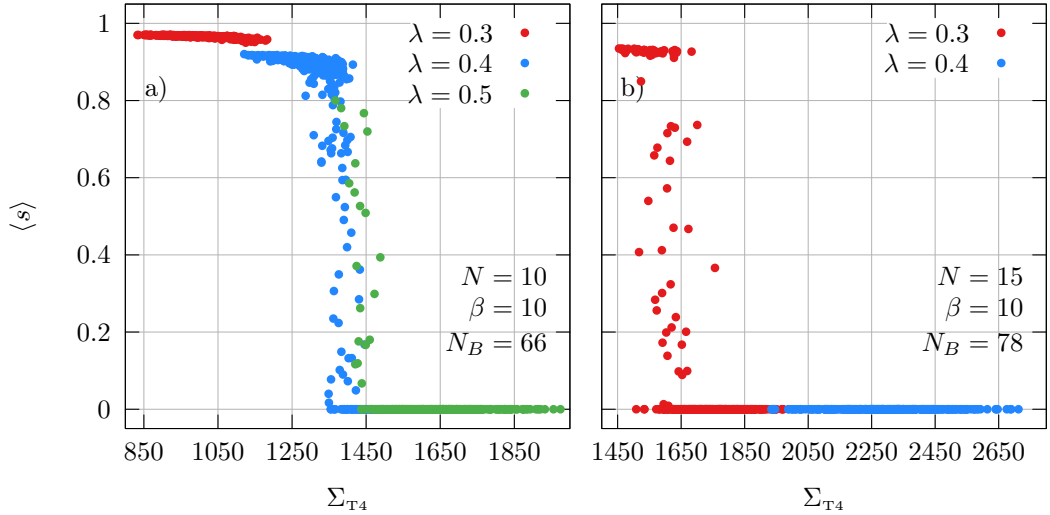
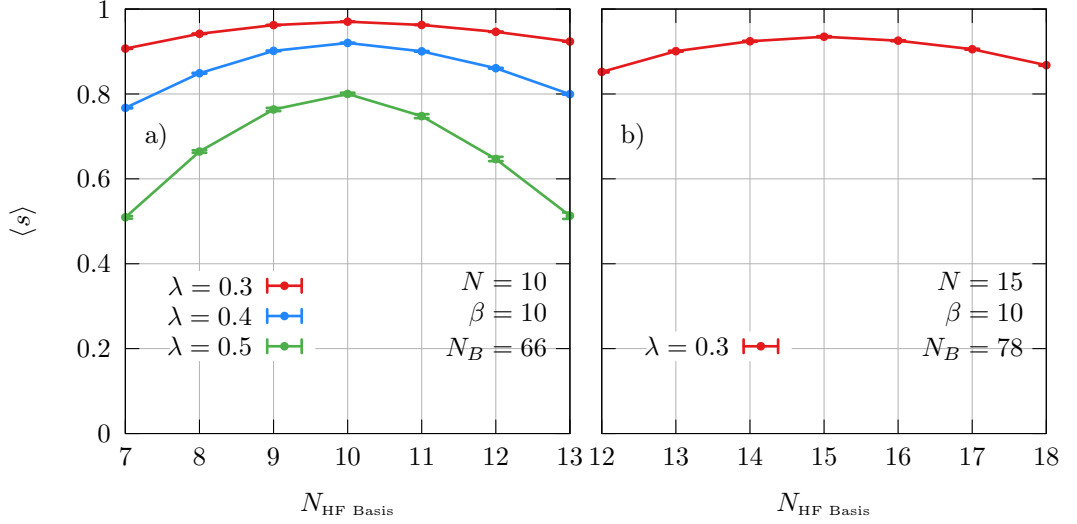**Figure 6.12.:** Same as Fig. 6.11 but only for ground state HF basis sets and a) $N = 10$ particles in $N_B = 66$ basis functions and b) $N = 15$ particles in $N_B = 78$ basis functions.

smallest values of the sum of type 4 kinks, while the largest value itself rapidly drops for increasing lambda so that for $\lambda = 1.0$, even the best (largest) average sign is almost zero. In addition, the same kink sum of $\Sigma_{T4} \approx 900$ can lead to a vanishing but also a very good average sign. This applies not only for different but also for the same coupling parameter. Even though, for fixed coupling, there is no strict monotonic decrease of the average sign with increasing sum of type 4 kinks, a strong correlation between these two quantities is obvious and the best sign is found for the smallest sum. As expected, for $\beta = 10$, there seems to be no significant difference between the ground state (left graphic) and the grand canonical HF basis (right graphic).

Fig. 6.12 pictures the same quantities but for $N = 10$ and $N = 15$ particles in $N_B = 66$ and $N_B = 78$ basis functions, respectively. While for $N = 10$ particles and $\lambda = 0.3$ (red points), the average sign is almost one in each of the 300 basis sets, for $\lambda = 0.5$, there are only very few points with a non-vanishing average sign. Yet, the best are again realized for the smallest sum of kinks, both for $N = 10$ and $N = 15$ particles. It is important to notice that the absolute value of the sum of type 4 kinks only plays a role for the same basis size and coupling[6]. For 6 particles in 45 basis functions (Fig. 6.11), $\Sigma_{T4} > 1000$ leads to a vanishing average sign, whereas for 10 particles in 66 basis functions, the average sign is nearly one up to $\Sigma_{T4} = 1200$. From the definition of Σ_{T4} (cf. Eq. (6.2)), this behavior is expected.

---

[6]The dependence of the smallest Σ_{T4} value on the particle number is rather weak (not shown).
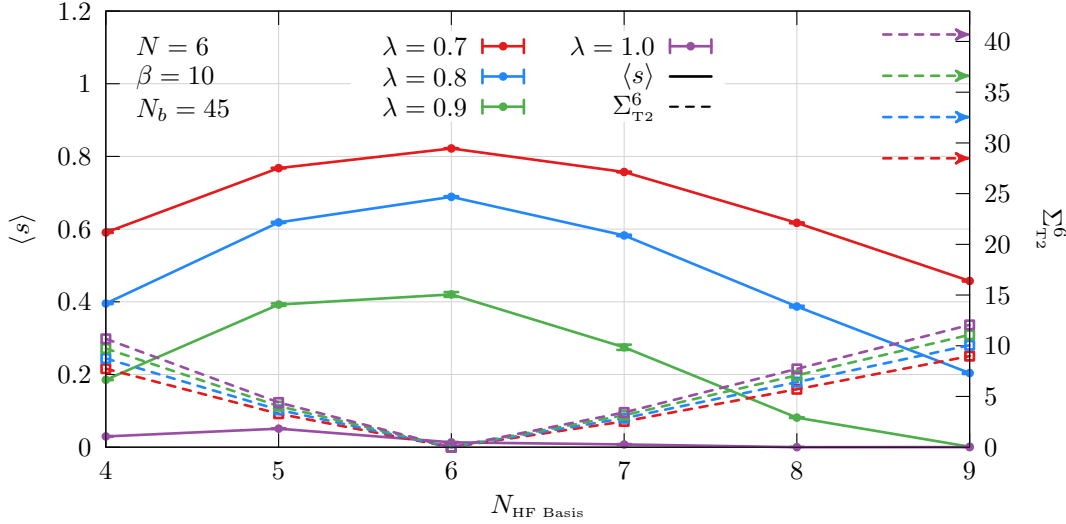
Figure 6.13.: Solid lines: Average sign of a CPIMC WA calculation of $N = 6$ particles in $N_B = 45$ basis functions at $\beta = 10$ for three different coupling parameters. The utilized HF basis sets have been obtained from ground state HF calculations with the same parameters but with $N_{\text{HF Basis}}$ particles. Dashed line: Sum of type 2 kinks Σ_{T2}^6 of the utilized basis, where the lowest 6 HF orbitals are assumed to be occupied, i.e., only for $N_{\text{HF Basis}} = N = 6$ it is $\Sigma_{\text{T2}}^6 = \Sigma_{\text{T2}}^{|\{n_p\}\rangle_{\text{HF}}} = 0$. Dashed arrows indicate the value of Σ_{T2}^6 in the ideal basis.

From the results presented in Fig. 6.11 and 6.12 the strategy to find the best of all possible HF basis sets for fixed system parameters is obvious: Further iterate the self-consistent solution of the HF equation sufficiently long and use the solution that corresponds to the smallest sum of type 4 kinks.

We can also compute the ground state HF basis by solving the HF equation for the same basis size and coupling but for a different particle number (N_{HF}) than the one used for the CPIMC calculation (N). The dependence of the average sign on different HF particle numbers for the basis computation is shown in Fig. 6.13 (solid line) for the same system parameters as in Fig. 6.11. For fixed coupling, the course of the average sign is well described by parabolas with its maximum at $N_{\text{HF}} = N$. Since all pictured particle numbers $N_{\text{HF}} \neq 6$ correspond to open shell configurations, further iteration of the first self-consistent solution is not required for those[7]. For $N_{\text{HF}} = 6$, the average sign corresponds to the largest in Fig. 6.11. Interestingly, these (4) points perfectly fit into the parabola shape representing its maximum (except that for $\lambda = 1.0$).

---

[7]From Sec. 6.2 we know that for open shells the sum of type 4 kinks is the smallest right after convergence of the solution and remains constant for many iterations (cf. Fig. 6.1), i.e., each of the corresponding basis sets would lead to the same average sign.

Figure 6.14.: Same as Fig. 6.13 but for a) $N = 10$ particles in $N_B = 66$ basis functions and b) $N = 15$ particles in $N_B = 78$ basis functions. Only the sign dependence on the HF particle number is pictured.

In addition, for higher coupling, the parabolas slightly deform with a larger sign for $N_{\mathrm{HF}} = N - 1$ than for $N_{\mathrm{HF}} = N + 1$. Fig. 6.14 also shows the average sign for different HF particle numbers but for $N = 10$ and $N = 15$ particles in the CPIMC calculation (same parameters as in Fig. 6.12). Obviously, the parabolas almost become straight lines for smaller coupling. However, we can conclude that we should use the same particle number for the computation of the HF basis and for the CPIMC calculation as this yields the best average sign.

Finally, the reason for the better average sign in the HF basis compared to the ideal basis shall be explained. For this purpose, we recall the definitions of the sum of type 2 and 4 kinks (Eq. (6.2)):

$$\Sigma_{\mathrm{T2}}^{|\{n_p\}\rangle_{\mathrm{HF}}} := \sum_{i \neq k}^{N_B} |f_{ik}| = h_{ik} + \sum_{p \neq i,k}^{N_B} w_{ipkp}^{-} \langle n_p \rangle \ ,$$

$$\Sigma_{\mathrm{T4}} := \sum_{\substack{i,j,k,l=0 \\ i<j,k<l, \\ i \neq k, i \neq l, j \neq k, j \neq l}}^{N_B} |w_{ijkl}^{-}| \ .$$

As already mentioned, Σ_{T4} is nothing but the sum over the modulus weight of all type 4 kinks in a CPIMC WA calculation with the corresponding parameters. The smaller the modulus weight of a specific kink, the smaller is the probability for this kink to be realized in one of the sampled paths. Consequently, if the modulus sum over all kink weights is reduced, then there are on average fewer

kinks in the paths. Since each kink comes with three sources of a possible sign change of the whole path weight (matrix element, phase factor and $(-1)^K$ (cf. Eq. (3.26))), on average fewer kinks is strongly connected to a larger average sign. However, this is not the whole truth since the acceptance probability for a kink to be added in a certain path not only depends on its modulus weight but also on the change in the diagonal energy when adding this kink. The change in the diagonal energy, of course, depends on the orbitals involved in the kink and on the occupation numbers at the time at which the kink shall be added in the path[8]. This is why a smaller sum of type 4 kinks not necessarily implies a better sign, which explains the non-monotonic behavior of the average sign in the Figs. 6.11 and 6.12.

Further, the modulus of the Fock-matrix element $|f_{ik}|$ equals the modulus weight of the kink $s = (i, k)$ only if the occupation numbers in the path at the time of the kink exactly equal the HF occupation numbers, i.e., if

$$|\{n\}(\tau)\rangle = |\{n_p\}\rangle_{\text{HF}} \; , \tag{6.3}$$

where τ denotes the time of the kink. Sure, only for ground state HF this can be exactly fulfilled since for canonical and grand canonical HF we have an ensemble of ONVs resulting in average occupation numbers instead of only a single ONV. However, for the moment let us consider ground state HF. Then, for N particles, the HF determinant consists of the first N orbitals being occupied. When using the corresponding HF basis for a CPIMC simulation, then no type 2 kink can be added at all times in the paths where Eq. (6.3) is fulfilled because for each self-consistent solution of the HF equation all $|f_{ik}|$ must vanish. At times where the ONV differs from the HF (ground state) by only a single (or more) occupation number(s), most kinks will have a small but finite weight. Hence, these have a finite probability to be added at such times. This is illustrated in Fig. 6.13, where the value of Σ_{T2}^6 is shown for different particle numbers of the HF basis (N_{HF}). There, Σ_{T2}^6 denotes the sum over all modulus weights of type 2 kinks assuming the first 6 HF orbitals are occupied, i.e., it vanishes for $N_{\text{HF}} = 6$, whereas for $N_{\text{HF}} \neq 6$ it has a finite value, which becomes larger the more N_{HF} deviates from 6 particles. Since the simulation in Fig. 6.13 has been performed for $N = 6$ particles and $\beta = 10$, the ONV with the lowest 6 orbitals occupied is the most probable. Therefore, the average number of type 2 kinks is at most reduced when using the HF basis with $N = N_{\text{HF}}$. For comparison, the positions of the dashed arrows in Fig 6.13 indicate the value of Σ_{T2}^6 in the ideal basis. Instead of zero for $N_{\text{HF}} = 6$, depending on the coupling, Σ_{T2}^6 is between 25 and 40 in the ideal basis, which results in a vanishing average sign for the illustrated parameters. Even for $N_{\text{HF}} = 9$, the value is three times smaller in the HF basis. As a result, the average number of type 2 kinks is

---

[8]This has been explained in detail in Sec. 3.5.1.
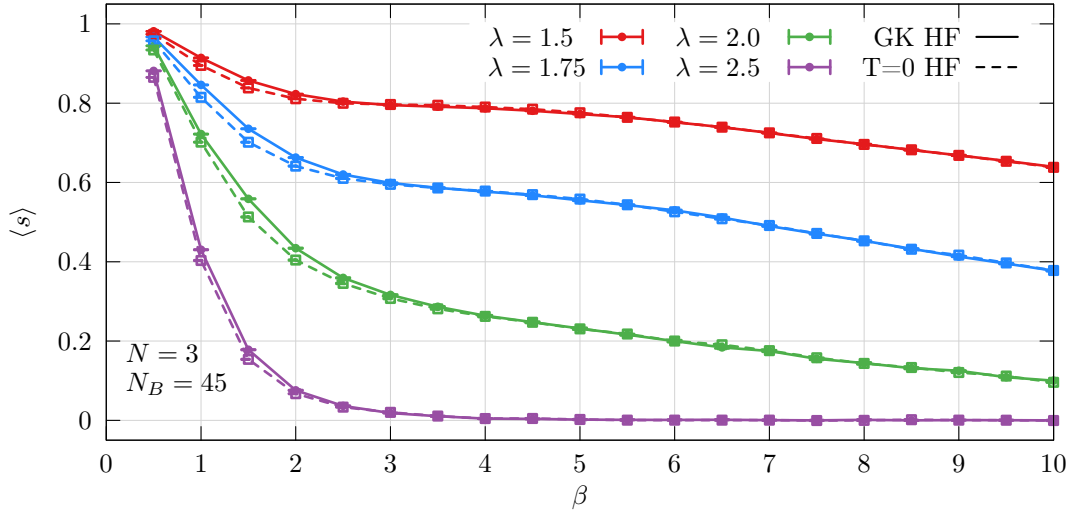
Figure 6.15.: Average sign $\langle s \rangle$ vs. inverse temperature β for CPIMC calculations in the grand canonical (solid line) and the ground state HF basis (dashed line) for $N = 3$ particles in $N_B = 45$ basis functions and different coupling parameters.

significantly reduced in the HF basis, and hence a much better average sign is observed. We refer to this property of the HF basis as an effective *blocking* of the type 2 kinks.

In addition, it turned out that the smallest sum of type 4 kinks of the HF basis sets is approximately equal to that of the ideal basis for the same parameters. Consequently, if we use the best HF basis instead of the ideal basis for the CPIMC calculation, only the average number of type 2 kinks is significantly smaller, while the average number of type 4 kinks is only slightly reduced.

So far, we have only studied the behavior of the average sign for CPIMC calculations at very low temperatures, in fact $\beta = 10$ only. Of course, for higher temperatures, the average occupation numbers in the sampled paths significantly differ from the HF ground state. According to the given explanation of the HF blocking, for higher temperatures, we would expect a larger average sign in the FTHF basis than in the ground state HF basis. In Fig. 6.15 the dependence of the average sign on the inverse temperature is pictured for CIPIMC calculations both in the grand canonical (solid line) and the ground state HF basis (dashed line), where the simulation has been performed for $N = 3$ particles in $N_B = 45$ basis functions and different coupling parameters. Indeed, the average sign for $\beta < 3$ is smaller in the ground state HF basis, but surprisingly, only slightly smaller. It seems that the well-known general effect of an increasing average sign with increasing temperature (cf. Eq. (2.13)) is more important than a better blocking in the FTHF basis. In addition, the

average sign does not exponentially decrease with increasing β, which we expect according to Eq. (2.13). Instead, for $\beta > 3$ it is rather a straight line with small negative slope. For the illustrated coupling parameters and an inverse temperature $\beta < 2$, the chosen basis size is far too small. In fact, for $\beta = 0.5$ convergence of the observables is ensured for $N_B > 91$. If plotting the same graph for $N_B = 91$, then the average sign would indeed decrease exponentially. For $\beta > 4$, convergence is already ensured for the illustrated $N_B = 45$ basis functions, i.e., in practice, the average sign in the CPIMC approach does not decrease exponentially with beta.

We summarize the important results concerning the utilization of the HF basis in CPIMC calculations. First, compared to the ideal basis, the type 2 kinks are successfully blocked in the HF basis. Second, for fixed parameters of the HF calculation, each of the various solutions of the HF equation are equivalent concerning the blocking of the type 2 kinks. Yet, the weight of the type 4 kinks varies massively, where the smallest sum of type 4 kinks is approximately the same as for the ideal basis and results in the best average sign. Third, even for larger temperatures the FTHF basis yields no significant advantage compared to the ground state HF basis. Therefore, the ground state HF basis for the same parameters as for the CPIMC WA calculations is used, while for particle numbers corresponding to closed shells, we have to further iterate the HF solution until a sufficiently small value for the sum of type 4 kinks is obtained.

6.4. Comparison of the density with CI and HF

For this work, there has been no access to another method that provides exact results for the MGF. Therefore, the MGF could only be compared to exact CI results[9] in the limiting case of a fixed time argument $\tau = 0^-$ or $\tau = \beta^-$, i.e., for the particle density. According to the Eqs. (2.26) and (3.22), the particle density is given by

$$n(\mathbf{r}) = \langle \hat{\Psi}^\dagger(\mathbf{r}) \hat{\Psi}(\mathbf{r}) \rangle = \sum_{ij} n_{ij} \Phi_i^*(\mathbf{r}) \Phi_j(\mathbf{r}) = \sum_{ij} (-\mathcal{G}_{ji}(0^-, 0)) \Phi_i^*(\mathbf{r}) \Phi_j(\mathbf{r}) \ .$$

(6.4)

Hence, we have two different estimators for the density; one that receives contributions from closed paths only (Eq. (4.3)) and the estimator for the MGF (Eq. (4.19)) that receives contributions from open paths only. If the closed path estimator is evaluated for closed paths of all particle numbers, then the grand canonical one-particle density matrix is obtained, while evaluating the

---

[9]The used CI program is included in the HF code from the former group member Dr. D. Hochstuhl.

estimator only for paths with a certain particle number yields the canonical expectation value for that particle number. Further, getting a contribution to the estimator of the MGF at $\tau_p = 0^-$ corresponds to an "almost" closed path that has a defined particle number since $\tau_p = \tau_{\mathrm{ir}} - \tau_{\mathrm{ma}} = 0^-$. Thus, we have grand canonical and canonical results for $\mathcal{G}_{ij}(0^-, 0)$, too.

All presented data is obtained from 25-30 hour CIPIMC WA calculations on standard single core CPUs. For each quantity, the Monte Carlo cycle has been chosen such that the auto-correlation of the samples is sufficiently small. Additionally, the convergence of the basis size is ensured for all shown results. The HF and CI calculations have been performed for the same basis size as the CPIMC calculation so that even the small, remaining error due to a finite basis is equal for the compared results. The CPIMC WA program works for both a fixed chemical potential or a desired average particle number. To estimate the error of the density (Eq. (6.4)), a Gaussian error propagation of the statistical error of all elements of the density matrix is carried out.

Fig. 6.16 shows a cut through the radially symmetric density of the two-dimensional test system[10] for a CIPIMC calculation in the ideal (left graphic) and the HF basis (right graphic). In addition, the deviation to the CI density is plotted for the MGF estimator (red curve), the closed path estimator (blue curve) and the canonical HF calculation (green curve). The system parameters are specified in the graphic. First, within the statistical errors, the MGF estimator in the ideal basis coincides with CI, while in the HF basis, its statistical errors become much smaller[11] yielding a perfect agreement with the CI density. In contrast, while the closed path estimator in the ideal basis coincides (within the error bars) with the CI density, too, it has an extremely large error in the HF basis. After we have understood the blocking of the type 2 kinks in the HF basis, the explanation for this behaviour is simple when remembering the actual form of the closed path estimator (cf. Eq. (4.3)), where we receive a contribution to n_{ij} for each kink $s = (i, j)$ in the sampled closed path. This contribution is given by one over the weight of the kink. In the HF basis, as explained in Sec. 6.3, the weight of all type 2 kinks is significantly reduced resulting in fewer type 2 kinks in the paths. Therefore, we rarely get contributions to the closed path estimator of a certain element of the one-particle density matrix, but if we get one, then it will be a huge number. The sample history for these matrix elements looks very similar to that of the poor MGF estimators discussed in Chap. 4 (see e.g. Eq. (4.13) and the sample history in Fig. 4.1). Hence, the closed path estimator is not employable in the HF basis. On the other hand, the MGF estimator profits

---

[10]In the graphs, $n(r)$ is shown, where r is the distance to the center of the harmonic trap, i.e., the particle number is given by $N = \int_0^\infty \mathrm{d}r 2\pi r n(r)$.

[11]Note that in the graphic showing the deviation, relative statistical errors are plotted, which, of course, become larger when the density is almost zero.
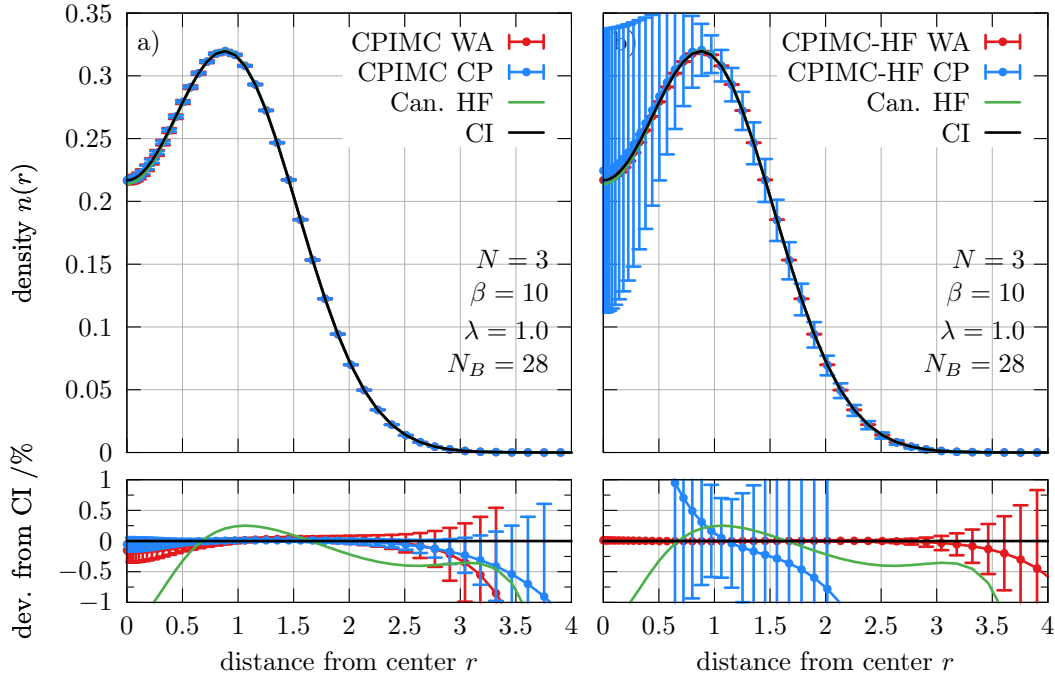
Figure 6.16.: Density $n(r)$ and deviation from CI (bottom plot) for CPIMC calculations in the ideal basis (left) and in the HF basis (right) both for the MGF estimator (red curve) and the closed path estimator (blue curve). The system parameters are shown in the graph.
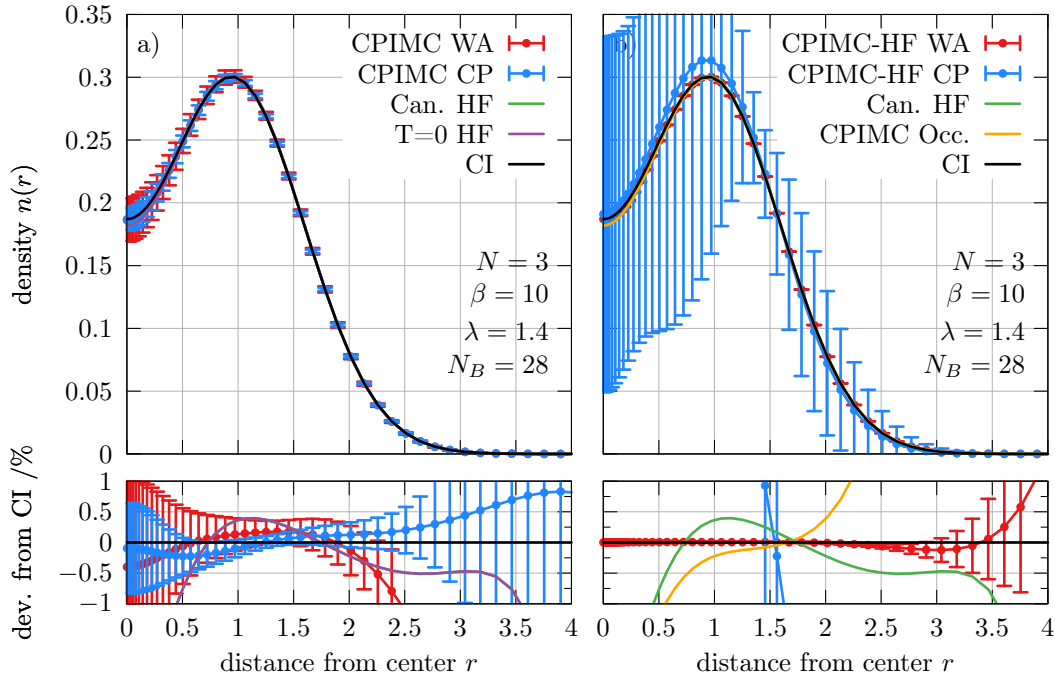
Figure 6.17.: Same as Fig. 6.16 but for $\lambda = 1.4$. The yellow curve is obtained by neglecting the off-diagonal elements of the density matrix.

from the HF blocking because the peaks in its sample history (cf. Fig. 4.3) occur if Ira can only be shifted within a very small time interval due to a near left and right kink on Ira's orbital. And, due to on average fewer kinks in the HF basis, such configurations are sampled less frequently, whereby the variance of the estimator is reduced.

In Fig. 6.17 the same quantities are plotted for the same test system, but the coupling is increased from $\lambda = 1.0$ to $\lambda = 1.4$. The additional yellow curve will be discussed later on. For this coupling parameter, in the ideal basis (left graphic), we have no exact data for the density, and hence not for the MGF, too. The statistical error of the closed path estimator is about 0.7%, while that of the MGF estimator is even larger. However, using the HF basis, we can still produce very accurate data for the density matrix with the MGF estimator. Note that the result of the closed path estimator is what can be obtained from standard CPIMC without the WA[12], i.e., with the WA in combination with the HF basis, we can provide exact data for the one-particle density at significantly higher coupling. In fact, even for $\lambda = 1.7$ and $\lambda = 2.0$, which is shown in Fig. 6.18, the results are still acceptable. Especially for $\lambda = 1.7$ (left graphic), the relative statistical error of the MGF estimator (about 0.1%) is comparable to that of the closed path estimator for $\lambda = 1.0$ in the ideal basis (cf. left graphic in Fig. 6.16).

In addition, in the Figs. 6.16 - 6.18, the canonical and/or ground state HF density is plotted, while, due to $\beta = 10$ in all graphics, both are practically equal (cf. left graphic in Fig. 6.17). The deviation of the HF densities for $r > 0.5$ doubles as lambda is increased from $\lambda = 1.0$ (0.25%, Fig. 6.16) to $\lambda = 1.7$ (0.5%, Fig. 6.18). Near the center of the trap ($r < 0.5$), the HF density shows much larger deviations from the CI density. This is not surprising as a cut through the density is plotted in the graphs, i.e., $N = \int_0^\infty \mathrm{d}r 2\pi r n(r)$. Naturally, an increase of the coupling also causes the particles to move apart (or outwards), which we observe in the change of the density profile.

Due to a perfect agreement with the exact CI results in the Figs. 6.16 - 6.18, we can conclude that the estimator of the MGF produces correct results (within statistical errors). Moreover, for the estimator of the MGF $\mathcal{G}_{ij}(\tau_p, 0)$, it is irrelevant if we sample for a certain particle number only, at $\tau_p = 0^-$ or at any other $\tau_p \in (0, \beta)$. The only difference lies in fewer samples for some times τ_p and orbitals i and j, which results in larger (relative) statistical errors. Therefore, it is very unlikely that the results for the MGF at times $\tau_p \neq 0^-$

---

[12]In the beginning of Sec. 3.3, it has been mentioned that one of the drawbacks of the standard CPIMC method consisted in the poor results for the one-particle density matrix. Obviously, within the HF basis and with the MGF estimator in the WA, this problem could be significantly reduced.
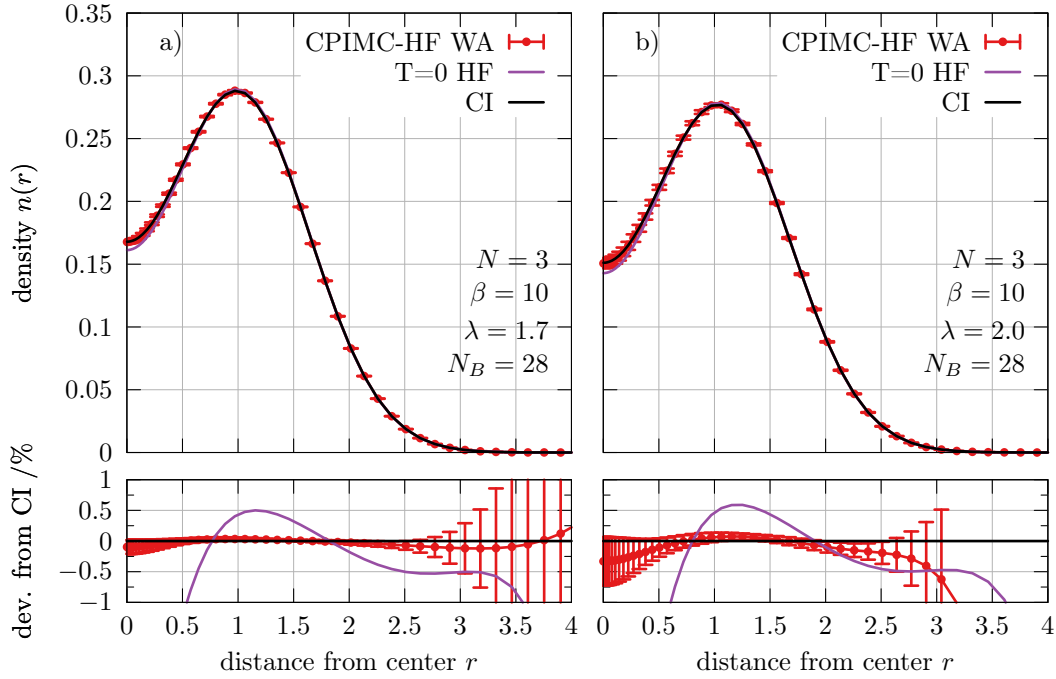
Figure 6.18.: Same as Fig. 6.16 but for a) $\lambda = 1.7$ and b) $\lambda = 2.0$ both in the HF basis. Only CI (black curve), the MGF estimator (red curve) and the ground state HF (violet curve) are plotted.
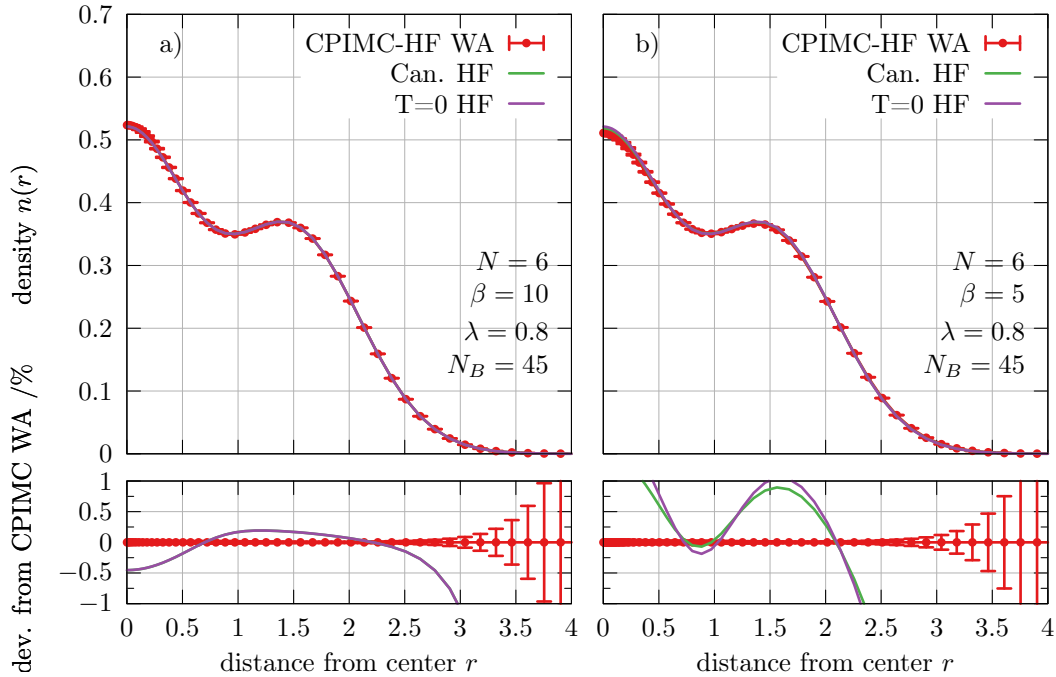

Figure 6.19.: Density n(r) and deviation from the MGF estimator for canonical and ground state HF for a) $\beta = 10$ and b) $\beta = 5$. CI calculations are not feasible for the specified system parameter.

do not coincide with the correct result within the (true) statistical errors[13]. In addition, comparing the density computed from the whole density matrix $\mathcal{G}_{ij}(0^-, 0)$ with the exact CI density is a fairly good comparison as all elements contribute to the density.

From now on, the HF basis is always used for the presented CPIMC results. Staying in the canonical ensemble, Fig. 6.19 shows the density for $N = 6$ particles in $N_B = 45$ basis functions at a coupling of $\lambda = 0.8$ for an inverse temperature $\beta = 10$ (left) and $\beta = 5$ (right graphic). This system size is already far too large for CI calculations[14]. Therefore, the deviation of the canonical and ground state HF density from the (exact) MGF estimator is plotted. For $\beta = 10$ (left graphic), again both canonical and ground state HF coincide showing a deviation of about 0.5% to the MGF estimator. Interestingly, for $\beta = 5$ (right graphic), the HF densities deviate more than 1% from CPIMC, while the canonical HF density is slightly better. Apparently, FTHF is not able to correctly represent the change in the density due to an increase of the temperature (for these system parameters)[15].

Next, Fig. 6.20 shows the grand canonical density for the same system parameters as in Fig. 6.19, i.e., the chemical potential μ is chosen such that we obtain roughly six particles. In addition, instead of $\beta = 10$ and $\beta = 5$, the densities in Fig. 6.20 are plotted for $\beta = 2$ (left) and $\beta = 5$ (right). As expected, compared to $\beta = 5$, the density profile is significantly smeared out at $\beta = 2$. In analogy to the canonical HF, the grand canonical HF density deviates up to 1.5% from the CPIMC density[16].

Finally, the grand canonical[17] densities for $N \approx 30$ particles in $N_B = 91$ basis functions are plotted in Fig. 6.21 for the ideal system (left) and for a coupling of $\lambda = 0.2$, both at an inverse temperature $\beta = 5$. In the ideal case, the grand canonical (green curve) agrees perfectly with the CPIMC density (red curve), while for $\lambda = 0.2$, grand canonical HF deviates up to 0.1% from the CPIMC result. Since the HF approximation takes into account the interaction in terms of a mean-field, this approximation is expected to become better for larger particle numbers and smaller coupling. Yet, with CPIMC, the concrete deviation can be precisely determined. Unfortunately, a slightly larger coupling

---

[13]Of course, if we have too few samples for some element $\mathcal{G}_{ij}(\tau_p, 0)$, then the samples might be not Gaussian distributed and the computed statistical error is of no meaning. Yet, this applies to any estimator in Metropolis Monte Carlo.

[14]The complexity of CI calculations is of the order $\mathcal{O}\left(\binom{N_B}{N}^3\right)$.

[15]The HF energies for $\beta = 5$ are still very good. It is $E_{\text{CPIMC}} = 20.606$, $E_{\text{Can. HF}} = 20.569$ and $E_{\text{T=0 HF}} = 20.543$. That is a deviation of 0.18% for canonical HF and 0.3% for ground state HF from the (exact) CPIMC energy.

[16]Of course, exactly the same chemical potential has been used for the HF and the CPIMC calculation.

[17]Canonical HF calculations are not feasible for $N_B = 91$ basis functions and $N > 3$ particles (cf. Chap. 5).
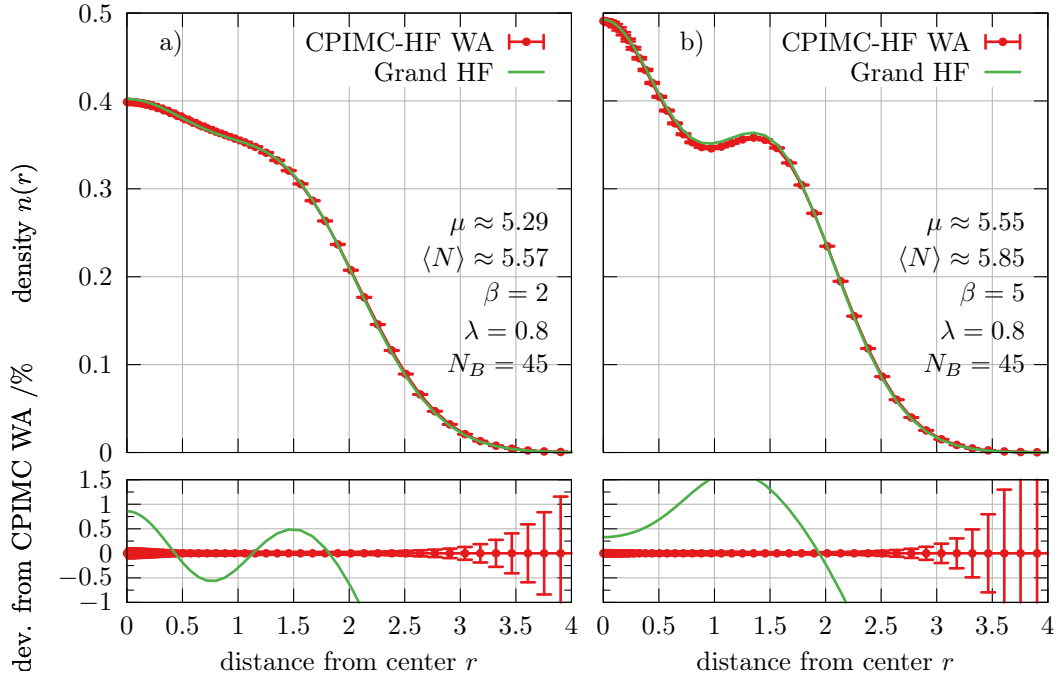
Figure 6.20.: Grand canonical density and deviation of the HF density from CIPIMC (bottom plot) for roughly six particles at $\beta = 2$ (left) and $\beta = 5$ (right).
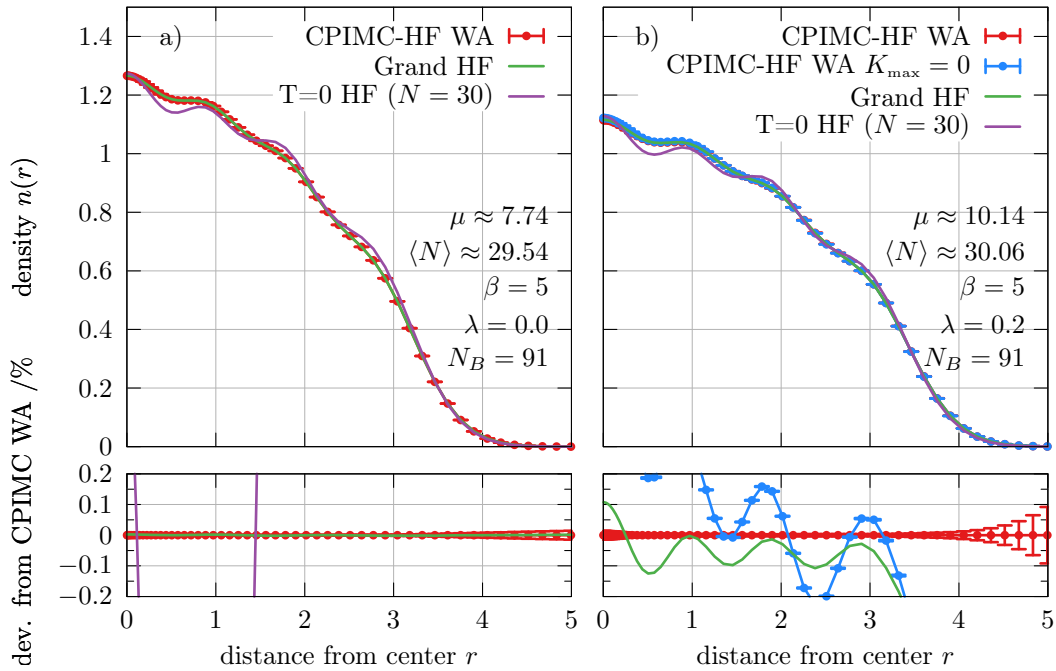

Figure 6.21.: Same as Fig. 6.20 but for roughly 30 particles at $\beta = 5$ for the ideal ($\lambda = 0$) system (left) and for $\lambda = 0.2$ (right). In addition, the ground state HF density for $N = 30$ particles (violet curve) and the CPIMC result with the restriction of no kinks (blue curve) is plotted.

of $\lambda = 0.225$ is (currently) not possible with CPIMC in the grand canonical ensemble, even though the average number of kinks in the sampled path for $\lambda = 0.2$ is about 0.4. Consequently, the average sign is nearly one. This problem will be discussed at the end of this work in Sec. 6.6. However, if we restrict the number of kinks exactly to zero in the CPIMC simulation (blue curve in Fig. 6.21), then the result for the density is even worse than the FTHF density. Additionally, in Fig. 6.21 the ground state HF density for $N = 30$ particles is plotted (violet curve), which significantly deviates from the density at $\beta = 5$ (see right graphic, where $N = 30.06$).

6.4.1. Density of the different HF solutions

In Sec. 6.2, we have observed that the ground state HF equation for $N = 5$ particles at $\lambda = 0.8$ possesses a solution corresponding to a local minimum of the energy (cf. Fig. 6.2). The existence of such metastable solutions is well-known [19]. Further, in unrestricted HF (UHF) calculations[18] [19], the densities of HF calculations may not be rotationally symmetric even if the Hamiltonian is invariant under rotations. This is referred to as the *symmetry breaking* of UHF [34]. Since our test system consists of spin polarized fermions, we do not expect a symmetry breaking of the HF solution. In Fig. 6.22, the density profile $n(r, \Phi)$ obtained from the HF solution with the higher energy (after 150 iterations) and with the lower energy (after 700 iterations) is shown for different (fixed) polar angles Φ. In addition, the deviation of the densities for the different angles from $\Phi = 0$, i.e., from $n(r, 0)$, is plotted. Obviously, both solutions are rotationally symmetric[19]. Thus, at least concerning the spatial symmetry, both solutions are correct.

The left graphic in Fig. 6.23 compares the canonical CPIMC density (violet curve) with the canonical HF density corresponding to the solutions after 150 (red curve) and 750 (blue curve) iterations of the FTHF equation (cf. Fig. 6.7). Both HF densities are not even near the correct CIPIMC density obtained from the MGF estimator. Thinking of classical particles, it seems that the higher energy solution (red curve) corresponds to the configuration of one particle being at the center of the trap and the remaining four in the outermost shell, while the lower energy solution corresponds to all five particles being in the outermost shell. This is in agreement to what has been discussed in Sec. 6.2 about the lower energy solution belonging to an initial density matrix describing a stronger interacting system. Interestingly, an appropriate linear combination of the density of both HF solutions (green curve) coincides with

---

[18]In UHF, one uses different orbitals for spin up and down particles, in contrast to restricted HF (RHF), where the spatial part of the HF orbital is equal for spin up and down particles.

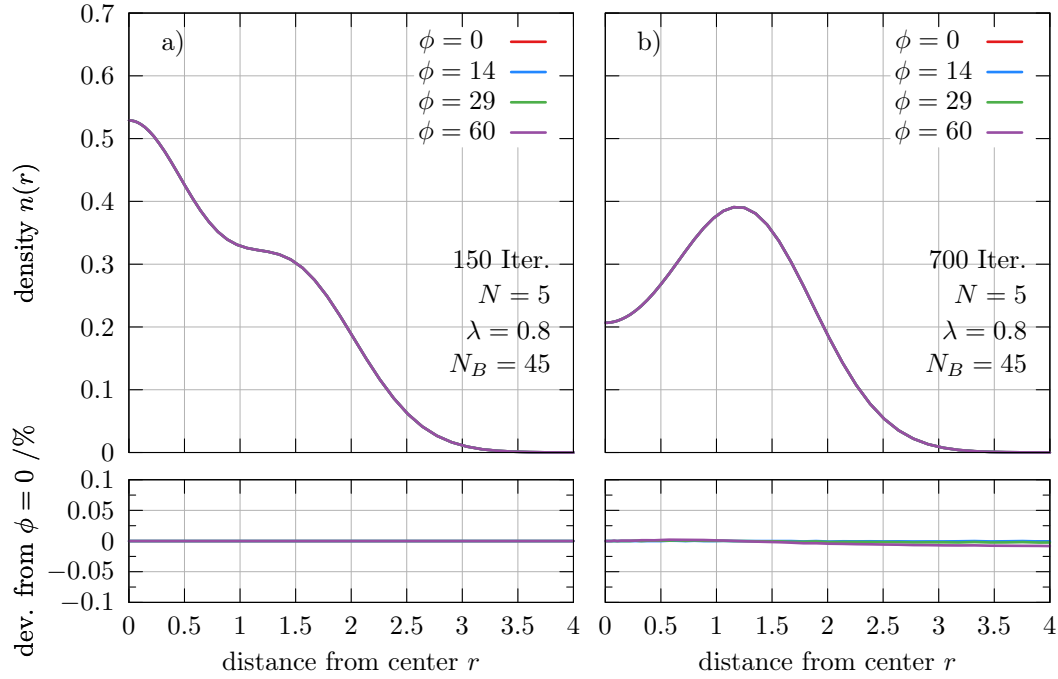[19]This has also been checked for polar angles $60 < \Phi < 360$.

Figure 6.22.: Ground state HF density profile $n(r, \Phi)$ under different polar angles Φ and deviation from $\Phi = 0$ (bottom plot) after a) 150 and b) 750 iterations of the HF equation (cf. Fig. 6.2)
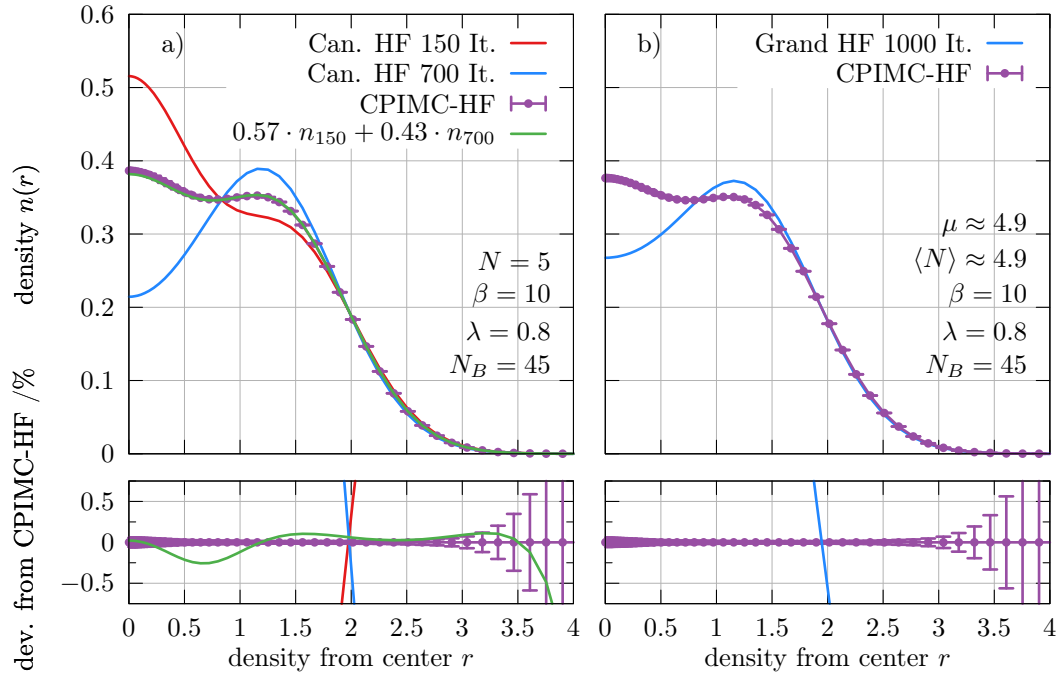

Figure 6.23.: a) Canonical density and the deviation from CPIMC (bottom plot) for the canonical HF solutions after 150 (red) and 750 iterations (blue) (cf. Fig. 6.7) and a linear combination of both (green) b) Grand canonical CPIMC and HF density after 1000 iterations (cf. Fig. 6.9).

the CPIMC density up to 0.25%. However, neither the first nor the second solution of the canonical HF equation for these system parameters represents the correct ensemble average concerning the density profile.

For the grand canonical HF equation, we could not observe a metastable solution for $N \approx 5$ (cf. Fig. 6.9). In the right graphic of Fig. 6.23, the grand canonical CPIMC and HF density after 1000 iterations are plotted. Even though, the grand canonical HF density is somewhere in between the two canonical densities, it strongly deviates from CPIMC.

From the results of this section, we conclude that FTHF provides fairly good results for the density with deviations up to about 2% percent for fewer particles and a coupling of $\lambda \approx 0.5 - 1.0$. For larger systems and even weaker coupling, the HF densities agree with CPIMC up to 0.1%. Yet, for smaller systems, this seems to apply only for particle numbers corresponding to closed shells[20] (even in the grand canonical ensemble), while for open shells (e.g. $N = 5$), the HF densities can become unphysical. Further investigation of this topic has been beyond the scope of this work[21]. In my opinion, it is likely that such metastable or unphysical solutions do not exist for larger systems, e.g., for $N \approx 30$ (open shell), the grand canonical HF and CPIMC density agree within 0.1% (cf. Fig. 6.21).

6.5. Results for the MGF

In this section, the results for the time dependent MGF are presented. First, for the complete time dependent MGF in the ideal and the HF basis sets. Afterwards, the diagonal elements of the MGF are compared to the MGF in the HF approximation.

6.5.1. Complete MGF in the ideal and HF basis

Fig. 6.24 shows the complete MGF $\mathcal{G}_{ij}(\tau)$ in the ideal (upper graphic) and in the HF basis (lower graphic). The parameters for the test system are specified in the caption. The orbital indices are on the x- and y-axis and the imaginary time τ is plotted along the z-axis. The actual value of $\mathcal{G}_{ij}(\tau)$ is determined by the color bar, where grey indicates "almost zero". Unfortunately, a logarithmic color bar can not be used due to positive and negative values of the off-diagonal elements of the MGF. Further, since $\mathcal{G}_{ij}(\beta^-) = n_{ji} = n_{ij}$ (symmetric matrix), for constant $\tau = \beta^-$, Fig. 6.24 shows the elements of the one-particle density matrix. In the ideal basis (upper graphic), there are only a few non-vanishing

---

[20] $N = 3$ and $N = 6$ correspond to closed shells.

[21] It remains to be checked if there are more such metastable and, concerning the density, incorrect HF solutions for different (open shell) particle numbers.
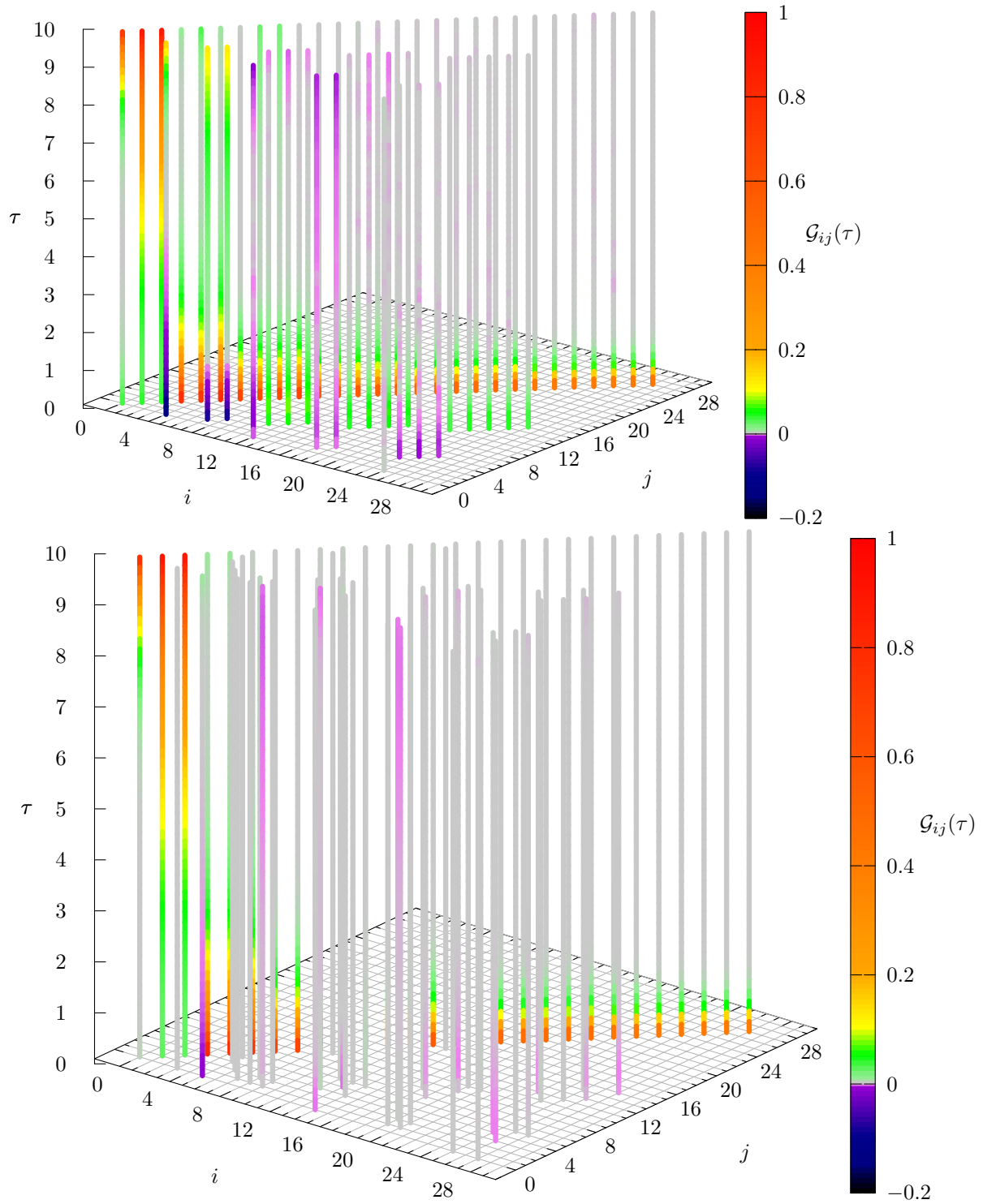
Figure 6.24.: Complete time-dependent MGF $\mathcal{G}_{ij}(\tau)$ in the ideal (top graphic) and HF basis (bottom graphic) for a $N \approx 3$ particles ($\mu = 4$) in $N_B = 28$ basis functions for a coupling of $\lambda = 1.4$ and an inverse temperature $\beta = 10$. The value of $\mathcal{G}_{ij}(\tau)$ is determined by the color bar.

off-diagonal elements of the MGF with values from roughly -0.2 up to 0.1. On the other hand, in the HF basis, there are more non-vanishing elements, while the values are significantly reduced by modulus, i.e., the quantity

$$\sum_{i \neq j} \int_0^\beta \mathrm{d}\tau \, |\mathcal{G}_{ij}(\tau)|$$

is much smaller in the HF than in the ideal basis. However, if we neglect the off-diagonal elements of the one-particle density matrix in the computation of the density, then this results in large deviations from the correct result. This is demonstrated by the yellow curve in the left graphic of Fig. 6.17, where the density for the same parameters as in Fig. 6.24 is plotted. Further, when increasing the coupling to $\lambda = 2.0$ (not shown), in the HF basis, there are much more elements of the MGF that do not vanish, while all of them have small values (by modulus). In contrast, in the ideal basis, there are exactly the same non-vanishing elements for $\lambda = 1.4$ and $\lambda = 2.0$ with larger values (by modulus) for $\lambda = 2.0$. Completely vanishing elements of the MGF, or equivalently of the density matrix, occur if the corresponding type 2 kink has zero weight. Thus, even though there are on average fewer kinks in the sampled paths for calculations in the HF basis, there are much more different, possible kinks compared to the ideal basis. In the ideal basis, less than 10% of the theoretically possible kinks actually have a non-vanisihnig weight.

6.5.2. Comparison to the MGF in HF approximation

In HF approximation, the MGF is given by [35]

$$\mathcal{G}_{ij}(\tau) = \begin{cases} e^{-\tau(\epsilon_i - \mu)} \cdot (1 - \langle \hat{n}_i \rangle) \delta_{ij} & \tau \in (0, \beta] \\ e^{-\tau(\epsilon_i - \mu)} \cdot (- \langle \hat{n}_i \rangle) \delta_{ij} & \tau \in [\beta, 0) \end{cases}, \tag{6.5}$$

with the HF orbital energies ϵ_i and the average (grand canonical) HF occupation numbers

$$\langle \hat{n}_i \rangle = \frac{1}{e^{\beta(\epsilon_i - \mu)} + 1} \, ,$$

i.e., the MGF is diagonal in the HF basis $\{|i\rangle\}$. Hence, after we solved the FTHF equation, we can compute the MGF in HF approximation according to Eq. (6.5) without additional effort. Of course, Eq. (6.5) only represents the actual MGF in HF approximation provided that we have obtained the true HF solution.

However, after we have compared the CPIMC densities with the HF densities, it is reasonable to compare the diagonal elements of the MGF in HF approximation with those obtained from CPIMC calculations (in the same HF
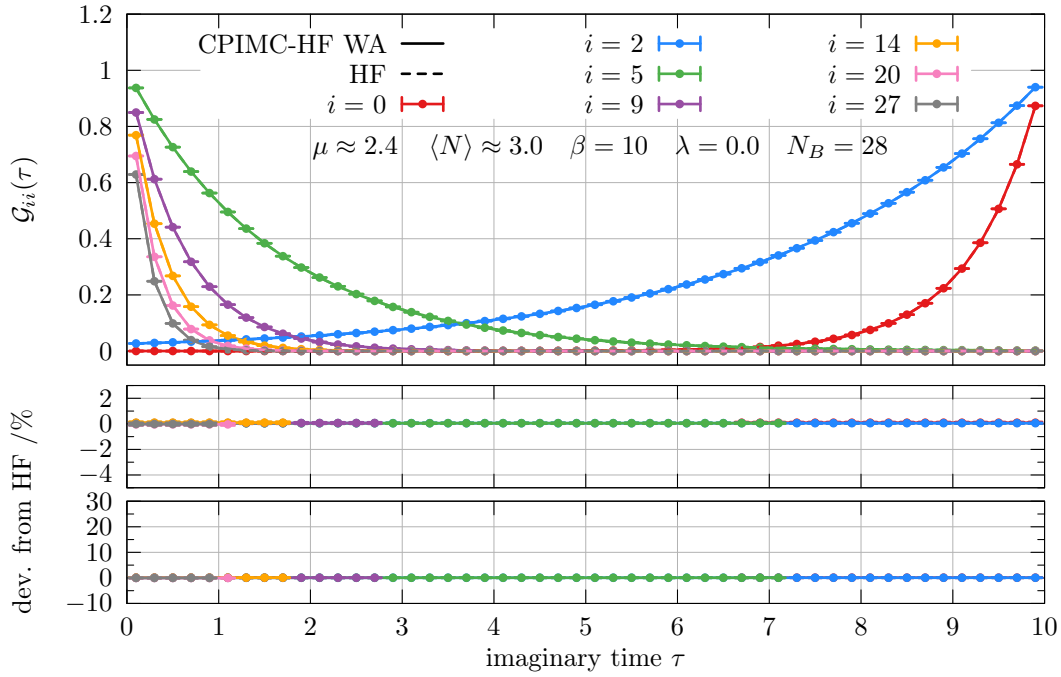
Figure 6.25.: Diagonal elements of the CPIMC MGF (solid lines) and the MGF in HF approximation (dashed lines). Below, the deviation of the CPIMC from the HF MGF for $\mathcal{G}_{ii}(\tau) > 10^{-3}$ is shown on two different scales. The system parameters are specified in the graphic.
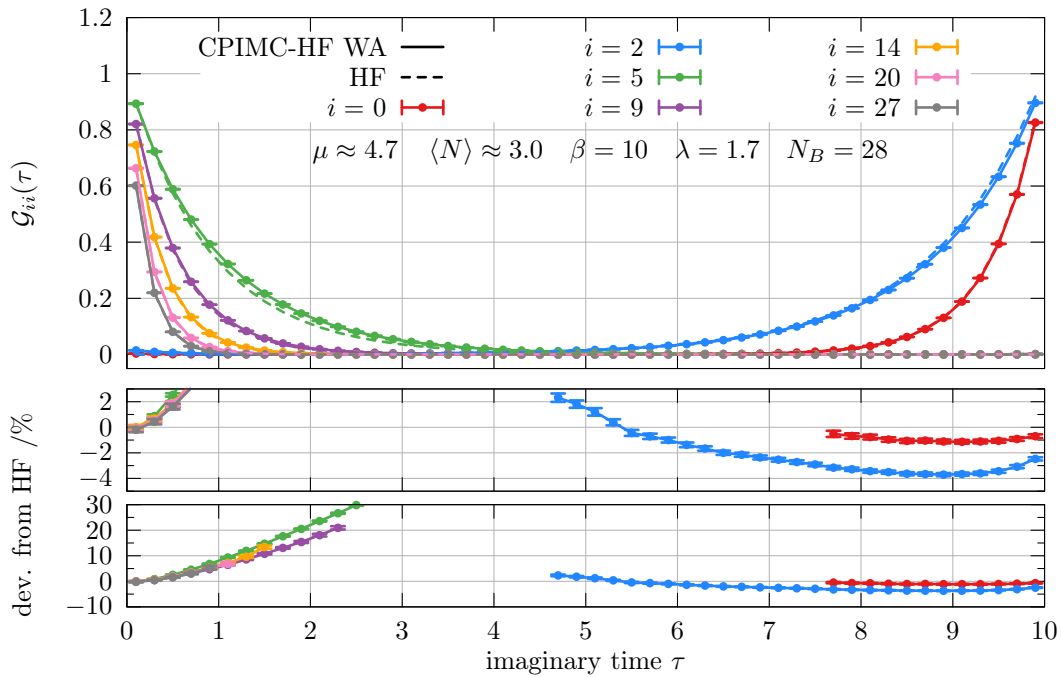

Figure 6.26.: Same as Fig. 6.25 but for a coupling of $\lambda = 1.7$.

basis). This is illustrated in Fig. 6.25 for the ideal system (see parameters in the graphic). For each shell of the test system, one diagonal element is plotted. In the ideal system, the elements of the MGF in each shell are exactly equal due to the degeneracy of the orbital energies, while in the interacting system, most of the orbital energies are two-fold degenerate due to the rotational symmetry of the system. Further, for weak coupling, the MGF elements of one shell show very similar behavior and hence, for a better overview, it is sufficient to only consider one element per shell. From Eq. (6.5) it follows that in Fig. 6.25 at $\tau = \beta^- = 10^-$, the value of the MGF element $\mathcal{G}_{ii}(\tau)$ is nothing but the average occupation number $\langle \hat{n}_i \rangle$, while at $\tau = 0^+$ it is $\mathcal{G}_{ii}(\tau) = 1 - \langle \hat{n}_i \rangle$. In addition, Fig. 6.25 shows the deviation of the CPIMC MGF from the HF MGF on two different scales, where the deviation is only plotted for times where $\mathcal{G}_{ii}(\tau) > 10^{-3}$. As expected, in the ideal system, the CPIMC and HF MGF perfectly agree. Besides the consistency of the CPIMC MGF in the limit of the density with the CI density (cf. Sec. 6.4), this is another important indicator for the correctness of the implemented estimator of the MGF.

Fig. 6.26 shows the same quantities but for a coupling of $\lambda = 1.7$. The chemical potential has been adjusted such that the average particle number is again three. The average occupation numbers show a deviation of up to 2% (blue curve at $\tau = 10$), which is in agreement with the deviation of the HF density from the CI density for these parameters (cf. Fig. 6.18). The course of the occupied elements of the MGF[22] obtained from the CPIMC calculation deviates by up to 4% from the HF MGF (blue curve), even for larger values of the MGF (see blue curve at $\tau \approx 9$). On the other hand, for the unoccupied elements of the MGF, the deviation from HF is much larger reaching up to $10 - 20\%$ at times where the MGF is not yet decreased to very small values (see for example the green curve at $\tau \approx 2$). For smaller coupling, e.g., $\lambda = 0.5$, there are still deviations up to a few percent for those unoccupied elements (not shown). These deviations strongly increase with stronger coupling.

Next, we investigate the behavior concerning the deviation from HF for increasing temperature. Fig. 6.27 and 6.28 show the diagonal elements of the MGF for a larger system of $\langle N \rangle \approx 6$ particles with a coupling parameter $\lambda = 0.8$ at two different inverse temperatures $\beta = 10$ and $\beta = 2$, respectively. For $\beta = 10$, we observe similar deviations as for $\langle N \rangle \approx 3$ particles at a coupling of $\lambda = 1.7$ (cf. Fig. 6.26). For higher temperatures, the deviations of the CPIMC MGF elements from those in HF approximation are strongly enhanced[23]. Especially for those orbitals that are partially occupied at $\tau = \beta$

---

[22]We refer to $\mathcal{G}_{ii}(\tau)$ as an occupied element of the MGF if $i \leq \langle N \rangle$, i.e., if the average occupation number $\langle \hat{n}_i \rangle = \mathcal{G}_{ii}(\beta^-)$ is significantly greater than zero for large β. Analogously, if $i > \langle N \rangle$, then it is called an unoccupied element of the MGF.

[23]For the results of the density, the HF approximation becomes worse with increasing temperature, too (see Fig. 6.19).
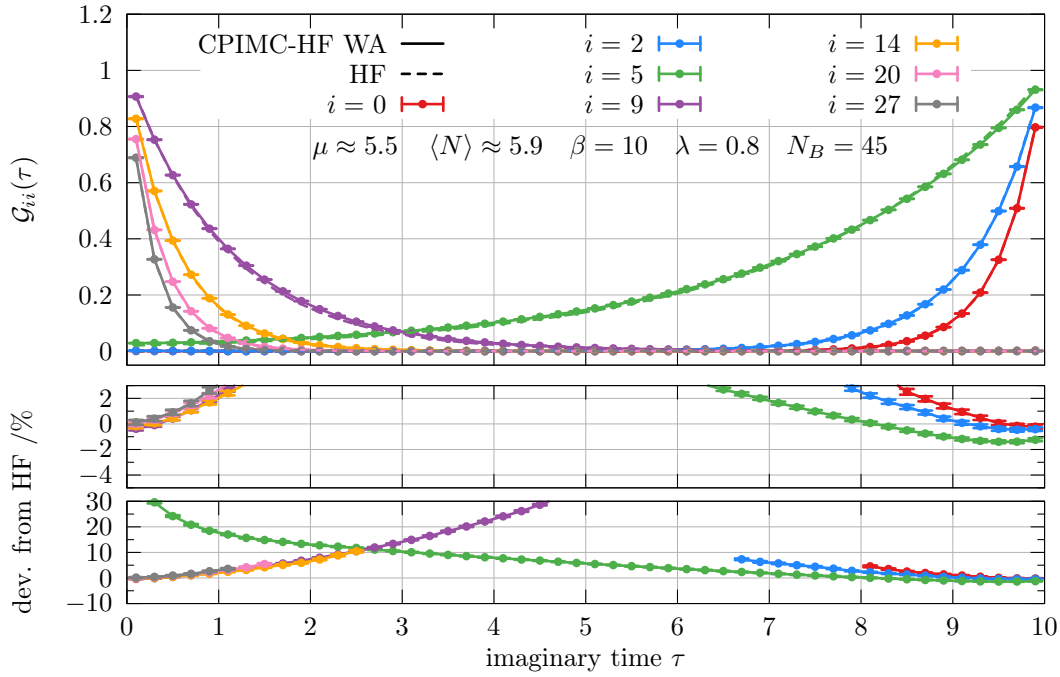
Figure 6.27.: Same as Fig. 6.25 but for a larger system of $\langle N \rangle \approx 6$ particles at $\lambda = 0.8$.
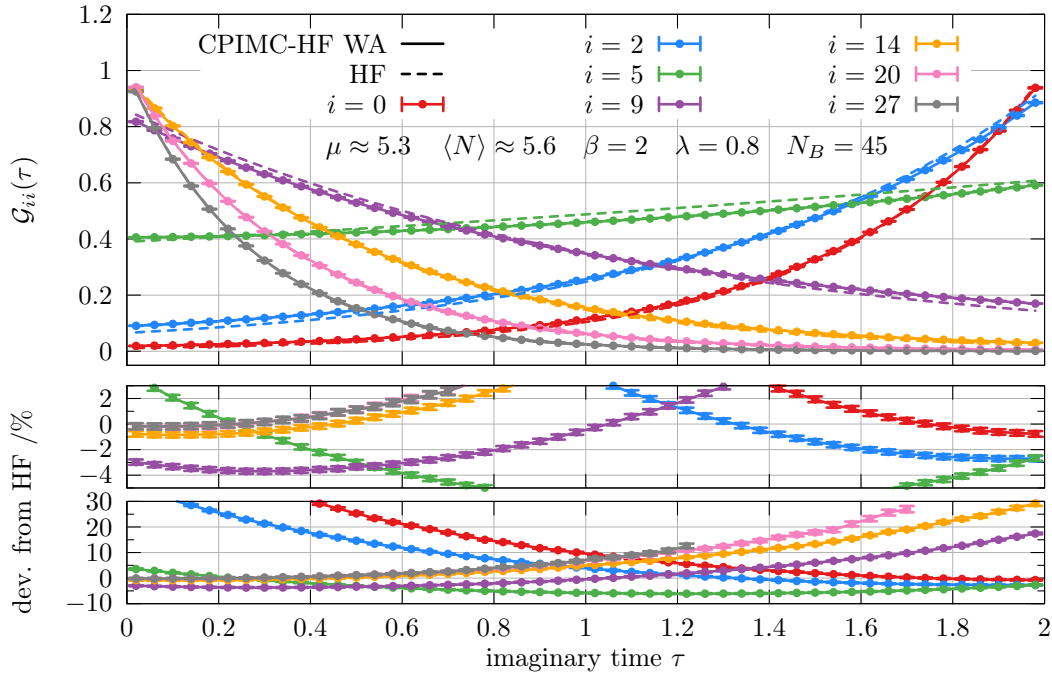

Figure 6.28.: Same as Fig. 6.27 but for a higher temperature of $\beta = 2$. The chemical potential has been adjusted to again obtain $\langle N \rangle \approx 6$ particles.

($i = 5$ and $i = 9$), there are extremely large deviations, even at $\tau = 0^-$. This enhancement of the deviation from HF already occurs at $\beta = 5$ (not shown).

Finally, Fig. 6.29 shows the diagonal elements of the MGF for $\langle N \rangle \approx 30$ particles at a coupling of $\lambda = 0.2$ and an inverse temperature $\beta = 5$. For the same parameters, the HF and CPIMC density coincide up to 0.1% (cf. Fig. 6.21). This is different for the elements of the MGF. Here, the MGF in HF approximation deviateas by up to approximately 2% from CPIMC.

It is known that the results for the MGF may be used to reconstruct the one-particle spectral function $A(\omega)$ by inverting the transformation

$$\mathcal{G}(\tau) = \int_{-\infty}^{\infty} d\omega A(\omega) \frac{e^{-\tau\omega}}{1 + e^{-\beta\omega}} \; .$$

There exist different methods to invert this transformation, but all of them require very precise input data for the MGF at discrete points $\mathcal{G}(\tau_p)$ because the inversion is well-known to be an ill-posed problem ([16, 15, 14] and references therein), i.e., due to the statistical error of the MGF, the solution for the spectral function may not be unique. Further, systematic deviations of a few percent, as observed for the HF approximation in this section are even worse than larger statistical errors. Such systematic deviations result in completely different spectra[24]. Hence, even though the HF density for larger, weakly coupled systems is quite accurate, using the MGF in HF approximation for the reconstruction of the spectra most likely yields completely wrong results. Of course, this remains to be confirmed. In addition, the HF approximation not only becomes worse with increasing coupling, which is what we expect, but also with increasing temperature. An analysis of this question goes beyond this work.

We conclude that the MGF seems to be much more influenced by correlation effects than the energy or the density, and for the reconstruction of reliable spectra, the exact results obtained from CPIMC calculations are essential.

6.6. The sign problem in the CPIMC WA

Since the main obstacle of the CPIMC method is the fermion sign problem, which limits the range of accessible parameters, we now discuss the sign problem concerning the investigated test system.

Fig. 6.30 shows the dependence of the average (canonical) sign on the coupling parameter λ for $\beta = 10$ (upper graphic) and $\beta = 5$ (lower graphic). The CPIMC calculations have been performed for various particle numbers N and basis

---

[24]This has been observed by the current master student T. Dornheim, who has spent some time on testing different methods for the inversion of transformations like Eq. 6.5.2.
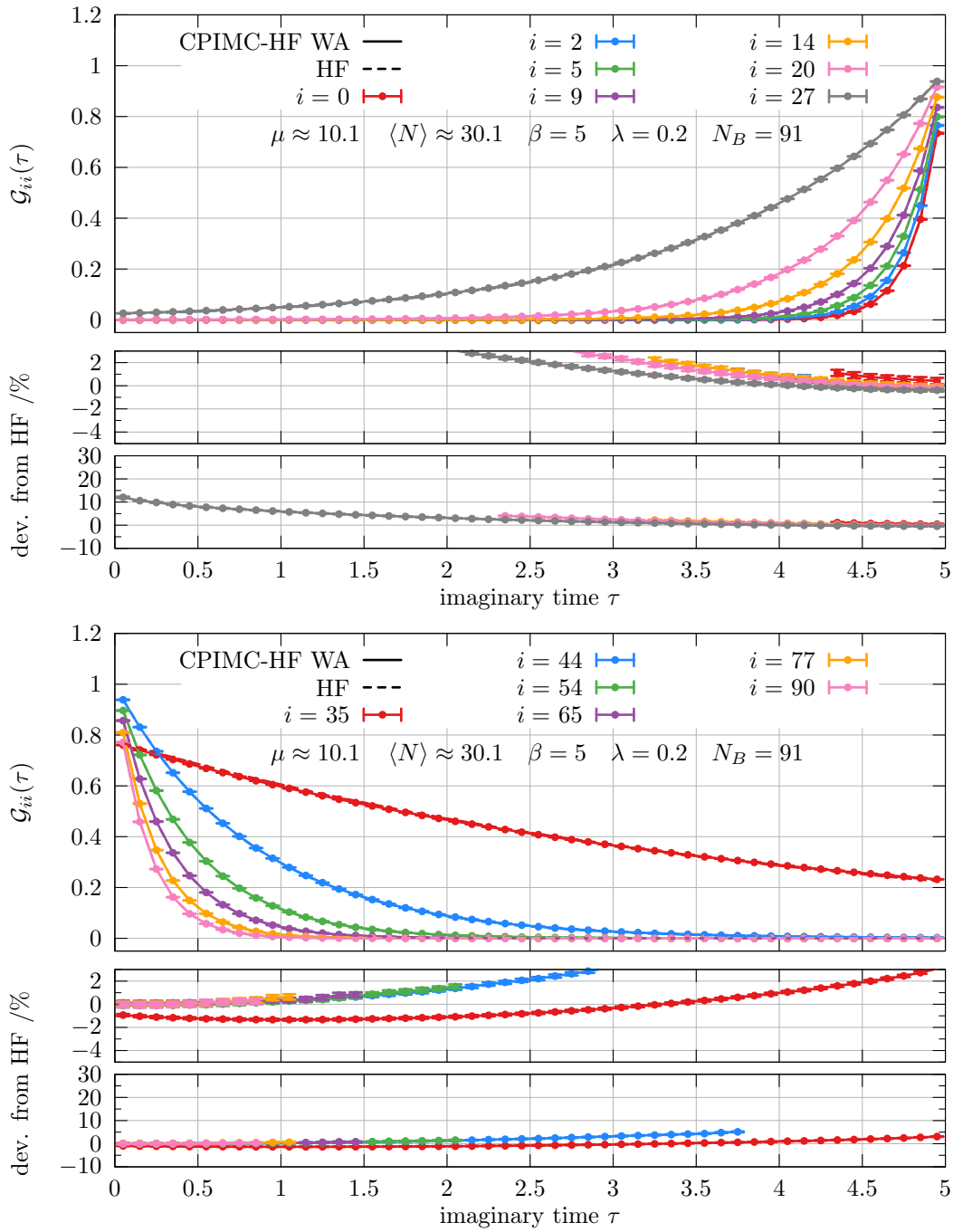
Figure 6.29.: Diagonal elements of the CPIMC MGF (solid lines) and the MGF in HF approximation (dashed lines) for $\langle N \rangle \approx 30$ particles at a coupling of $\beta = 10$. In the top (bottom) graphic, the occupied (unoccupied) elements are plotted. The deviation of the CPIMC MGF from the HF MGF is shown on two different scales for $\mathcal{G}_{ii}(\tau) > 10^{-3}$.
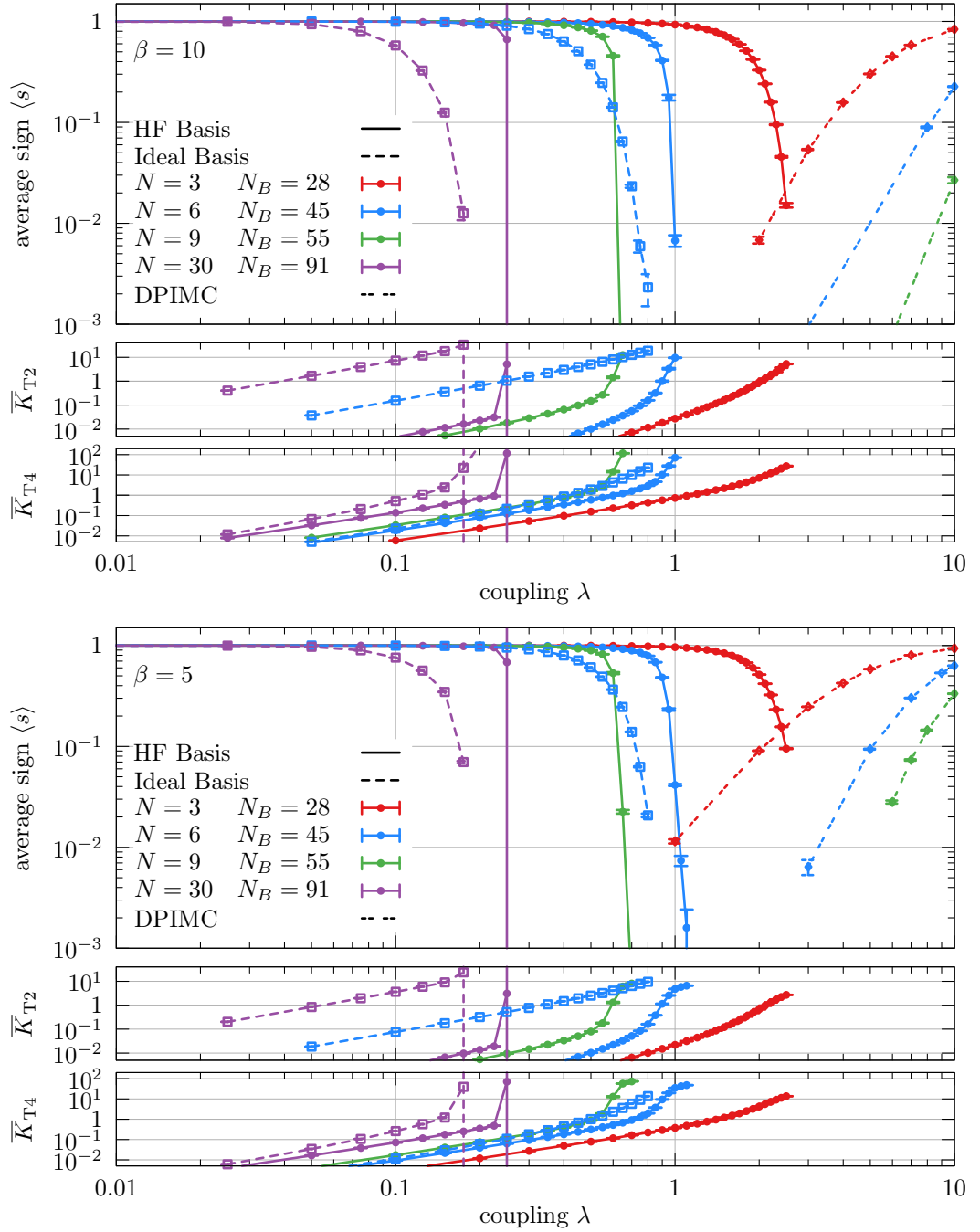
Figure 6.30.: Dependence of the average (canonical) sign $\langle s \rangle$ on the coupling parameter λ at $\beta = 10$ (top graphic) and $\beta = 5$ (bottom graphic) for different particle numbers N and number of basis functions N_B. The CPIMC calculation has been performed both in the HF basis (dots and solid lines) and in the ideal basis (squares and dashed line). The lower graphs show the average number of type 2 (4) kinks $\overline{K}_{T2}$ ($\overline{K}_{T4}$) in the CPIMC simulation. In addition, the average sign of the DPIMC method (dotted line) is shown (data courtesy of T. Dornheim). Note that all axes are logarithmic.

sizes[25] N_B both in the ideal[26] and HF basis. Further, the average number of type 2 (4) kinks $\overline{K}_{T2}$ ($\overline{K}_{T4}$) in the sampled closed paths are plotted. In addition, the average sign of the DPIMC method for some particle numbers is presented[27]. In contrast to the other CPIMC calculations in this work, these results have been obtained without using the worm steps, i.e., only using the steps (7-13) explained in Sec.

3.5 so that only closed paths of a fixed particle number are sampled.

First, we focus on the upper graphic for $\beta = 10$. The average sign in the ideal basis (squares) starts to decrease much earlier than in the HF basis. In the ideal basis, the average sign drops more slowly compared to the HF basis, where it abruptly drops to zero at some critical coupling (blue and violet dots and squares). Independent of the basis, the average number of kinks grows exponentially with the coupling parameter yielding (almost) straight lines on the logarithmic scale. The average number of type 2 kinks is reduced by roughly two to three orders of magnitude in the HF basis, while the average number of type 4 kinks is reduced by up to one order of magnitude. This almost doubles the coupling parameter in the HF basis for which results with CPIMC can be obtained.

Moreover, the rapid decrease of the average sign corresponds to an over-exponential increase of the average number of kinks with the coupling (i.e., these bend upwards on the logarithmic scale). For larger particle numbers in the HF basis, the average number of kinks grows rapidly beyond some critical coupling (green and violet curve). For $N = 9$ particles (green curve), the average number of type 4 kinks increases from 14 at $\lambda = 0.6$ ($\langle s \rangle \approx 0.5$) to 117 at $\lambda = 0.65$ ($\langle s \rangle \approx 10^{-4}$). Similarly, for $N = 30$ particles, the number of type 4 kinks suddenly increases from 1 to 100 yielding an extremely large error.

At the moment, we think that there is a problem with the currently used Monte-Carlo steps that occurs at large kink numbers (>100). It seems that fairly complex structures containing many kinks can be build up on very short time scales, while it takes extremely long to again remove all these kinks. This is due to the fact that only very few kinks can actually be removed since we have to properly change another kink if one is removed. In other words, it is possible to build up extremely entangled configurations which can not be untangled in a sufficiently short time. That means the used Monte-Carlo steps are in principle ergodic but not in practice if there are paths in the samples containing a large amount of kinks. It turned out that the explanation for the large error of the last point for $N = 30$ particles is the following: At the beginning of the simulation, we always sample closed paths containing very

---

[25]The basis size is chosen such that the observables are converged.

[26]For the ideal basis, only the results for $N = 6$ and $N = 30$ particles are plotted for a better overview.

[27]The data for the DPIMC calculations has been provided by the group member T. Dornheim.

few kinks (< 10) for a long time. Then, at some point, a very complex path containing many kinks (≈ 600) is generated. Afterwards, we are "stuck" in such configurations containing an extremely large number of kinks because the steps to remove the kinks become too inefficient. Of course, this results in an extremely large statistical error and has to be investigated in more detail in the future.

However, for the other presented particle numbers, such a behavior is not observed and the over-exponential growth of the number of kinks after some critical coupling parameter seems to be correct. Further, the larger the particle number, the smaller is the coupling parameter interval in which the average sign drops from nearly one to zero. Therefore, even if we would improve the Monte Carlo steps so that complex kink structures can be entangled or removed within a few Monte Carlo steps, this would not allow for calculations of $N = 30$ particles at a coupling of $\lambda = 0.4$.

Increasing the temperature from $\beta = 10$ to $\beta = 5$ does not change the situation qualitatively (see bottom graphic in Fig. 6.30). For even higher temperatures than $\beta = 5$, the increase of the average sign according to Eq. (2.13) is compensated by a larger number of basis functions required to ensure the convergence of the observables.

Furthermore, the average sign of the DPIMC calculation shows the already mentioned complementary behavior to that of CPIMC. For $N = 3$ particles (red curve) at $\beta = 10$, the average sign of DPIMC crosses that of CPIMC above $\langle s \rangle = 10^{-2}$, which is sufficient to obtain reliable results. For $N = 6$ (blue curve), both average signs cross somewhere below $\langle s \rangle = 10^{-3}$ leaving a gap of coupling parameters that is not accessible with any of both methods[28]. The size of this gap strongly increases with the particle number and the inverse temperature.

Finally, Fig. 6.31 shows the average particle number and the average (grand canonical) sign (upper graphs) vs. the chemical potential, i.e., the paths have been sampled with the CPIMC WA utilizing all 13 Monte Carlo steps (see Sec. 3.5). The value of the coupling parameter is fixed to $\lambda = 1.0$ and the calculations have been performed for two different inverse temperatures $\beta = 10$ and $\beta = 5$ in $N_B = 45$ basis functions. Up to a chemical potential of $\mu = 5$, which corresponds to an average particle number $\langle N \rangle \approx 4$, the average sign smoothly decreases to $\langle s \rangle \approx 0.6$. At $\mu = 5.2$, we would expect an average sign of 0.4 and an average particle number of $\langle N \rangle \approx 4.5$, but instead, the average number of kinks explodes from approximately 10 to more than 100 resulting in a large error for $\beta = 2$ (red curve) and a vanishing sign for $\beta = 10$ (blue curve). Moreover, at $\mu = 5$, the ratio of sampled closed to open paths nearly drops to zero, i.e., due to the large amount of kinks, the worm cannot be removed

---

[28]In practice, calculations providing reliable results are feasible if the average sign is larger than approximately 10^{-3}.
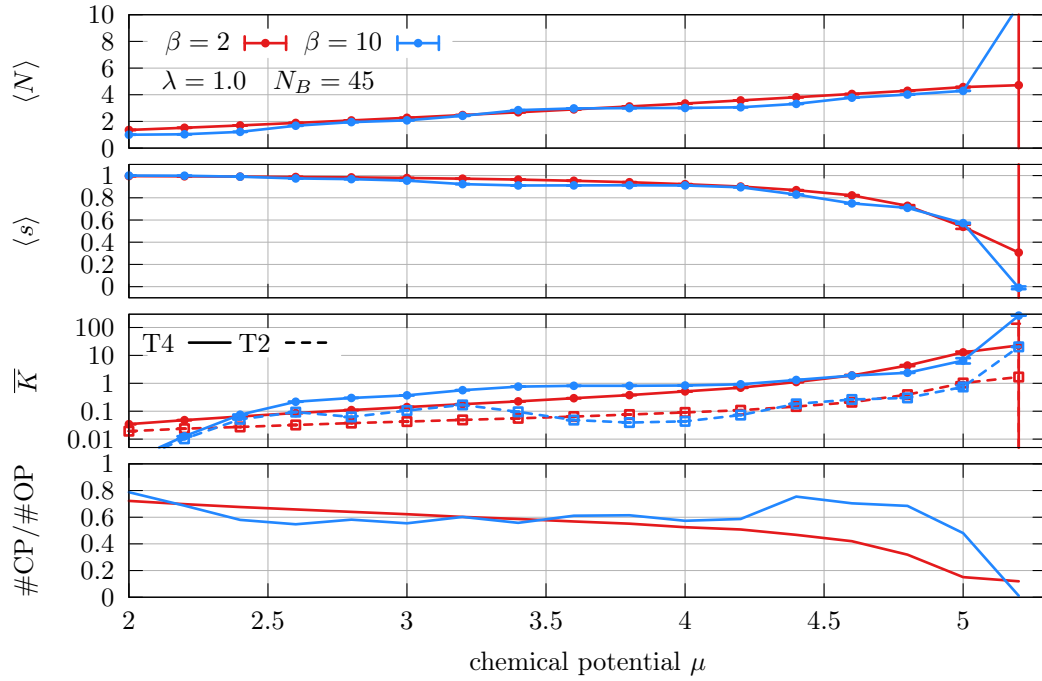
Figure 6.31.: Expectation value of particle number $\langle N \rangle$, average (grand canonical) sign $\langle s \rangle$, average number of kinks $\overline{K}$ (type 2 and 4) and the ratio of the total number of closed to open paths, versus the chemical potential μ. The system parameters are specified in the topmost plot.

any more. Hence, we do not obtain any additional closed paths samples for the grand canonical observables. Consequently, the average particle number $\langle N \rangle > 10$ for $\beta = 10$ at $\mu = 5.2$ is completely wrong and so is the statistical error.

For a given particle number, the sign problem is expected to be worse in the grand canonical ensemble compared to the canonical ensemble, simply because the configuration space of paths with varying particle number is larger than that for a fixed particle number. Yet, for $N = 6$ particles at $\beta = 10$, we still have a good average (canonical) sign $\langle s \rangle \approx 0.2$ at $\lambda = 0.95$ (cf. Fig. 6.30). In addition, according to the course of the average (grand canonical) sign for $\mu < 5.0$, even $\mu = 5.5$ should be feasible for the parameters in Fig. 6.31. The explanation for this unfavorable behaviour in grand canonical simulations is obvious. If there ought to be paths in the grand canonical simulation with a significantly large particle number, then these usually have many kinks so that we again encounter the problem of the Monte Carlo steps being inefficient, i.e., we get "stuck" in such configurations with many kinks and large particle numbers. Therefore, the (false) average particle numbers from some critical chemical potential onwards are observed to be always far too large (see blue curve in Fig. 6.31). Therefore, solving the problem with the currently used Monte Carlo steps would extend the range of parameters for which correct results can be obtained for grand canonical observables and the MGF.

7. Summary and outlook

In this work, together with T. Schoof, the development of the presented, fairly complex WA for the CPIMC approach could be finished. Without modifications, the algorithm can be used to simulate strongly degenerate, spin polarized[1] fermions with an arbitrary pair-interaction and external potential. In particular, within this work, the addition and removal of type 4 kinks with two worms (Sec. 3.5.2) and major parts of the steps[2] 7-13 described in Sec. 3.5 have been implemented. Further, the code to find the missing configurations which has been necessary to solve the ergodicity problem (Sec. 3.5.2) has been implemented. Additionally, the proper theoretical formulation of the CPIMC WA presented in Sec. 3.2, 3.3 and 3.4 has not been published anywhere else for continuous systems.

In the next major part of this wok, different estimators for the MGF have been developed and tested, which were all unemployable due to a far too large variance of the resulting samples. Eventually, a sophisticated estimator could be found that reduced the variance of the computed MGF by up to five orders of magnitude (Sec. 4.2).

Afterwards, the ground state and finite temperature HF methods have been applied to a two-dimensional test system of spin-polarized, Coulomb interacting fermions in a harmonic trap. A further result of this work consists in the observation that the value of the two-particle integrals varies significantly for different self-consistent solutions of the corresponding HF equation (Sec. 6.2). An investigation of the average sign of CPIMC calculations in different HF basis sets revealed that the largest average sign is obtained if the modulus sum over all two-electron integrals is minimal (Sec. 6.3). Thus, a fast and reliable method of finding the best HF basis for CPIMC calculations has been established. In addition, the mechanism that reduces the sign problem in the HF basis compared to that in the ideal basis has been understood and explained in detail within this work (end of Sec. 6.3).

The perfect agreement of the obtained results for the MGF in the limit of the density with the CI density verified the correctness of the method in Sec. 6.4. Further, together with the HF basis, the developed estimator for the MGF provides much better results for the density than those computed with

---

[1] A generalization to spin restricted fermions is possible without much additional effort.

[2] In total, I have implemented about six thousand lines of the currently used CPIMC WA code that consists of roughly twenty thousand lines.

standard CPIMC [10]. A comparison of the CPIMC densities with the HF densities showed that for smaller systems, where a higher coupling is feasible in the CPIMC calculations, the HF densities deviate by up to $1-3\%$ from the exact result. On the other hand, for larger systems, where only small coupling parameters are possible with CPIMC, the HF approximation improves, yielding deviations about 0.1% from the exact CPIMC density. This is different for the MGF. Here, the deviations of the HF approximation from the MGF obtained from CPIMC calculations are significant even for very small coupling parameters and large systems (Sec. 6.5.2). In addition, it turned out that the HF approximation apparently becomes worse not only for increasing coupling but also for increasing temperature[3]. Since an ill-posed problem has to be solved for the reconstruction of the one-particle spectra, where the MGF serves as input data, reliable spectra require the exact MGF from CPIMC calculations, which takes into account all correlation effects.

Finally, the fermion sign problem has been discussed in Sec. 6.6 to give a concrete impression of the accessible parameter range with the presented method. Unfortunately, there is still an ergodicity problem of the used Monte Carlo steps that slightly reduces the actually possible coupling parameter for larger particle numbers.

The actual reconstruction of the spectra from the MGF and the comparison with those in HF approximation is subject to future investigations. Due to the weak coupling, one could also compare the results with the MGF obtained from solving the Dyson equation with some suitable approximation for the self-energy [36]. Further, the MGF from RPIMC calculations [4] could be used to reconstruct the spectra and compared to CPIMC. Moreover, the sampling of the two-particle MGF could be implemented since this gives access to the dynamical structure factor. The corresponding estimator will be more elaborate but the principle idea of the estimator presented in this thesis can be used, too. The two-particle MGF is directly linked to the two-particle density matrix, i.e., in addition to the structure factor, this yields exact results for the two-particle correlation function.

In my opinion, there are only two exact ways of further reducing the sign problem within the CPIMC approach. First, one could find an even more sophisticated representation of the partition function[4]. Second, there might be a better basis than the HF basis. For example, the minimization of the two-particle integrals may be incorporated in the variation that results in the HF equation. Concerning the reduction of the sign problem with approximations, there are many things that could be investigated with respect to the resulting systematic errors. Starting from the ground state determinant with the lowest

---

[3]Of course, this is not what we expect since correlation effects in general become more important the lower the temperature.

[4]This includes blocking as described in [8].

orbitals being occupied, the number of allowed excitations that are taken into account can be restricted, i.e., only certain determinants can be realized in the paths. This approximation is widely used in CI calculations and referred to as *Restricted Active Space* (RAS) [37]. Next, the maximum number of allowed kinks can be restricted. This approximation has the advantage that there is only one parameter to be adjusted, and the resulting energy monotonically converges to the exact energy with increasing number of allowed kinks. Even more sophisticated than just restricting the maximum number of kinks might be the introduction of an artificial kink potential, which decreases with increasing kink number.

Of course, the ergodicity problem of the Monte Carlo steps for very large kink numbers may be solved. Moreover, the CPIMC WA could be applied to other physical systems of interest.

I finish this work with its first sentence: The ab initio simulation of interacting fermionic many-body systems without approximations represents a challenging and highly interesting research field of theoretical physics and chemistry.

A. Diagrams
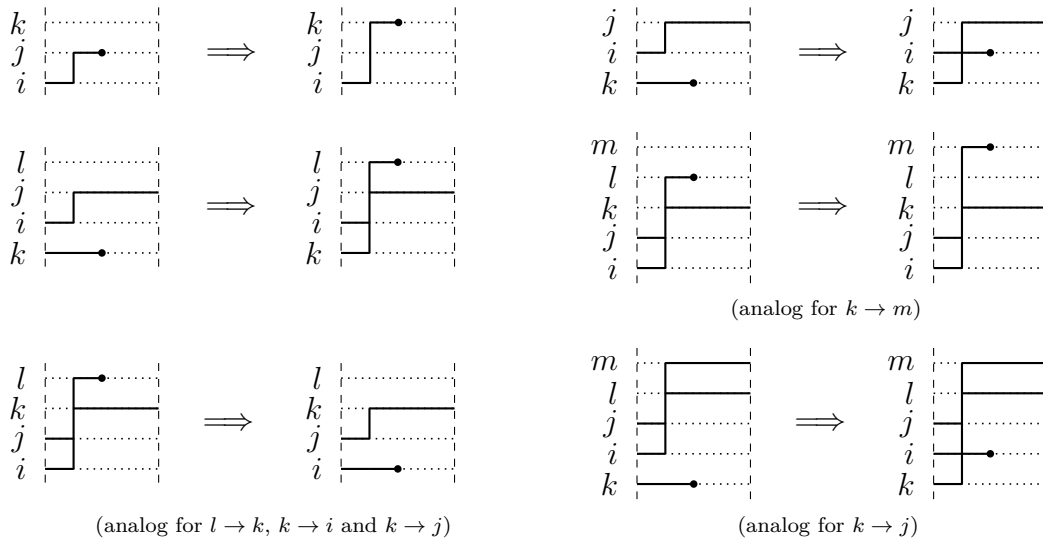
Figure A.1.: All 11 possibilities of changing the next kink left of Ira by placing Ira on a free orbital. Thereby, a type 2 kink can be changed into a type 4 kink and vice versa.
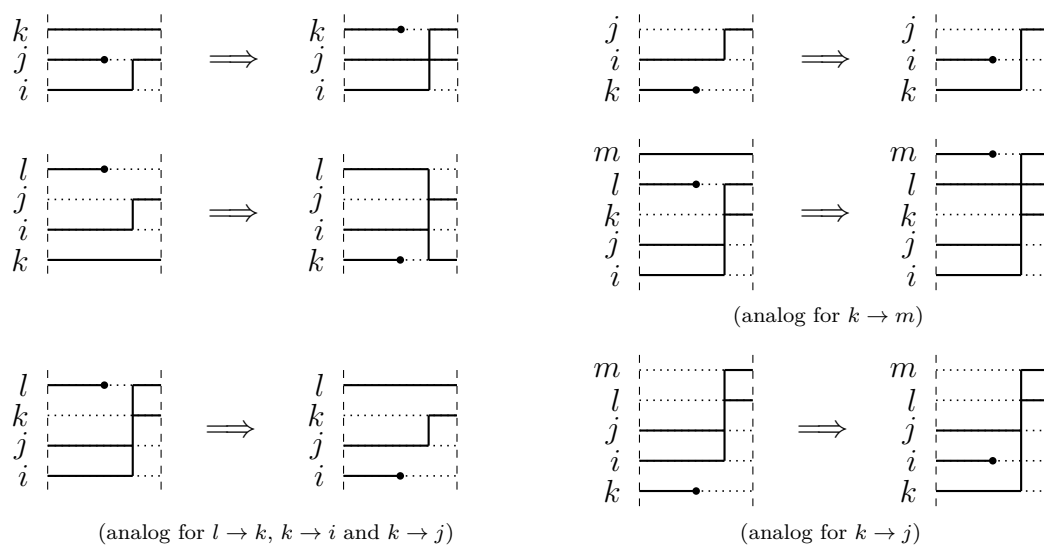
Figure A.2.: All 11 possibilities of changing the next kink right of Ira by placing Ira on an occupied orbital. Thereby, a type 2 kink can be changed into a type 4 kink and vice versa.
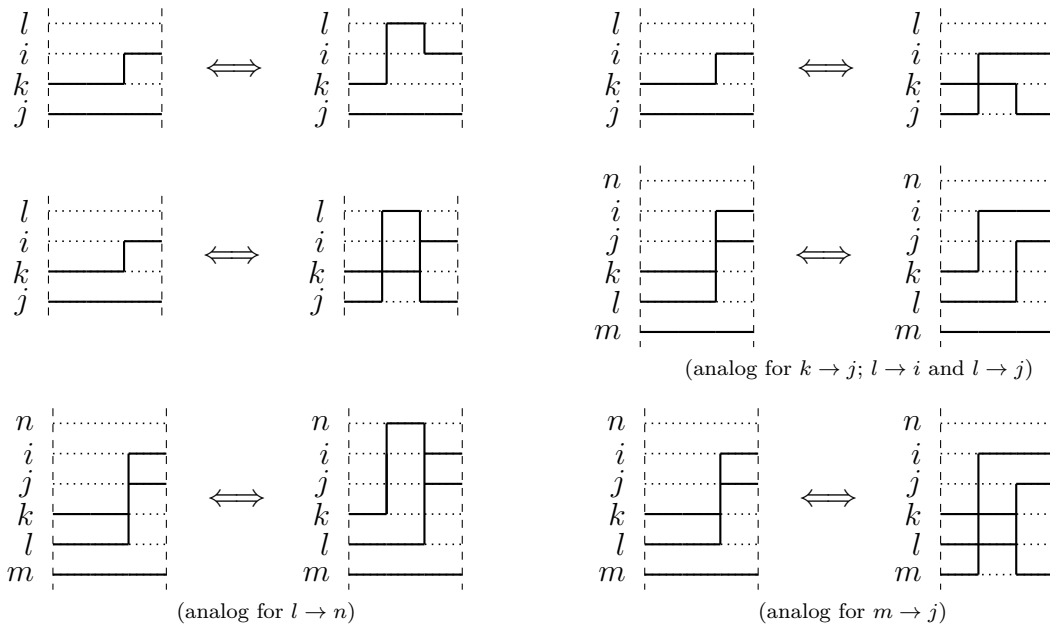
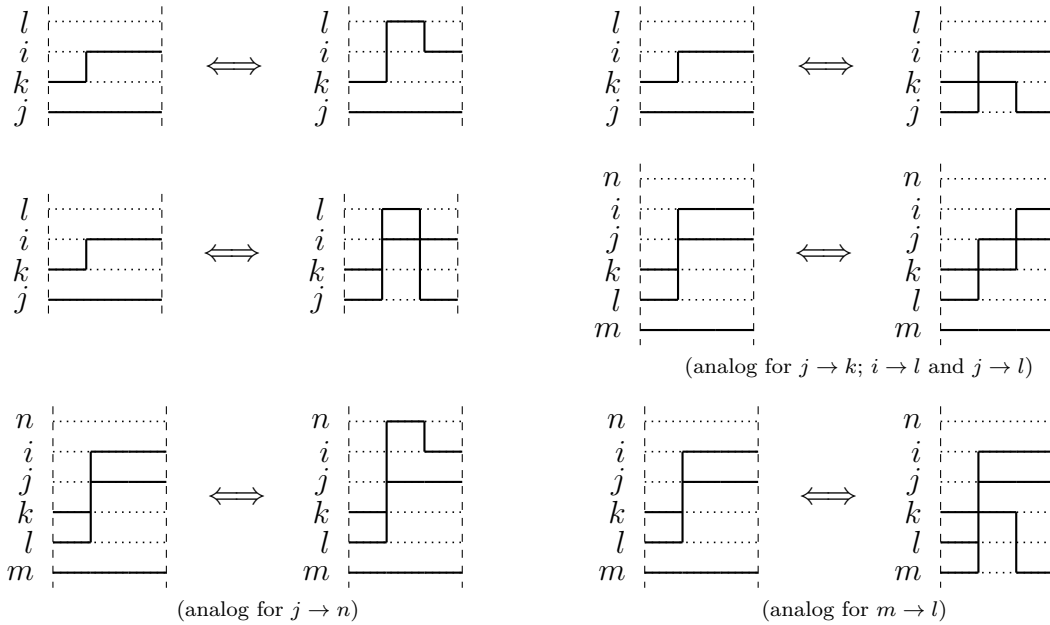**Figure A.3.:** All 11 possibilities to add a type 2 kink left of the kink to be changed via a one-particle excitation.

Figure A.4.: All 11 possibilities to add a type 2 kink right of the kink to be changed via a one-particle excitation.

127
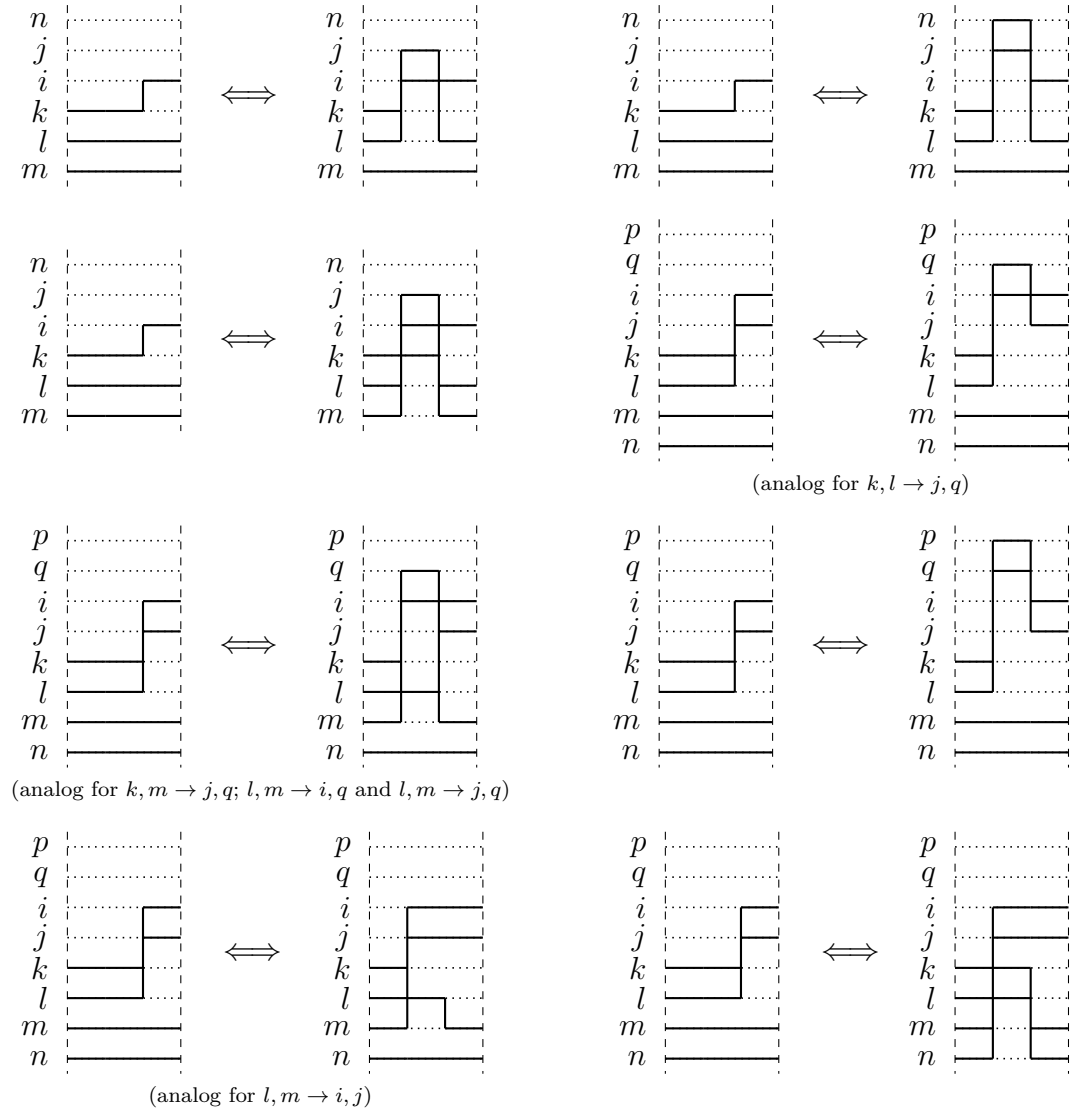
Figure A.5.: All 13 possibilities to add a type 4 kink left of the kink to be changed via a two-particle excitation.

(analog for $i, j \rightarrow l, q$)

(analog for $i, m \rightarrow l, q$; $j, m \rightarrow k, q$ and $j, m \rightarrow l, q$)

(analog for $j, m \rightarrow k, l$)
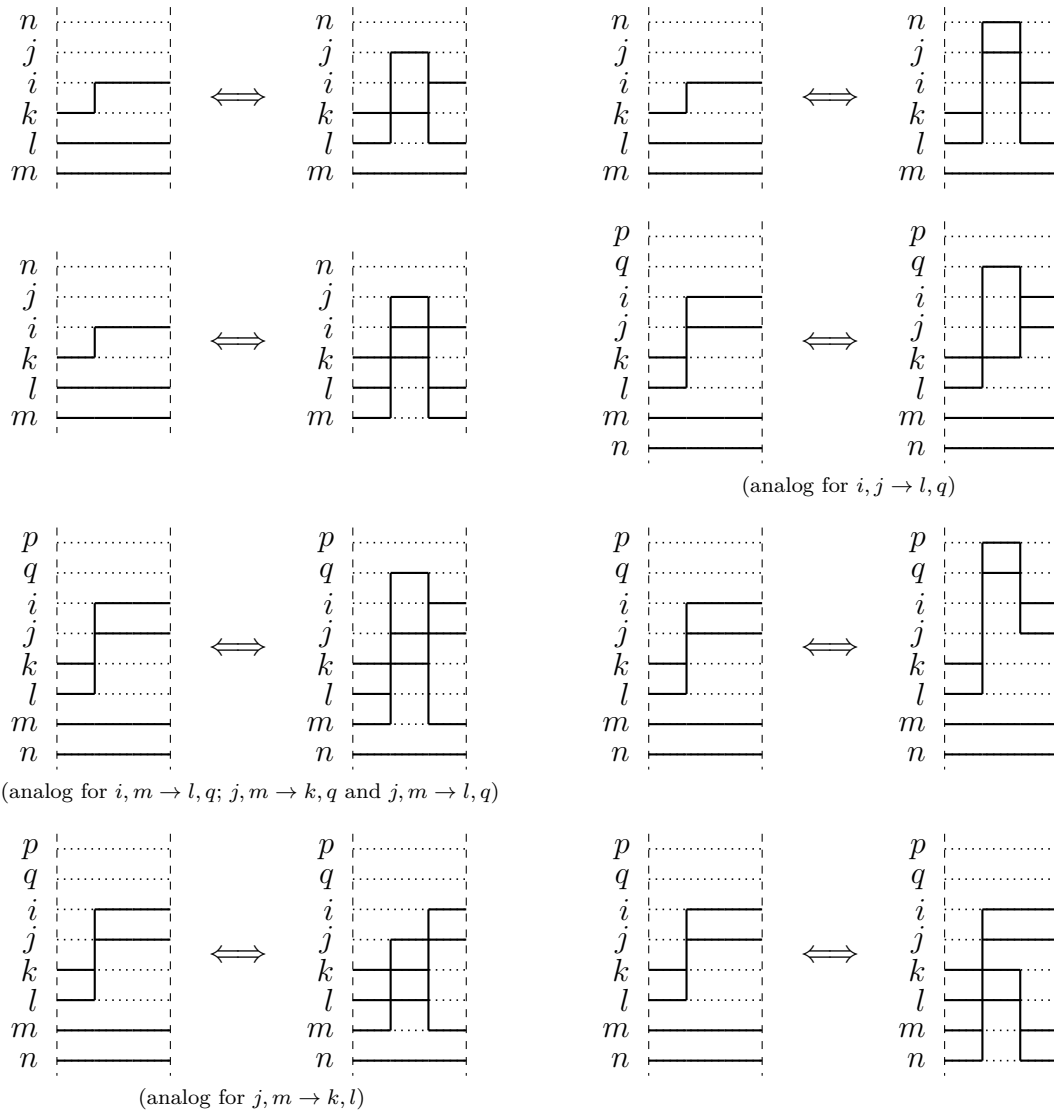
Figure A.6.: All 13 possibilities to add a type 4 kink right of the kink to be changed via a two-particle excitation.

Bibliography

[1] D. M. Ceperley, Rev. Mod. Phys. **67**, 279 (1995).

[2] A. Filinov, N. V. Prokof'ev, and M. Bonitz, Phys. Rev. Lett. **105**, 070401 (2010).

[3] R. Feynman, *Quantum mechanics and path integrals* (McGraw-Hill, New York, 1965).

[4] D. Ceperley, in *Monte Carlo and Molecular Dynamics of Condensed Matter Systems* (Editrice Compositori, Bologna, Italy, 1996).

[5] M. Troyer and U. Wiese, Phys. Rev. Lett. **94**, 170201 (2005).

[6] V. S. Filinov, M. Bonitz, W. Ebeling, and V. E. Fortov, Plasma Phys. and Controlled Fusion **43**, 743 (2001).

[7] A. V. Filinov, M. Bonitz, and Y. E. Lozovik, Phys. Rev. Lett. **86**, 3851 (2001).

[8] R. Egger, W. Häusler, C. H. Mak, and H. Grabert, Phys. Rev. Lett. **82**, 3320 (1999).

[9] T. Schoof, M. Bonitz, A. Filinov, D. Hochstuhl, and J. W. Dufty, Contrib. Plasma Phys. **51**, 687 (2011).

[10] T. Schoof, S.Groth and M. Bonitz, *Introduction to Configuration Path Integral Monte Carlo, Chapter in: Complex Plasmas: Scientific Challenges and Technological Opportunities edited by M. Bonitz, K. Becker, J. Lopez and H. Thomsen* (Springer, 2014).

[11] T. Schoof, *Thermodynamische Eigenschaften entarteter, korrelierte Fermionen, Diplomarbeit (in German)* (Kiel University, 2011).

[12] N. V. Prokof'ev, B. V. Svistunov, and I. S. Tupitsyn, J. Exp. Theor. Phys. Lett. **64**, 911 (1996).

[13] A. W. Sandvik and J. Kurkijärvi, Phys. Rev. B **43**, 5950 (1991).

[14] A. Filinov and M. Bonitz, Phys. Rev. A **86**, 043628 (2012).

[15] M. Boninsegni and D. M. Ceperley, J. Low Temp. Phys. **104**, 339 (1996).

[16] A.S. Mishchenko, N. V. Prokof'ev, A. Sakamoto and B. V. Svistunov, Phys. Rev. B **62**, 6317 (2000).

[17] N. V. P. M. Boninsegni., B. V. Svistunov, and I. S. Tupitsyn, Phys. Rev. E **74** (2006).

[18] N. V. Prokof'ev, B. V. Svistunov, and I. S. Tupitsyn, J. Exp. Theor. Phys. **87**, 310 (1998).

[19] A. Szabó and N. S. Ostlund, *Modern quantum chemistry: introduction to advanced electronic structure theory* (Courier Dover Publications, 1996).

[20] D. Hochstuhl, *Nonequilibrium Green functions approach to ionization processes*, Diplomarbeit, Universität Kiel (2008).

[21] N. D. Mermin, Annals of Physics **21**, 99 (1963).

[22] *Introduction to Computational Methods in Many Body Physics*, edited by M. Bonitz and D. Semkat (Rinton Press Inc, Princeton, 2006).

[23] N. Metropolis, A. W. Rosenbluth, M. N. Rosenbluth, A. H. Teller, and E. Teller, J. Chem. Phys. **21**, 1087 (1953).

[24] W. Janke, in *Quantum Simulations of Complex Many-Body Systems: From Theory to Algorithms*, edited by J. Grotendorst, D. Marx and A. Muramatsu, John von Neumann Institute for Computing (NIC, Jülich, 2002).

[25] T. Nakamura, Phys. Rev. B **57**, R3197 (1998).

[26] A. P. Lyubartsev, J. Phys. A **38**, 6659 (2005).

[27] T. Helgaker, P. Jorgensen, and J. Olsen, *Molecular Electronic-Structure Theory*, 1st ed. (Wiley, Chichester, Hoboken, 2000).

[28] F. Schwabl, *Quantenmechanik für Fortgeschrittene (QM II)*, 5th ed. (Springer, Berlin, 2008).

[29] H. F. Trotter, Proc. Amer. Math. Soc. **10**, 545 (1959).

[30] N. V. Prokof'ev, *Worm algorithm for classical and quantum statistical models*, Lecture notes at "Advanced School on Quantum Monte Carlo Methods in Physics and Chemistry", 2008, Trieste, online at `http://mcwa.csi.cuny.edu/umass/lectures.html`.

[31] M. Pourfath, *Numerical Study of Quantum Transport in Carbon Nanotube Based Transistors*, Dissertation, Universität Wien (2007).

[32] M. Heimsoth, *Unrestricted Hartree-Fock Theory of Nonideal Bose systems* (Diploma thesis, Kiel University, 2009).

[33] Maretis and Dimitris, Journal of Chemical Physics **71**, 917 (1997).

[34] U. Giovannini, Phys. Rev. B **77**, 035325 (2008).

[35] *Many-Particle Physics*, edited by G. D. Mahan (Springer, 2000).

[36] K. Balzer and M. Bonitz, *Nonequilibrium Green's functions approach to inhomogeneous systems* (Springer, Heidelberg, New York, 2013) ISBN 364235081X 9783642350818.

[37] D. Hochstuhl, *Multiconfiguration methods for the numerical simulation of photoionization processes of many-electron atoms (PhD thesis)* (Kiel University, 2013).

Acknowledgements

Erklärung

Die vorliegende Arbeit ist von mir selbständig und ausschließlich unter Zuhilfenahme der angegebenen Quellen und Hilfsmittel angefertigt worden.

Kiel, den

_____   _____

(Ort)   (Datum)   (Unterschrift)